UNIVERSITY OF CALIFORNIA

Santa Barbara

Diatom community transcriptomic responses to abiotic stressors

A dissertation submitted in partial satisfaction of the

requirements for the degree Doctor of Philosophy

in Marine Science

By

Michael Andrew Maniscalco

Committee in charge

Professor Mark A. Brzezinski, Chair

Professor Kimberlee Thamatrakoln, Rutgers The State University of New Jersey

Professor Alyson Santoro

Professor Debora Iglesias-Rodriguez

September 2022

The dissertation of Michael Andrew Maniscalco is approved.

Alyson Santoro

Debora Iglesias-Rodriguez

Kimberlee Thamatrakoln

Mark Brzezinski, Committee Chair

June 2022

Diatom community transcriptomic response to abiotic stressors

ACKNOWLEDGEMENTS

I wish to thank my advisors Dr. Mark Brzezinski and Dr. Kimberlee Thamatrakoln and committee members Dr. Alyson Santoro and Dr. Debora Iglesias-Rodriguez for their guidance and advice throughout my thesis. I would also like to thank Dr. Kelly Bidle for fostering my scientific curiosity and independence and encouraging me to pursue a graduate degree. Professors, staff, and fellow graduate students of University of California Santa Barbara and Rutgers University have been endlessly generous with their time and energy. Their formal and informal mentorship have shaped me into a better scientist and person.

The field work and research in this thesis was supported and made more enjoyable by the many collaborators involved including Jozef Nissimov, Fedor Kouzminov, Jeremy Schreier, Natalie Cohen, Kelsey Ellis, Adrian Marchetti, Benjamin Twining, Kay Bidle, Christopher Johns, Ivia Closset, and Heather McNair. None of the field work involved in this thesis would have been possible without the expertise and organization of Janice Jones.

I cannot express the depths of my gratitude toward the greater marine science community at UCSB who welcomed me with open arms and open doors since I stepped foot in town. Your continual support and willingness to, sometimes literally, pick me up when I was down has helped make the long weeks feel shorter and ensured that every day was full of joy and adventure. I want to thank my family and friends who have supported me from afar over the past several years. Lastly, I would like to thank Caroline for the never-ending warmth, laughter, and pranks that she has brought into my life.

CURRICULUM VITAE OF MICHAEL ANDREW MANISCALCO

Education

University of California Santa Barbara (UCSB), Santa Barbara, CA

Ph.D., Marine Science *June 2022*

Primary advisors: Dr. Kimberlee Thamatrakoln and Dr. Mark Brzezinski

Rutgers University, New Brunswick, NJ

B.S. Biotechnology *May 2011*

Research Positions

Environmental Data Initiative Fellow, Mount Desert Island Bio Labs, Bar Harbor, ME *Summer 2022*

- Assembled and curated a multidecadal harmful algal bloom dataset
- Published the dataset in the Environmental Data Initiative repository

Graduate Research Assistant, UCSB, Santa Barbara, CA *2014-2022*

- Assembled, managed, analyzed, and visualized complex datasets
- Perform weekly phytoplankton enumeration for harmful algal bloom monitoring
- Presented research findings at five national and international conferences
- Collaborated with interdisciplinary teams in partnerships across several universities as part of integrative field studies
- Investigated the transcriptomic response of natural diatom communities to environmental stressors including identifying molecular indicators for biogeochemical processes
- Developed, troubleshot, and implemented RNAseq assembly, annotation, and analysis pipelines to assess differential abundance of transcripts within marine eukaryotic microbial communities
- Performed phylogenetic analysis of viral and eukaryotic genes

Research Assistant/Laboratory Manager, Rider University, Ewing, NJ *2011-2014*

- Used standard microbial culturing methods, qPCR, and protein assays to investigate and characterize a suite of archaeal circadian genes
- Managed lab operations and developed standard operating procedure
- Created and supervised projects for several undergraduate mentees

Publications

Maniscalco M, Brzezinski MA, Thamatrakoln K. Diatom molecular strategies for acclimating to variable light in a dynamic coastal regime. In prep.

Maniscalco M, Brzezinski MA, McNair HM, Krause JW, Thamatrakoln K. Physiological interactions between nitrogen limitation and cooccurring silicon limitation within a Monterey Bay diatom bloom. In prep.

Maniscalco M, Brzezinski MA, Lampe RH, Cohen NR, McNair HM, Ellis KA, Brown M, Till CP, Twining BS, Bruland KW, Marchetti A, Thamatrakoln K. Diminished carbon and nitrate assimilation drives changes in Si stoichiometry in an iron-limited diatom assemblage. *Accepted*.

Ladd TM, Catlett D, **Maniscalco M,** Kim SM, Kelly RL, John SG, Carlson CA, Iglesias-Rodríguez MD. Wildfire ash deposition fertilizes coastal marine ecosystems. submitted

Kranzler CF, Brzezinski MA, Cohen NR, Lampe RH, **Maniscalco M,** Till CP, Mack J, Latham JR, Bruland KW, Twining BS, Marchetti A, Thamatrakoln K. Impaired viral infection and reduced mortality of diatoms in iron-limited oceanic regions. Nat. Geosci. 14: 231–237. doi:10.1038/s41561-021-00711-6

Krause JW, Brzezinski MA, Largier JL, McNair HM, **Maniscalco M.,** Bidle KD, Allen AE, and Thamatrakoln K. 2020. The interaction of physical and biological factors drives phytoplankton spatial distribution in the northern California Current. Limnol. Oceanogr. 65: 1974–1989. doi:10.1002/lno.11431

Kranzler, CF, Krause, JW, Brzezinski, MA, Edwards, BR, Biggs, WP, **Maniscalco, M,** McCrow, JP, Van Mooy, BAS, Bidle, KD, Allen, AE, Thamatrakoln, K. 2021. Silicon limitation facilitates virus infection and mortality of marine diatoms. Nat. Microbiol. 4: 1790–1797. doi:10.1038/s41564-019-0502-x

Maniscalco M, Nannen J, Sodi V, Silver G, Lowrey PL and Bidle KA. 2014. Light-dependent expression of four cryptic archaeal circadian gene homologs. *Front. Microbiol*. 5:79. doi: 10.3389/fmicb.2014.00079

Presentations

Maniscalco. M, McNair, H, Lampe, R.H., Cohen, N.R., Ellis, K., Marchetti, A., Twining, B.S., Till, C.P., Brown, M., Coale, T., Bruland. K.W., Brzezinski, M.A., and Thamatrakoln, K. 2020. Diatom community transcriptomic response to nitrate and silicon limitation. Oral Presentation. Ocean Science Meeting. San Diego, CA.

Maniscalco. M, McNair, H, Lampe, R.H., Cohen, N.R., Ellis, K., Marchetti, A., Twining, B.S., Till, C.P., Brown, M., Coale, T., Bruland. K.W., Brzezinski, M.A., and Thamatrakoln, K. 2018. **The stoichiometry of staying** skinny**: Increased Si:N uptake without changes in frustule silica content in an iron stressed diatom assemblage.** Oral Presentation. Silicamics Meeting. University of Victoria, Victoria, BC, Canada.

Maniscalco. M, McNair, H, Lampe, R.H., Cohen, N.R., Ellis, K., Marchetti, A., Twining, B.S., Till, C.P., Brown, M., Coale, T., Bruland. K.W., Brzezinski, M.A., and Thamatrakoln, K. 2018. Molecular drivers behind increased Si:N uptake in an iron stressed diatom assemblage. Oral Presentation. Ocean Science Meeting. Portland, OR.

Maniscalco, M., Krause J.W., Allen, A.E., Brzezinski, M.A., Thamatrakoln. K. 2015. Building Bridges Between Molecular and Physiological Aspects of Diatom Silicification. Oral Presentation. Molecular Life of Diatoms. Seattle, WA.

Maniscalco, M., Minichino, D. and Bidle, K. 2014. Examining the Role of Four Cryptic Circadian-genes in the Stress Response of *Haloferax volcanii.* Poster presentation. *American Society for Microbiology Meeting.* Boston, MA.

Teaching and mentoring

Teaching Assistant, UCSB, Santa Barbara, CA 2018-2022

- Designed weekly lessons for over 80 students in marine ecology, environmental processes, marine microbiology, and introductory biology lab courses
- Assessed students writing and provided regular constructive feedback

- Met with students individually and in groups to review difficult concepts

Middle School Science Educator, UCSB-CSEP, Santa Barbara, CA 2014-present

- Facilitate and run hands-on activities with junior high school students and their families to stimulate science interest and conversation through the Family Ultimate Science Exploration (FUSE), Center for Science and Engineering Partnerships (CSEP), UC Santa Barbara, Santa Barbara, CA.

Center for Science & Engineering Partnerships Grad Assistant 2017-2018

- Coordinate and train volunteers to make sure they are prepared and comfortable teaching the lessons each week.

Mentoring Experience

Soren Ibsen, reference/mentor for junior high science fair project	2017
Daniel Shedlovskiy, undergraduate intern	2015-2016
Christopher Marrocco, undergraduate intern	2013-2014
Kaitlyn Uhrick, undergraduate intern	2013-2014
Danielle Minichino, undergraduate intern	2012-2014
Nicole Ritzer, undergraduate intern	2011-2013
Gillian Davis, undergraduate intern	2011-2012
Amanda Walker, undergraduate intern	2011-2012

University and Departmental Service

Diversity, Equity, Inclusion, and Wellness group	2019-present
UCSB Marine Science graduate program DEI working group	2019-present
Marine Science Graduate Program Chair's committee	2016-2021
Program Representative, EEMB Grad Student Advisory Council	2016-2018
Member, Grad Students for Diversity in Science	since 2016
Marine Science Seminar Coordinator	2016-2017

Honors and Awards

Fellowships

Environmental Data Initiative Fellow	Summer 2022
Nejat B. Ezal Fellow, University of California	Summer 2019
Eugene Cota-Robles Fellow, University of California	2014-2017
IGPMS/EEMB Block Grant	Summer 2014
IGPMS/EEMB Block Grant	Summer 2015

ABSTRACT

Diatom community transcriptomic response to abiotic stressors

By

Michael Andrew Maniscalco

Diatoms serve as a critical link between the marine carbon (C), nitrogen (N), and silicon (Si) biogeochemical cycles through an obligate requirement for silicon for frustule formation. The siliceous frustules of diatoms serve as ballast, leading to the disproportionate contribution of diatoms to organic carbon export compared to similarly sized non-siliceous cells. Despite accounting for ~30% of marine primary production, diatom growth and productivity are limited in much of the surface ocean by the availability of dissolved iron (dFe), nitrate (NO_3^-), and silicic acid ($Si(OH)_4$). Furthermore, as obligate phototrophs living in the sunlight region of the ocean, diatom cells can become increasingly light-limited as light quality and quantity decreases over depth. These physiological limitations can lead to shifts in phytoplankton community composition and act as controls on phytoplankton physiology, marine biogeochemical cycling, and carbon export.

With the growing abundance of marine nucleic acid sequencing data through large collaborative projects such as EXPORTS [1], BIOS-SCOPE, BioGEOTRACES [2], Global Ocean Sampling [3], Tara Oceans [4], and Bio-GO-SHIP [5], which all share an interest in moving toward linking cellular metabolism with ocean processes, there is a need to develop

and test relationships between molecular markers, phytoplankton physiology, and related biogeochemical stocks and rates. By relating metatranscriptomic patterns to biogeochemical stock and rate measurements during diatom blooms in the California Upwelling Zone we evaluate the ecological relevance of diatom transcriptomic fingerprints of iron, nitrogen, silicon, and light limitations based on those previously characterized in laboratory studies, while also exploring potentially undiscovered Si related genes.

The first chapter of this dissertation (Chapter 1) explores the transcriptomic and physiological changes that occur in iron limited diatom assemblages that led to bulk increases in biogenic silica relative to particulate organic carbon and nitrogen. Under Fe-limitation, diatom dominated communities can double the respective ratios of biogenic silica (bSi) to particulate organic carbon (C) and nitrogen (N), which has implications for carbon export efficiency given the ballasted nature of the silica-based diatom cell wall. Understanding the drivers of this altered cellular stoichiometry will foster a predictive understanding of how diatom carbon export is affected by low Fe. In a simulated upwelling experiment, water from the 10ºC isotherm was transported from depth, incubated shipboard, and left untreated or amended with dissolved Fe or the Fe-binding siderophore desferrioxamine-B (+DFB) to induce Fe-limitation. The phytoplankton communities within all treatments became dominated by diatoms, which displayed hallmark signatures of Fe-limitation in the +DFB treatment, including elevated particulate Si:C and Si:N ratios. Single-cell, taxon-resolved measurements of elemental content revealed no increase in bSi content during Fe-limitation despite the higher transcript abundance of silicon associated genes. We posit that the observed increase in bSi relative to C and N was primarily due to reductions in

C fixation and N assimilation, driven by lower transcript expression of key Fe-dependent genes.

Chapter 2 pairs biogeochemical measurements of Si uptake with metatranscriptomic analysis of communities incubated with and without added dissolved Si to investigate the molecular response of diatom communities to different nutrient statuses. Steep gradients in macronutrients in the surface ocean near Monterey Bay, CA allowed for the sampling of macronutrient replete phytoplankton communities as well as communities experiencing N-limitation, and N and Si co-limitation. Metatranscriptomic analysis revealed that N-limited communities exhibited dynamic shifts in N and C transcriptional patterns. Despite a 97% reduction in biomass-specific silica production rates, only modest additional changes in transcript abundance occurred with N and Si co-limited communities. Transcript abundance of previously characterized Si-metabolism associated genes did not appear to be correlated with changes in Si-limitation. However, several not yet characterized Si-responsive genes were revealed to be potential indicators of kinetic Si-limitation. Transcriptomic data implied that additional Si-limitation within N and Si co-limited samples served a protective role of reducing the degree of N-limitation and the associated heavy physiological toll.

The last chapter of this dissertation (Chapter 3) investigates the extent to which ambient light availability at the lower depths of the euphotic zone (EZ) impacted water biogeochemistry and diatom community physiology. As light intensity decreased at the base of the EZ (1-5% incident irradiance) all diatom communities reduced bSi-normalized silica production rates. However, there was poor correlation between changes in bSi production rates and silicon transporter transcript abundance. Biogeochemical markers of light limitation, such as decreased ratio of chlorophyll *a* to particulate organic carbon, correlated

with reduced transcript abundance of genes related to photosystem II as well as nitrate transport and reduction. In stratified conditions, diatom communities at the base of the euphotic zone exhibited widespread reduction of transcripts for genes related to light harvesting, photosystem II, photosynthetic electron transport, oxidative phosphorylation, and nitrogen assimilation. However, in less stratified water columns diatom communities exhibited minimal changes in transcript abundance and were likely better poised to deal with rapid changes in light availability.

The combined results from this dissertation offer a comprehensive understanding of diatom community transcriptomic response to several of the determinant abiotic drivers of biogeochemical cycling within the dynamic California Upwelling Zone. Furthermore, this work validates and supports the use of prior and additional transcriptomic markers of diatom physiology.

Table of Contents

Chapter 1: Diminished carbon and nitrate assimilation drive changes in diatom elemental stoichiometry independent of silicification in an iron-limited assemblage

Abstract:

In the California Current Ecosystem, upwelled water low in dissolved iron (Fe) can limit phytoplankton growth, altering the elemental stoichiometry of the particulate matter and dissolved macronutrients. Iron-limited diatoms can increase biogenic silica (bSi) content >2-fold relative to that of particulate organic carbon (C) and nitrogen (N), which has implications for carbon export efficiency given the ballasted nature of the silica-based diatom cell wall. Understanding the molecular and physiological drivers of this altered cellular stoichiometry would foster a predictive understanding of how low Fe affects diatom carbon export. In an artificial upwelling experiment, water from 96 m depth was incubated shipboard and left untreated or amended with dissolved Fe or the Fe-binding siderophore desferrioxamine-B (+DFB) to induce Fe-limitation. After 120 h, diatoms dominated the communities in all treatments and displayed hallmark signatures of Fe-limitation in the +DFB treatment, including elevated particulate Si:C and Si:N ratios. Single-cell, taxon-resolved measurements revealed no increase in bSi content during Fe-limitation despite higher transcript abundance of silicon transporters and silicanin-1. Based on these findings we posit that the observed increase in bSi relative to C and N was primarily due to reductions in C fixation and N assimilation, driven by lower transcript expression of key Fe-dependent genes.

Introduction:

Diatoms play a key role in global biogeochemistry, accounting for ~30% of marine primary production [6]. Through an obligate silicon (Si) requirement for frustule formation,

diatoms serve as the critical link between the ocean carbon (C) and Si cycles, and disproportionately contribute to organic carbon export compared to similarly sized non-siliceous cells [6]. In the late spring and summer, phytoplankton productivity in the coastal California Upwelling Zone (CUZ) is fueled by wind-driven upwelling events that transport deep waters to the surface that are rich in both silicic acid ($Si(OH)_4$) and nitrate (NO_3^-). The concentrations of both $Si(OH)_4$ and NO_3^- in these waters often exceed 20 μmol L^{-1} [7]. Along stretches of narrow continental shelf, the deep ferricline and lack of contact with Fe-laden sediment can result in upwelled water deplete in dissolved Fe (dFe) relative to nitrate (>12 μmol L^{-1} NO_3^-:1 nmol L^{-1} dFe) that has the potential to push the system into Fe-limitation, similar to open ocean high nutrient, low chlorophyll (HNLC) regions [8].

Fe-limited HNLC regions are considered 'hot spots' of diatom silica burial [9] and they can be areas of enhanced carbon export efficiency [10], with the underlying driving mechanism often cited as an increase in the molar ratio of particulate Si to C and nitrogen (N) that results in enhanced mineral ballast and a more efficient biological pump [10]. Alterations in elemental stoichiometry (here Si:C:N) can arise through a variety of changes, including phytoplankton community structure and cellular physiology [7, 11, 12]. For example, Fe-limitation can shift the phytoplankton community away from non-silicifying taxa or toward more heavily silicified diatom species [13]. Interspecific reductions in cell size [14] or changes in cell shape [15] in response to Fe-limitation can impact the overall cellular stoichiometry, given that biogenic silica (bSi) content is more dependent on cell surface area (SA), while particulate organic carbon (POC) and particulate organic nitrogen (PON) are more related to cell volume (V). The remarkable physiological plasticity of diatoms allows cells to alter bSi [16], N [17], and C [11] content somewhat independently in

response to environmental conditions altering cellular elemental stoichiometry. During Fe-limitation, some diatom species produce more heavily silicified frustules, which has been hypothesized to be due to slower growth rates given that silicon uptake and silica production, are closely tied to the cell cycle [10, 18–20]. Increased expression of silicon transporters (*SITs*), a conserved family of membrane-bound proteins responsible for Si uptake into the cell [21], under Fe-limitation has been suggested to be a mechanistic driver behind more heavily silicified frustules [22, 23]. Similar to increases in cellular bSi content, altered elemental stoichiometry could also arise due to reductions in C and N in Fe-limited diatoms, as has been reported in both laboratory- [23, 24] and field-based studies [25–27]. This has been attributed to the replacement of high Fe-requiring proteins involved in C and N assimilation with Fe-independent, but less efficient, analogs under low Fe availability such as the substitution of the Fe-containing photosynthetic electron transport chain proteins, ferredoxin and cytochrome c_6 with flavodoxin [28] and plastocyanin [29]. Similarly, decreased expression and activity of Fe-dependent nitrate and nitrite reductases [30, 31] during periods of low Fe availability contribute to reduced N assimilation [26, 27].

Given the significant contribution of diatoms to sinking flux in the ocean [32], it is important to understand the mechanisms driving changes in diatom elemental stoichiometry and subsequent impacts on the magnitude of organic matter export into the mesopelagic. Bulk measures of bSi, POC and PON have been invaluable in providing insight into the net community response to Fe-limitation. However, recent studies using single diatom cell-based analyses have failed to find a relationship between Fe limitation and increased silica ballast [16-17] requiring a reassessment of the factors driving increases in Si:C and Si:N under Fe limitation. We previously described the molecular response of a diatom-dominated,

phytoplankton community to simulated upwelling and Fe availability in waters overlying a narrow region of the continental shelf of the CUZ [33, 34]. Here, we combine bulk and single-cell elemental measurements of Fe-limited diatoms to assess the contribution of silica production and cellular silica content to observed increases in Si:C and Si:N. Metatranscriptomic analysis of that same community further enabled interrogation of the underlying molecular drivers of the observed response. In addition to transcriptomic indicators of C and N metabolism, we explore the viability of two well-characterized, and highly conserved proteins silicon transporters (*SITs*) responsible for the uptake of dissolved Si, and silicanin-1 (*Sin1*), a diatom-specific protein [35] involved in silica biomineralization [36] – as molecular indicators of silicon metabolism in natural communities.

Results:

Initial water mass characteristics

To investigate the response of diatoms to upwelling, a trace-metal clean Teflon diaphragm pump and tubing was used to collect seawater from 96 m in the upwelling zone off coastal California, corresponding to the 10°C isotherm as presented by Lampe et al. [33]. Satellite-derived sea surface temperatures (SST) combined with shipboard measurements of SST, wind velocity, and low surface nitrate + nitrite concentration, here-after referred to as nitrate (NO_3^-) concentration, indicated that upwelling-favorable conditions were not present upon arrival at our study site or for the previous 13 days [33], setting the potential upper limit on the length of time phytoplankton cells had spent at depth. Initial (T0) phytoplankton abundance in the experimental water was low as indicated by chlorophyll *a* concentration (Chl *a;* >5 μm), 0.05 μg L^{-1}, bSi concentration, 0.19 μmol L^{-1}, and diatom cell abundance, 5.8 x 10^3 cells L^{-1} (Fig. 1A). The initial community also had low photosynthetic efficiency

(F_v/F_m = 0.25 ± 0.03) and a total particulate carbon (TPC) and nitrogen (TPN) ratio of 31.5 (>5 µm) , ~5-fold higher than the Redfield ratio of 6.6 (Fig. 1B-C, Table S4). High TPC:TPN is not atypical of deep or freshly upwelled waters in the CUZ and likely indicates prior N-limitation [37, 38] and/or a high C-rich detrital fraction.

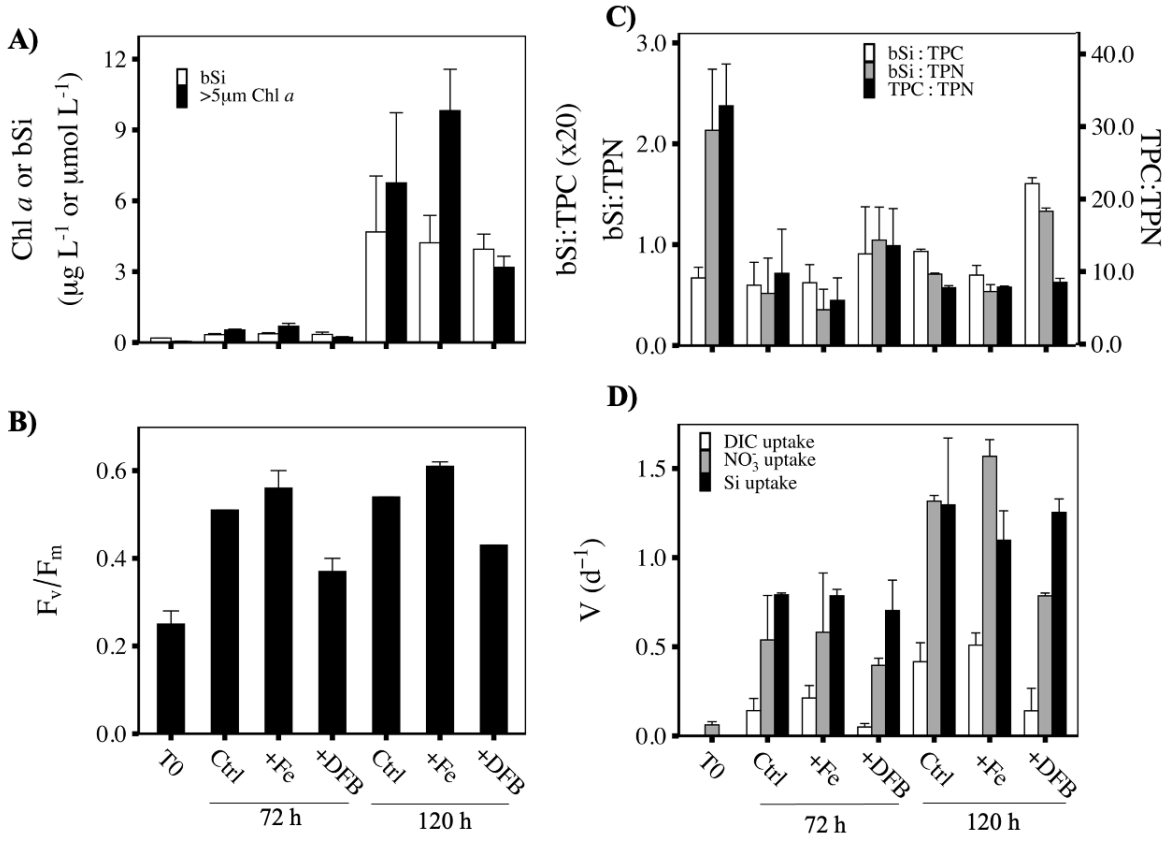

Figure 1-1: Physiological and biogeochemical characteristics of the initial upwelled water and incubations. Measurements of the initial water mass (T0) and control (Ctrl), iron (+Fe) and DFB (+DFB) additions at 72 and 120 h for (A) biogenic silica, bSi (µmol L^{-1}; white) and Chl a (µg L^{-1}; black) concentrations, (B) the maximum photochemical quantum efficiency of PSII (F_v/F_m), (C) molar ratio (µmol L^{-1}:µmol L^{-1}) of bSi to total particulate carbon (bSi:TPC; white) or nitrogen (bSi:TPN; grey), and TPC:TPN (black) and (D) dissolved inorganic carbon (DIC; d^{-1}; white),nitrate (NO_3^-) uptake rates (d^{-1}; grey), and Si uptake (d^{-1}; black). Chl a, TPC, and TPN data are for the >5 µm size fraction. Mean and standard deviation are shown (n = 3). One-way ANOVA and Tukey's HSD post hoc test results and significance are shown in Table S5.

The deep water was rich in NO_3^- and $Si(OH)_4$, with concentrations of both near 22 µmol L^{-1} (Fig. S1, Table S1). The initial dFe concentration, 0.82 nmol L^{-1}, was below the average of ~1 nmol L^{-1} typical of the CUZ [39], but was likely sufficient to support growth of the sparse initial phytoplankton community. However, the high NO_3^-:dFe ratio (26 µmol L^{-1}

NO_3^-: 1 nmol L^{-1} dFe) was more than double the threshold of 12 µmol L^{-1} NO_3^-:1 nmol L^{-1} dFe, indicating that nutrient utilization and biomass accumulation would lead to eventual Fe limitation [8].

Bloom progression under varied iron availability

Seawater was subsampled into incubation bottles and left unamended (Ctrl), augmented with either 5 nmol L^{-1} $FeCl_3$ (+Fe) to relieve potential Fe limitation, or 200 nmol L^{-1} of the siderophore desferroxamine-B (+DFB) to induce Fe limitation. Bottles were incubated in flow-through surface seawater cooled incubators (12-18°C) screened to 33% incident irradiance. After 72 h, the phytoplankton assemblage responded positively on a photosynthetic level to the simulated upwelling in all of the treatments, with F_v/F_m increasing markedly from 0.25 ± 0.03 at T0 to 0.51 ± 0.00, 0.56 ± 0.04, and 0.37 ± 0.03 in the Ctrl, +Fe, and +DFB treatments, respectively, indicating a recovery of photosynthetic efficiency. The addition of DFB limited the increase of F_v/F_m to ~70% of that measured in the Ctrl and +Fe treatments (Fig. 1B).

Biomass (Chl *a,* bSi, TPC, and TPN) started to increase by 72 h and became significantly higher by 120 h in all treatments compared to T0 (Fig. 1A, Table S2). By 120 h, Chl *a* concentration increased in the Ctrl and +Fe treatments to 6.76 ± 2.97 and 9.82 ± 1.75 µg L^{-1}, respectively, but was significantly lower (3.18 ± 0.47 µg L^{-1}) in the +DFB treatment compared to the +Fe treatment. There was a similar increase in bSi by 120 h to 3.95-4.68 µmol L^{-1}, but this did not differ significantly between treatments (ANOVA, $p = 0.85$; Fig. 1A). Finally, the concentrations of TPC (24.6 ± 3.81 µmol L^{-1}) and TPN (2.97 ± 0.51 µmol L^{-1}) within the +DFB treatment remained ~50% below the +Fe treatment at 120 h, but this

fell just below the threshold of statistical significance (Tukey's HSD; $p = 0.065$ and $p = 0.068$, respectively; Table S5).

The addition of Fe resulted in a significant increase in the biomass-specific NO_3^- uptake rate by 120 h, 1.57 ± 0.09 d^{-1}, which was 19% higher than the Ctrl, 1.32 ± 0.03 d^{-1} (Tukey's HSD; $p = 0.01$), and ~70% higher than the +DFB treatment, 0.79 ± 0.02 (Tukey's HSD; $p < 0.001$; Fig. 1D, Table S3, S5). The dissolved inorganic carbon (DIC) uptake also increased ~75% at both 72 h, 0.21 ± 0.07 d^{-1}, and 120 h, 0.51 ± 0.07 d^{-1}in the +Fe treatment compared to +DFB (0.05 ±0.02 d^{-1} and 0.14 ± 0.13 d^{-1} at 72 and 120 h, respectively; Fig. 1D, Table S3). In contrast, the Si uptake rates at 72 h, 0.76 ± 0.09 d^{-1}, and 120 h, 1.22 ± 0.23 d^{-1} did not differ significantly between Ctrl, +Fe, or +DFB treatments.

The increased concentrations of bSi, TPC, and TPN across various treatments resulted in significant differences in the cellular elemental stoichiometry. The initial TPC:TPN of ~30 decreased to Redfield proportions [40] in all treatments (Ctrl, 7.6 ± 0.3, +Fe, 7.7 ± 0.1, and +DFB, 8.3 ± 0.5) by 120 h (Fig. 1C). Both bSi:TPC and bSi:TPN increased in the +DFB treatment by 120 h (0.08 ± 0.003 and 1.33 ± 0.03, respectively) compared to the +Fe treatment (0.03 ± 0.004 and 0.54 ± 0.07, respectively; Fig. 1C, Table S4). Despite substantial biomass accumulation within the incubations, $Si(OH)_4$ and NO_3^- concentrations both remained >14 μmol L^{-1} (Fig. S1), which is not considered rate limiting in the CUZ [41].

To assess changes in phytoplankton community composition, we used metatranscriptome sequence data to quantify the relative proportion of taxonomically annotated mRNA reads. Previous comparisons to cell enumeration via microscopy established that mRNA reads are a reasonable proxy for the relative abundance of active

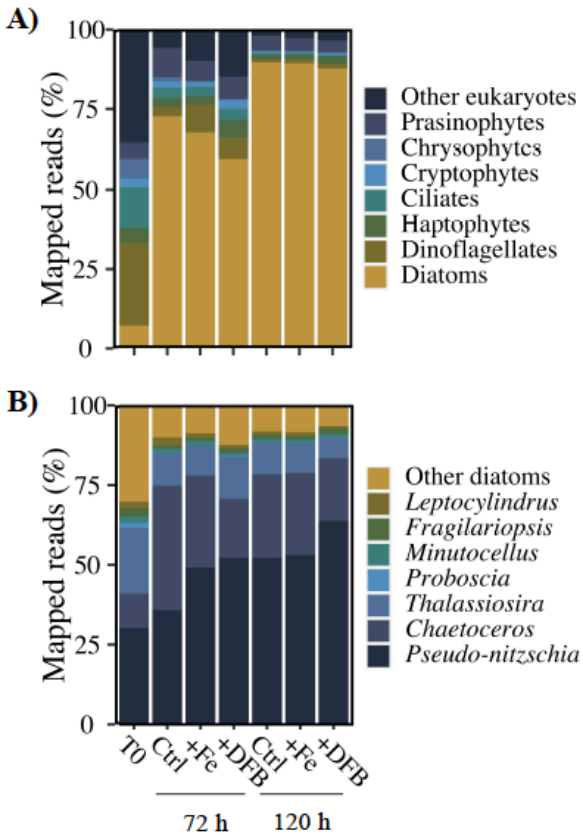

Figure 1-2: Community composition in initial water and throughout the incubation. Percentage of mapped transcriptomic reads belonging to each of the (A) major eukaryotic phytoplankton, and (B) diatom genera. Data shown from 120 h are the averages of replicates (n=3).

phytoplankton groups in this system [33]. A substantial fraction of the mRNA reads in the initial phytoplankton community were associated with dinoflagellate (26%) and diatom (7%) taxa, with the remaining 54% divided among 44 unique taxa (Fig. 2A and Table S6). Across all three treatments, there was a shift toward diatoms, which accounted for 60-73% of the sequence reads at 72 h and ~89% at 120 h (Fig. 2A). This is consistent with our previous report that diatom cell abundance in the Ctrl treatment increased from $5.8 \pm 2.5 \times 10^3$ cells L^{-1} to $\sim 2.5 \pm 0.2 \times 10^6$ cells L^{-1} [33]. *Thalassiosira* and the bloom-forming diatoms, *Chaetoceros* and *Pseudo-nitzschia*, were the dominant genera at both sampling timepoints, accounting for a combined 83-90% of total diatom reads across all treatments (Fig. 2B). Although qualitative differences in the relative abundance of *Pseudo-nitzschia* between treatments were present at 120 h, the mean contributions of *Pseudo-nitzschia* to total diatom reads in

Ctrl, 53 ± 17%, +Fe treatment, 52 ± 8%, and +DFB, 63 ± 5%, was not significantly different (ANOVA, p= 0.50; Fig. S2, Table S5). Furthermore, the genus level distribution of mRNA reads did not differ significantly in the overall community or the diatom community at 120 h (PERMANOVA; p = 0.40, p = 0.45, respectively). The large proportion of diatom reads, dominated by these three genera, provided an opportunity to interrogate genus-specific responses the increase in the bulk ratios of bSi to TPC and TPN at conditions of low dFe availability.

Molecular response to Fe-limitation

In addition to the aforementioned biogeochemical and physiological indicators of Fe-limitation within the +DFB treatment, all three dominant diatom genera mounted a molecular response to Fe-limitation. Relative to the +Fe treatment, transcripts of Iron Starvation Induced Protein 3 (ISIP3) were elevated in *Thalassiosira* and *Chaetoceros* in the +DFB treatment at both timepoints (Fig. S3A,B; [42]). Additionally, at 120 h *Thalassiosira* ISIP3 transcripts were significantly elevated in the Ctrl treatment compared to the +Fe treatment while *Chaetoceros* ISIP3 transcripts did not significantly differ between Ctrl and +Fe treatments (Fig. S3A,B, Table S5). For *Pseudo-nitzschia* the iron limitation index (*Ps-n* ILI) was >0.5 in the +DFB treatment at both 72 and 120 h, indicative of Fe limitation [43]. Negative *Ps-n* ILI values in Ctrl and +Fe treatments at both timepoints indicated a lack of Fe-limitation (Fig. S3C).

Carbon metabolism

Due to the high Fe requirement of the photosynthetic apparatus, Fe-limitation has a notable impact on C assimilation. When comparing the +DFB to the +Fe treatment we observed changes in the abundance of transcripts of genes involved in photosynthetic

electron transport consistent with a molecular response to Fe-limitation [23, 25, 44, 45]. Low RNA yield from samples collected at 72 h necessitated pooling of biological replicates prior to sequencing, limiting the ability to resolve statistically significant differences. However, these data revealed important trends that were recapitulated at 120 h.

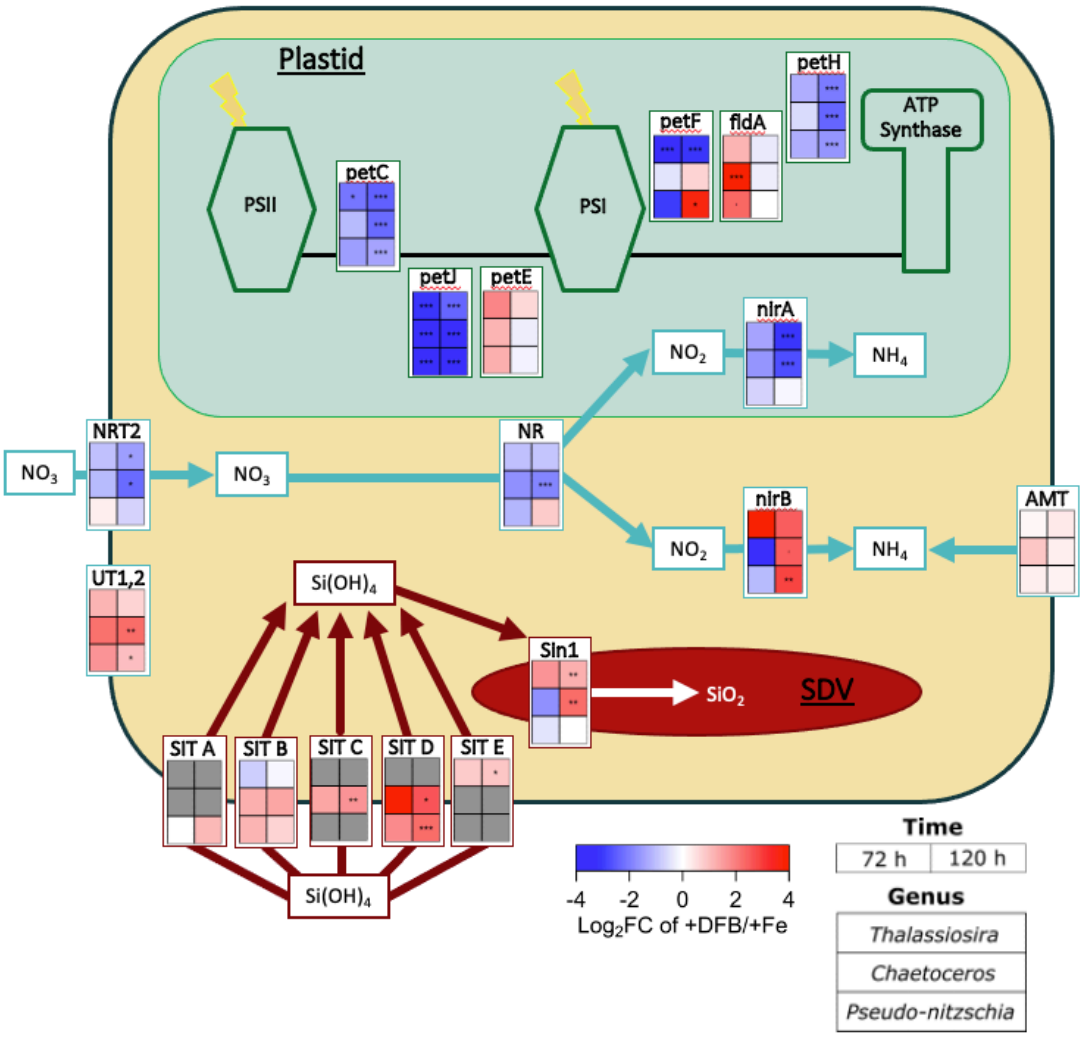

Figure 1-3: Differential transcript abundance of key cellular carbon, nitrogen, and silicon pathways under Fe limitation for the three dominant diatom genera, *Thalassiosira*, *Chaetoceros*, and *Pseudo-nitzschia*. Heatmap of changes transcript abundance (log_2 fold-change) in +DFB compared to +Fe treatment at 72 h (left column) and 120 h (right column) for *Thalassiosira* (top row), *Chaetoceros* (middle row), and *Pseudo-nitzschia* (bottom row). Grey boxes indicate genes that were not detected in either treatment. Asterisks denotes false discovery rate (FDR); · $p < 0.1$, * $p < 0.05$, ** $p < 0.01$, *** $p < 0.001$. Abbreviations are as follows: flavodoxin (*fldA*); plastocyanin (*petE*); ferredoxin (*petF*); cytochrome c6 (*petJ*); cytochrome b6/f complex (*petC*); ferredoxin-NADP+ reductase (petH); nitrate reductase (*NR*); nitrate transporter (*NRT2*); ferredoxin-nitrite reductase (*nirA*); NAD(P)H-nitrite reductase (nirB); ammonium transporter (AMT); urea transporters (*UT1,2*); Silicanin-1 (*Sin1*); *SIT* Clade A (*SIT* A); *SIT* Clade B (*SIT* B); *SIT* Clade C (*SIT* C); *SIT* Clade D (*SIT* D); *SIT* Clade E (*SIT* E).

At 72 h, *Thalassiosira, Chaetoceros,* and *Pseudo-nitzschia* in the +DFB treatment exhibited a >2-fold downward trend in the abundance of transcripts encoding the Fe-dependent electron transport proteins ferredoxin reductase (*petH*), cytochrome b_6f (*petC*), as well as the Fe-containing ferredoxin protein (*petF*), compared to the +Fe treatment (Fig. 3). At the same time, transcript coding for plastocyanin (*petE)* and flavodoxin (*fldA*), the Fe-independent analogs of *petJ* and *petF* [46, 47], respectively, were generally more abundant in the +DFB treatment (Fig. 3). Notably, transcripts coding for cytochrome c_6 (*petJ*), were significantly less abundant in all three diatom genera at both 72 h and 120 h. By 120 h, genus-specific patterns in *petF* expression emerged with transcripts encoding *petF* within *Thalassiosira* continuing to be significantly less abundant in the +DFB treatment, while *Pseudo-nitzschia petF* transcripts were significantly elevated relative to the +Fe treatment (Fig. 3). In addition, at 120 h all three genera no longer exhibited higher transcript abundance of *fldA* in +DFB compared to +Fe treatment, despite prior significant differential abundance of *fldA* in *Chaetoceros* at 72 h.

Nitrogen metabolism

The impact of Fe limitation on N assimilation may also drive increased bSi:TPN characteristic in low Fe regimes [11, 48]. Transcripts for genes encoding ferredoxin-dependent nitrate reductase (*NR*), nitrite reductase (*nirA*), and a nitrate transporter (*NRT2*) were generally less abundant in the +DFB treatment compared to the +Fe treatment for *Thalassiosira* and *Chaetoceros* throughout the incubation. At 120 h, transcripts for all three genes were significantly lower in *Chaetoceros*, while those for *nirA* and *NRT2* were significantly less abundant in *Thalassiosira* (Fig. 3). Transcripts encoding for ferredoxin independent NADH-nitrite reductase protein [49], *nirB,* were >2-fold more abundant in the

+DFB treatment relative to +Fe in *Thalassiosira* by 72 h, and in *Chaetoceros* and *Pseudo-nitzschia* by 120 h, though the increase was not significant in *Thalassiosira* at either timepoint (Fig. 3). While the abundance of ammonium transporters (*AMT*) transcripts was unaffected by Fe availability, transcripts encoding urea transporters (*UT*) were generally more abundant in the +DFB treatment in all three diatom genera at both 72 h and 120 h, and significantly more abundant in the +DFB treatment in *Chaetoceros* and *Pseudo-nitzschia* at 120 h. Elevated levels of UT transcripts may have helped diatoms exploit an alternative source of nitrogen that is more efficiently assimilated without the added Fe required for reducing nitrate and nitrite (Fig. 3; [50]).

Silicon metabolism

Unlike C and N metabolism, there are no established molecular markers for Si metabolism. The expression of specific clades of diatom *SITs* has been linked to silica production under Fe-limiting conditions [22]. For *Sin1,* expression may be associated with changes in biomineralization that impact the amount of Si deposited per unit area of cell wall [51], referred to here as the degree of silicification. Phylogenetic analysis of *SIT* sequences revealed the presence of genera-specific *SIT* clades (Table S7, [52]), with *Thalassiosira* expressing *SITs* from clades B and E, *Chaetoceros* expressing *SITs* from clades B, C, and D, and *Pseudo-nitzschia* expressing *SITs* from clades A, B, and D (Fig. 3, Fig. S4). In all three genera, respective *SIT* clades C, D, and E transcripts were generally more abundant in the +DFB treatment compared to +Fe at 72 h and and progressed to were significantly higher abundance at 120 h (Fig. 3). Similar qualitative increases at 72 h were observed for clade A and B *SIT* transcripts in *Pseudo-nitzschia*, and clade B transcripts in *Chaetoceros* (Fig. 3). For *Sin1*, transcripts from *Chaetoceros* and *Pseudo-nitzschia* qualitatively decreased at 72 h

but increased in *Thalassiosira* in the +DFB compared to +Fe treatment. By 120 h, *Thalassiosira* and *Chaetoceros* had significantly more (>2-fold) *Sin1* transcripts in the +DFB treatment relative to in the +Fe treatment.

Diatom cell morphology and Si content

The fluorescent dye PDMPO (2-(4-pyridyl)-5-((4-(2-dimethylaminoethylaminocarbamoyl) methoxy) phenyl) oxazole) was used in combination with confocal microscopy to measure single-cell rates of bSi production (Si $cell^{-1}$ d^{-1}) and production of new siliceous frustule surface area (SA; μm^2 $cell^{-1}$ d^{-1}) at 72 h when molecular and biogeochemical measures first indicated a differential response to Fe availability. Together, these metrics were used to calculate the degree of silicification (Si μm^{-2}) of the frustule (Supporting Information, Eq. 1; [53]). Single-cell bSi measurements were grouped into four taxonomic classes corresponding to *Chaetoceros*, *Thalassiosira* (consisting of remaining cells with centric morphology), and two morphologically distinct groups of *Pseudo-nitzschia* (45 and 90 µm in apical length). Although PDMPO data is not available from samples at 120 h, the 72 h PDMPO data should be representative of the latter time point, as Si uptake was comparable between treatments within each time point, macronutrient status remained replete throughout the incubation, and Fe availability was similar within +Fe and +DFB treatments at 72 h and 120 h.

Despite morphological and physiological differences between *Thalassiosira* (Fig. S5 A-C)*, Chaetoceros* (Fig. S5 D-F)*,* and *Pseudo-nitzschia* (Fig. S5 G-I), there was no difference in the amount of new frustule SA produced by *Chaetoceros* or *Pseudo-nitzschia* in any of the treatments. In *Thalassiosira,* the rate of new frustule SA produced in the +DFB treatment, 1.73 ± 1.03 μm^2 $cell^{-1}$ d^{-1}, was 41% lower (t-test; $p = 0.04$) compared to the +Fe treatment, 2.92 ± 1.16 μm^2 $cell^{-1}$ d^{-1} (Fig. 4A). The reduction of the rate of new SA produced

by *Thalassiosira* cells within the +DFB treatment compared to the +Fe treatment was accompanied by a significant increase (t-test; $p = 0.01$) in SA:V (Fig. S6B). These morphological changes are likely associated with an overall reduction in the size of *Thalassiosira* cells because when the proportions of a cell are reduced, V decreases at a faster rate than SA, resulting in an increase in SA:V.

Previously Fe-limitation has been associated with increases in bulk bSi concentration, but we did not observe an increase in cell-specific silica production rates or in the degree of silicification by Fe-limitation (Fig. 4B**,**C) for *Thalassiosira, Chaetoceros,* or *Pseudo-nitzschia* (Fig. 4B,C). In fact, the >90 µm *Pseudo-nitzschia* cells exhibited a 2-fold higher silica production rate (Tukey's HSD; $p<0.05$), 0.66 ± 0.4 pmol Si cell^{-1} d^{-1}, in the +Fe treatment compared to the Ctrl, 0.33 ± 0.10 pmol Si cell^{-1} d^{-1} or the +DFB treatment, 0.35 ± 0.18 pmol Si cell^{-1} d^{-1} (Fig. 4B). This was primarily driven by a 47% increase in the degree of silicification relative to the Ctrl (Tukey's HSD; $p = 0.03$) and +DFB (Tukey's HSD; $p = 0.04$) treatments (Fig. 4C). In addition to increasing the cell specific silica production rate and degree of silicification, Fe addition also increased the mean length-normalized-width (LNW) of the larger *Pseudo-nitzschia* cells by 22 % relative to +DFB (Tukey's HSD; $p = 0.001$; Fig. S6A). This modest increase in the LNW of >90 µm *Pseudo-nitzschia* cells did not, however, result in an increase in SA:V (Fig. S6B).

Figure 1-4: Silicon metabolism-related parameters for diatom taxa obtained using PDMPO. Box plots of (A) new frustule surface area (µm^2 cell^{-1} d^{-1}), (B) bSi production (pmol Si cell^{-1} d^{-1}), and (C) degree of silicification (fmol Si µm^{-2}) in control (Ctrl; dark grey), +Fe (light grey), and +DFB (white) treatments at 72 h for *Thalassiosira* (all centric diatoms not including *Chaetoceros*), *Chaetoceros*, and *Pseudo-nitzschia* (45 and 90 µm size groups). The center line represents the median and the boxes display the upper and lower quartiles with whiskers extending 1.5 times the interquartile range. Open diamonds show the arithmetic mean of a given sample. Black dots represent data from individual cells. Samples with <5 cells imaged were excluded and denoted nd. Significance was determined within each taxonomic group by Welch two-sample t-test when comparing between two treatments or one-way ANOVA and Tukey's HSD post hoc test when comparing among three treatments. Different lowercase letters delineate the statistically significant different groups within a taxa ($p < 0.05$). The vertical axes are plotted on a logarithmic ($\log_{10}$) scale. Statistical test results and significance are shown in Table S5.

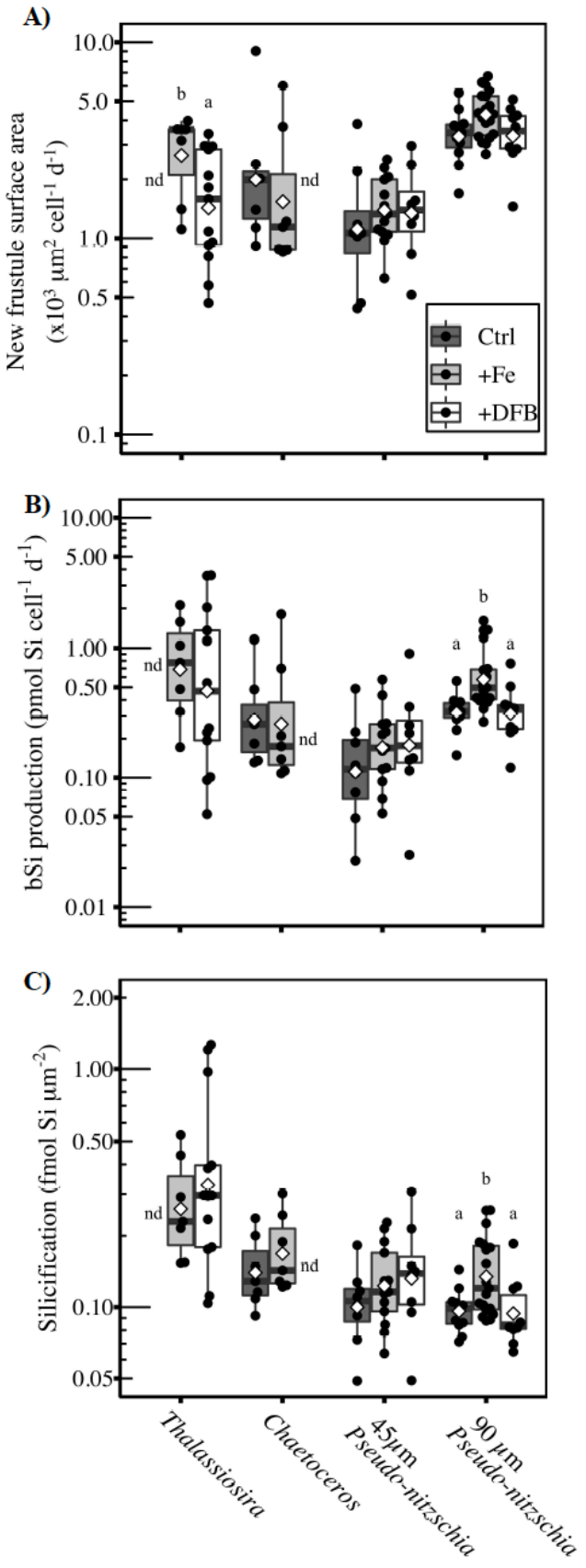
A)
New frustule surface area
(x10³ µm² cell⁻¹ d⁻¹)
10.0
5.0
1.0
0.5
0.1
b
a
nd
nd
Ctrl
+Fe
+DFB
B)
bSi production (pmol Si cell⁻¹ d⁻¹)
10.00
5.00
1.00
0.50
0.10
0.05
0.01
nd
nd
a
b
a
C)
Silicification (fmol Si µm⁻²)
2.00
1.00
0.50
0.10
0.05
nd
nd
a
b
a
Thalassiosira
Chaetoceros
45µm Pseudo-nitzschia
90 µm Pseudo-nitzschia

Discussion:

Fe limitation led to changes in cellular stoichiometric ratios

In the unamended Ctrl treatment, high initial NO_3^-:dFe (26 μmol L^{-1} NO_3^- :1 nmol L^{-1} dFe) indicated that nutrient consumption had the potential to drive the phytoplankton community into severe Fe-limitation [10, 54]. Yet, over the five-day incubation <30% of the initial nitrate was consumed and the unamended phytoplankton community only exhibited signs of mild Fe-limitation characterized by reduced photosynthetic efficiency and elevated molecular markers of Fe limitation compared to the +Fe treatment. The addition of DFB led to a distinct physiological and molecular response with photosynthetic efficiency, ISIP3 expression (for *Thalassiosira* and *Chaetoceros*) and *Pn*-ILI (for *Pseudo-nitzschia*) illustrative of Fe-limitation in this community.

Iron availability affected uptake rates and ultimately altered bulk elemental composition. Iron-limited communities were also characterized by diminished biomass-specific DIC and NO_3^- uptake rates. In contrast, biomass-specific $Si(OH)_4$ uptake rates and bSi concentrations remained similar between Fe treatments. Notably, Fe-limitation negatively impacted both C and N assimilation to a similar extent, such that the particulate C:N ratio was near Redfield proportions at the end (t= 120 h) of the incubation [40]. Collectively, these responses resulted in elevated ratios of Si:C and Si:N under Fe-limitation. Previous field campaigns in the CUZ have reported similar increases, as well as increased consumption of $Si(OH)_4$ relative to NO_3^- [7, 18, 55, 56], but the drivers of these shifting elemental ratios are often ambiguous. By combining measurements of bulk bSi with single cell silica production, single cell degree of silicification and metatranscriptomics, we were able to explore two possible over-arching drivers of this cellular elemental shift.

Increased SA:V as a driver of elevated Si:C and Si:N

Elevated cellular Si:C and Si:N can be driven by an increase in the total SA of silicified cells relative to the total V of cells in the phytoplankton community. One possible explanation for an increase in SA:V would be intraspecific reductions in diatom cell size [14, 57] or changes in cell shape such as LNW [15]. Given that the diatom cell is encased in a siliceous frustule and that biovolume is associated with C and N rich internal components, a shift toward species with a higher SA:V has the potential to increase Si:C and Si:N without necessarily increasing the degree of frustule silicification [58]. Our data demonstrate that Fe-limitation did not alter SA:V in the most abundant genera *Chaetoceros*, and *Pseudo-nitzschia* despite a reduction in LNW of the large size class of *Pseudo-nitzschia* in response to Fe-limitation. While cell SA:V increased within the *Thalassiosira* genera, the binning of all non-*Chaetoceros* centrics into this classification may have been a contributing factor.

Concomitant changes in total community SA:V and bulk ratios of Si:C and Si:N can also be related to changes in community composition, which has been observed in the chronically Fe-limited HNLC waters of the subtropical Pacific Ocean and Southern Ocean [59]. For example, Fe-limitation could induce a shift toward smaller diatom species with a higher SA:V and more efficient Fe uptake relative to other cellular requirements [60–62]. Alternatively, an increase in the proportion of diatoms within the phytoplankton community could increase the total siliceous-based SA relative to total phytoplankton-based V, causing a similar increase in Si:C and Si:N. Based on our metatranscriptome analyses, we did not observe a significant difference in community composition between Fe treatments in this study. This could be due to the ability of bloom-forming diatoms to outcompete other phytoplankton groups for nutrients during upwelling events [33], or an ability to assimilate

DFB-bound iron [63], albeit at far lower rates than unbound Fe. Irrespective of the mechanism, our observed increase in Si:C and Si:N in Fe-limited diatom communities seems unlikely to have been driven by modest changes in community composition as only *Thalassiosira* cells, which only contributed at most 13% of community composition at 72 h and 120 h respectively, differed significantly in cell-specific Si production or in the degree of silicification when comparing among taxa (Fig. S6C,D). As neither taxon-specific SA:V of the dominant diatom genera, nor community composition differed between Fe-replete and Fe-limited treatments, we posit that the observed increase in Si:C and Si:N in Fe-limited diatoms was driven by cellular shifts in Si, C, and/or N content.

Fe-limitation impacts on diatom Si, C and N content

Previous studies within the CUZ have reported increased Si:chlorophyll and Si:C and preferential utilization of $Si(OH)_4$ over NO_3^- under Fe-limiting conditions [7]. These changes have been largely attributed to increases in cellular bSi content based on laboratory culture experiments demonstrating an increase in silica per cell under Fe-limiting conditions in some, but not all diatom species [18, 19, 64]. The prevailing mechanistic explanation is that Fe-limitation prolongs cell-cycle progression and, given the close association between silica production and the cell-cycle [20], allows more time for silica to be incorporated into the frustule [65]. However, evidence from both culture [15, 24, 48, 55] and field based studies [11] suggest increased Si:C and Si:N in Fe-limited diatoms can also be due to reductions in cellular C and N content. The reliance of C and N assimilation on Fe-dependent proteins makes these processes particularly vulnerable to Fe-limitation. By decreasing the abundance of Fe-dependent proteins or substituting with an Fe-independent analog, cellular Fe quotas are reduced, but at the expense of C and N assimilation [28, 31, 66].

In our study, elevated Si:C and Si:N under Fe-limitation were driven primarily by decreases in cellular C and N without a concomitant increase in Si, proportionally similar to the plasticity exhibited by diatoms in previous findings [11, 17]. This is supported by decreases in both DIC and NO_3^- uptake as well as declines in Chl *a* concentration. A significant reduction of transcript abundance for genes encoding the high Fe-requiring photosynthetic electron transport proteins *petC*, *petH*, *petJ*, as well as those encoding Fe-dependent nitrate and nitrite reductase proteins was also observed under Fe-limitation. No concomitant increase in cell-specific silica production rates or in the degree of silicification under Fe-limitation was observed in the dominant diatom genera. In fact, the only significant change in silica production rate was a nearly 50% decrease by the large morphotype of *Pseudo-nitzschia* that was largely driven by a decrease in the degree of silicification. We did measure a reduction in the newly formed frustule surface area of Fe-limited *Thalassiosira*, a possible indicator of a slower growth rate, but no significant change in silica production or degree of silicification was detected. Despite the impaired molecular C- and N-assimilation pathways and reduced C and N quota, the consistent bulk and single-cell bSi measurements between Fe treatments suggest Fe-limited diatoms were still able to sustain cell division rates comparable to Fe-replete cells. Furthermore, we observed that Fe limitation did not increase Si content using synchrotron x-ray fluorescence (SXRF) analysis of cellular elemental composition in two similar incubations conducted on the same cruise but at different locations (38° 39.30 N, 123° 39.87 W and 42° 40.00 N, 125° 0.00 W, Twining, unpublished data). Previously, we demonstrated that SXRF- and PDMPO-based measurements of Si content provide comparable results [53]. At these two distinct sites, we found no difference

in Si cell^{-1} or biovolume-normalized Si content (Si L^{-1}) of *Chaetoceros* or *Pseudo-nitzschia* cells between Fe-replete and Fe-limited conditions (ibid).

Decoupled silicon metabolism transcript abundance and silicification

In contrast to C and N metabolism, our incomplete understanding of Si metabolism has thus far hindered the identification of viable molecular markers for silica production or Si limitation. We explored two of the more highly conserved and better characterized proteins – SITs and Sin1 [34, 37, 81] – as candidates for markers of silica production and degree of silicification, respectively. Although other diatom-specific proteins involved in silica biomineralization have been well-characterized [67, 68], poor sequence conservation across diverse diatom species precludes their use as molecular markers [35].

Expression of clades A and B *SITs* has been reported to specifically increase in response to Fe-limitation [22], but our data identified higher abundance of clades C, D, and E *SITs* under Fe-limitation. At the $Si(OH)_4$ concentrations typical of the CUZ (<30 µmol L^{-1} [69, 70]) active transport of Si should be facilitated by SITs [71] and closely linked to the rate of bSi production [72]. In our study, there was a general increase in *SIT* transcript abundance with Fe-limitation, but it was not consistent across *SIT* clades. For example, while clade C, D, and E *SIT* transcripts were significantly more abundant under Fe-limitation, those of clade A and clade B were not. Regardless, we did not observe a correlation between the changes in *Pseudo-nitzschia* cell-specific Si production and *SIT* transcript abundance at 72 h or between bulk Si uptake and *SIT* transcript abundance in *Thalassiosira, Chaetoceros,* and *Pseudo-nitzschia* at 120 h. This is not completely unexpected given findings of post-transcriptional and post-translational regulation of SITs [73, 74]. However, strong correlation between *SIT* protein abundance has been reported after prolonged (24 h) in Si-free media

[70], thus it could be useful to explore, in targeted studies, whether *SIT* transcript abundance is diagnostic of severe Si-limitation in field samples.

The biomineralization of silica is aided by *Sin1*, a highly conserved diatom-specific protein localized to the silica deposition vesicle and crucial for proper valve formation [35, 36]. We hypothesized that alterations in valve formation or Si content by Fe-limitation could be driven by changes in expression of *Sin1.* However, we observed strikingly different expression patterns of *Sin1* among the diatoms investigated in this study. Despite a lack of increase in the degree of silicification, both *Thalassiosira* and *Chaetoceros* cells exhibited increases in *Sin1* transcript abundance at the later timepoint. In contrast, *Pseudo-nitzschia* exhibited no difference in *Sin1* abundance between Fe-replete and Fe-limited treatments even through there was a lower degree of silicification in the larger size class of Fe-limited *Pseudo-nitzschia*. The lack of changes in cell silica content in response to Fe limitation has been observed in previous studies and calls into question the physiological drivers of *SIT* and *Sin1* transcript abundance in Fe-limited *Thalassiosira, Chaetoceros,* and *Pseudo-nitzschia* [22, 23].

One possible explanation for Fe-limitation driven changes in *SIT* and *Sin1* expression without concomitant increases in bSi production or degree of silicification may stem from the close connection between $Si(OH)_4$ uptake, silica production and the cell cycle. Studies in *T. pseudonana* have shown that *SITs* exhibit a diurnal pattern of expression [75, 76], and are expressed maximally during cell cycle stages associated with peak silica production [73]. In addition, transcriptomic-based studies on *T. pseudonana* and *Phaeodactylum tricornutum* report *Sin1* expression is most highly correlated with other genes involved in cell division [75, 76]. In assemblages with low species diversity, such as in this study, intra-specific cell

division can become partially entrained in the light:dark cycle [77]. Analyzing cell-cycle related transcripts within a single diatom species relies on the timing of cell-cycle progression being closely aligned (in phase) among the vast majority of cells present. While artificial upwelling and low species diversity may have initially entrained diatom cell cycles to the photocycle, the transcription of cell cycle related genes and timing of cell cycle progression [78] can be altered by limitation of nutrients such as Si, N, or Fe [20, 79, 80]. This may confound the interpretation of genus-specific transcription patterns of *SITs* and *Sin1* between Fe treatments if the cell cycles of each taxon were unsynchronized. While the C and N assimilation genes discussed here have only been reported to respond to diel cycles [81], any potential cell-cycle control of C- and N- assimilation genes would similarly complicate interpretation. Further work disentangling the role of individual members of the SIT family as well as individual SIT clades may provide a better picture of the cellular and biogeochemical significance of SITs.

Conclusions:

In this study a diatom-dominated phytoplankton community presented characteristic signs of Fe-limitation including elevated cellular Si:C and Si:N ratios. Other studies reporting similar findings often invoke higher Si content as a mechanistic explanation, with implications for subsequent sinking and export given the ballasted nature of the silica-based cell wall. However, using single-cell, taxon-resolved measurements of the degree of diatom cell silicification, we found no difference in Si content between Fe-replete and Fe-limited cells, and instead found significant reductions in both C and N assimilation. Increased transcript abundance of the highly conserved *SIT* and *Sin1* genes did not correlate with rates of silicon uptake, cell-specific silica production, or with the degree of silicification,

demonstrating that neither gene appear to be viable molecular markers for those respective processes within Fe-limited regimes. Our finding that none of the dominant diatom genera responded to Fe-limitation by thickening frustules complements previous field studies in both the Equatorial Pacific [11] and CUZ [53], lying in stark contrast to studies that suggest diatom frustule thickening is a common response to Fe-limitation. [7]. Thus, evaluation of drivers of carbon export and opal burial in Fe-limited regimes must also consider mechanisms that do not depend on increased silica ballasting, such as increased aggregation [82], reduced grazing and associated respiratory losses [10], and viral infection [83].

Methods:

Incubation setup

We conducted a deckboard multi-day incubation experiment at 35° 56.0710'N, 121° 44.0220'W within the California Upwelling Zone (CUZ) on board the *R/V* Melville (MV1405, Chief Scientist: Kenneth Bruland) from July 17-22, 2014. Details on incubation setup and downstream analysis are reported elsewhere [33, 34, 43]. Briefly, 200L of water was collected from 96 m into acid-cleaned HDPE drums using an air-driven PTFE deck pump fitted with PTFE tubing. Water was distributed into eighteen 10 L acid-cleaned cubitainers using trace-metal clean techniques. Each cubitainer was amended with either 5 nmol L^{-1} $FeCl_3$ (+Fe) or 200 nmol L^{-1} of the siderophore desferroxamine-B (+DFB), the latter to induce Fe limitation [84]. Unamended cubitainers served as controls (Ctrl). Cubitainers were incubated in plexiglass incubators shaded to ~33% incident irradiance and cooled with the flow-through seawater. At each timepoint, triplicate cubitainers were sacrificed at dawn for enumeration, dissolved and particulate analyses, cell-specific silica measurements, DIC and NO_3^- uptake rate measurements, F_v/F_m, and RNA.

Dissolved and particulate analyses

Samples for dissolved nutrient analysis (NO_3^- + NO_2^-, PO_4, $Si(OH)_4$) were filtered through a GF/F filter and stored at 4°C until analysis on the ship using a Lachat 8000 Quick Chem Flow Injection Analysis system [85]. Concentrations of NO_3^- + NO_2^- are referred to simply as NO_3^- as concentrations of NO_2^- were negligible. Reference materials for nutrients in seawater (Lots BY and CA, KANSO Technos, Osaka, Japan) were used for quality control. Samples for biogenic Si were filtered onto 0.6 μm pore-size polycarbonate filters and stored at -20°C. Samples were digested shipboard with 0.2 N NaOH in Teflon tubes, and measured using the ammonium molybdate colorimetric assay [86]. For the initial (T0) dissolved Fe measurements the seawater samples were shipboard filtered and analyzed spectrophotometrically with ultraclean methods after [87]. All other dissolved Fe concentration samples were acidified and stored in acid-cleaned LDPE bottles for at least two months before preconcentration and analysis with a Thermo Fisher Element XR inductively coupled plasma mass spectrometer [88, 89].

To assess total particulate carbon (TPC), total particulate nitrogen (TPN), and nitrate (NO_3^-) uptake rates, 618 ml sub-samples of seawater from each cubitainer were each spiked with $Na_{15}NO_3$ at no more than 10 % of the ambient NO_3^-concentration and incubated deckboard for 8 h in a flow-through plexiglass incubator shaded to 33% incident irradiance. Following incubation, samples were gravity filtered through a 5 μm polycarbonate filter (47 mm) then rinsed with an artificial saline solution onto a precombusted 25 mm GF/F filter. Filters were stored at -20°C until analysis. Prior to analysis, filters were dried at 50°C for 24 h, then run on an elemental analyzer paired with an isotope ratio mass spectrometer (EA-IRMS). Uptake rates (ρ, NO_3^- per unit time) were calculated using a constant transport model

(Eq. 3 from [90]). Biomass-specific NO_3^- uptake rates (V, NO_3^- per unit TPN per unit time) were also calculated according to the constant specific uptake model (Eq. 6; [90]). The reported values are considered conservative estimates or net uptake because ^{15}NO3 uptake rates were not corrected for possible losses of ^{15}N in the form of dissolved organic nitrogen [91].

To assess dissolved inorganic carbon (DIC) uptake 60 ml sub-samples from each cubitainer were distributed into acid-cleaned light and dark bottles. Each bottle was spiked with 1.2 μCi of $NaH^{14}CO_3$. A 1 ml subsample was taken from each bottle and added to vials containing 6 mol L^{-1} NaOH to trap and validate the initial inorganic $H^{14}CO3$ quantities. The light and dark bottles were incubated for 6.5–8 h in a deckboard flow-through plexiglass incubator 33% incident irradiance. Each 60 mL sub-sample was filtered onto 5 μm polycarbonate filters. Blank control bottles containing 1.2 μCi of $NaH^{14}CO_3$ were filtered onto a GF/F filter and had counts similar to dark bottles. Filters were vacuumed dried, placed in scintillation vials with 0.5 ml of 6 mol L^{-1} HCl, degassed for 24 h and counted using a Beckman Coulter LS 6500 scintillation counter. Reported values are light bottles minus dark bottles. Biomass-specific DIC uptake rates (V_{DIC}) were calculated by normalizing DIC uptake to TPC.

Biomass-specific Si uptake measurements were calculated for samples at 72 h and 120 h by taking the natural log of the change in $Si(OH)_4$ concentration of a sample at a given time point (n) relative to the mean value of within the corresponding treatment at the previous time point (n-1) normalized to the mean bSi concentration of the corresponding treatment at the previous time point.

$$V_b = ln\left(\left([\mathrm{Si(OH)_4}]_n - \left[\overline{\mathrm{Si(OH)_4}}\right]_{n-1}\right) \times \left(\left[\overline{\mathrm{bSi}}\right]_{n-1}\right)^{-1}\right) \text{(Eq. 1)}$$

Cell specific silica measurements

Cell-specific and community bSi production rates were measured at 72 h using 244 nmol L^{-1} of using 2-(4-pyridyl)-5-((4-(2-dimethylaminoethylaminocarbamoyl)methoxy)phenyl)oxazole (PDMPO; LysoSensor Yellow/Blue DND-160, Molecular Probes) and incubated deckboard for 6 h prior to sampling.

From each PDMPO incubation, 50 mls was removed and centrifuged at 1,230 RCF for 10 min. Pellets were resuspended in 10 mL of methanol and stored for >24 h at 4ºC to remove unbound PDMPO and photopigments. An aliquot (targeting 2-4 x 10^4 cells) was removed and 10 ml of MilliQ water was added to the remaining sample to remove precipitated salts and centrifuged (1,230 RCF, 10 min). All but 200 µL of supernatant was removed. Cells were then pipetted onto a polylysine-coated glass slide and left to dry. A #1.5 cover slip was adhered with ProLong Gold Antifade (Life Technologies), sealed with nail polish, and stored in the dark at 4°C [16, 53, 92].

PDMPO-labeled cells were imaged using an Olympus Fluoview 1000 Spectral Confocal microscope and analyzed as described [16, 53, 92]. In brief, cells were serially imaged in discrete 420 nm depths in short (PDMPO, ex 405/em 450-550 nm) and long (autofluorescence from photopigments, ex 559/em 617-718 nm) wavelengths to allow quantification of both the volume and surface area of newly produced silica, as well as total fluorescence. Images were assembled into 3D renderings (voxels) by digitally extrapolating between depths and removing photopigment fluorescence, ensuring only the PDMPO fluorescence was used in silica quantification. PDMPO fluorescence was converted into a

mass of bSi using a standard curve generated from laboratory-grown fully labelled diatom cells of known silica content [92]. The degree of cellular silicification (fmol Si μm^{-2}), or frustule thickness, was calculated by dividing the rate of silica production (pmol Si $cell^{-1}$ d^{-1}) by the rate of new surface area produced (µm^2 $cell^{-1}$ d^{-1}) :

$$Degree\ of\ silicification = \frac{Si\ production}{new\ frustule\ SA}$$

(Eq. 2)

The valve apical length and pervalvar width were used to calculate the total volume and surface area using formulae for a cylinder for *Thalassiosira and Chaetoceros.* Valve apical length and transapical width were used to calculate total volume and surface area using formulae for a prolate spheroid for *Pseudo-nitzschia*.

RNA extraction and metatranscriptome analysis

Samples for metatranscriptomic analysis were filtered onto 142 mm, 0.8 µm pore-size Pall Supor filters, flash frozen, and stored at -80º C. RNA was extracted using an Ambion ToTALLY RNA Kit with a glass bead beating step, and one round of DNase 1 (Ambion) treatment [33, 45]. Samples at 120 h were sequenced in biological triplicate, but T0 and 72 h samples yielded low quantities of RNA necessitating the pooling of biological triplicates prior to library prep [33] using an Illumina TruSeq Stranded mRNA Library Prep and running on an Illumina HiSeq 2000. Trimmed reads were *de novo* assembled into contiguous sequences (contigs) with ABySS v.1.5.2 [93] and annotated using BLASTX+ v.2.2.21. Taxonomic annotation was assigned with MarineRefII database and functional annotation was assigned using Kyoto Encyclopedia of Genes and Genomes (KEGG) [94]. KEGG Ortholog (KO) classifications of diatom urea transporters, nitrite reductase, ammonium

transporters were manually verified against known gene phylogenies and edited accordingly [95].

Iron Starvation Induced Proteins (ISIPs), silicon transporters (*SITs*), and silicanin-1 (*Sin1*) lack KO identifiers and were thus manually annotated using BLASTX+ v.2.5.0 [36, 52, 96]. To further classify *SIT* contigs into clades, using pplacer version 1.1.alpha19 with posterior probability calculated [97].

Reads from each site were trimmed for quality and removal of adapters using Trimmomatic v0.32 (paired-end mode, adaptive quality trim with 40 bp target length and strictness of 0.6, minimum length of 36 bp) [98]. Overlapping trimmed paired reads were interleaved into single reads with BBMerge v8.0. Merged pairs and non-overlapping paired-end reads were assembled into contigs using ABySS v1.5.2 with varied k-mer sizes [99]. The different k-mer size assemblies were merged using Trans-ABySS v1.5.3 to remove redundant contigs and contigs <120 bp [93]. Assemblies from all sites were merged with Trans-ABySS and duplicates further removed with GenomeTools v1.5.1 [100]. Read counts were estimated using the quasi-mapping method implemented in Salmon v0.73-beta with the seqBias option [101].

NCBI taxonomic IDs were assigned to contigs by best homology using BLASTX v2.2.31 (E-value $\leq 10^{-3}$) with MarineRefII database. Taxonomic information was mapped to the NCBI taxonomic IDs of each contig using the National Center for Biotechnology Information's (NCBI) Taxonomy Database [102], and manually curated) to ensure proper assignment and use of common phytoplankton taxonomic ranks (https://github.com/marchettilab/metatranscriptomicsPipeline. Gene function was assigned

using BLASTX (E-value ≤ 10^{-3}) with the Kyoto Encyclopedia of Genes and Genomes (KEGG; Release 75) [94]. For analysis of KEGG Orthologs (KO), the top hit with a KO number from the top 10 hits was chosen [34, 45]. KO classifications of diatom urea transporters, nitrite reductase, ammonium transporters were manually verified against known gene phylogenies and edited accordingly [95].

Iron Starvation Induced Proteins (ISIPs), silicon transporters (*SITs*), and silicanin-1 (*Sin1*) lack KO identifiers and were thus manually annotated using BLAST [36, 52, 96]. To further classify *SIT* sequences by clade, a maximum-likelihood tree was constructed from a reference alignment [52] using RAxML version 8.2.12 with the PROTGAMMAWAGF substitution model and 100 bootstraps [103]. Amino acid sequences corresponding to *SIT* contigs were aligned to the reference alignment using hmmalign and the HMM profile created from the reference alignment (built using hmmbuild 3.2.1). Associated alignment and tree files were packaged using taxtastic version 0.8.3. *SIT* contigs were placed on the reference tree using pplacer version 1.1.alpha19 with posterior probability calculated [97]. The most closely related reference sequence was assigned to each *SIT* contig using guppy version 1.1.alpha19. *SIT* clade assignments were included as KO identifiers for downstream analysis.

Prior to differential expression analysis, raw counts were aggregated within diatom genera by KO number. For genes lacking a KO number, e.g. SITs, ISIPs, Sin-1, etc., aggregation was done based on gene assignment through KEGG annotation or BLASTX query of supplemental databases. Genus-specific aggregation of functionally annotated reads reduces redundancy and allows the use of tools originally designed for single organism RNAseq analysis (e.g. DESeq2, edgeR). This is necessary for microbial community

transcriptomic analysis due to methodological and computational difficulties in resolving species-level, differential transcript expression [34, 45, 104–108]. However, this approach does not resolve species-level contig expression, nor does it *a priori* resolve clade-specific expression patterns for genes that belong to multigene families. In the case of SITs, individual clades were identified through phylogenetic analysis as previously done (Durkin et al. 2012, 2016), and manually annotated to allow interrogation of SIT transcripts at the clade level. Additionally, annotations for urea transporters 1 and 2 were grouped together because of there close phylogenic relationship and shared expression pattern in response to nitrogen supply [95]. A similar approach for other multigene families, such as the ammonium transporters (AMTs) and nitrate transporters (NRT2s) was not used because 1) there are no studies reporting a clade-specific response to Fe limitation and 2) expression of these genes in response to nitrogen supply does not appear to be clade-specific (Smith et al. 2019), thus interrogating clade-level expression patterns of these genes in our metatranscriptomes would be unlikely to yield interpretable results.

Phytoplankton analysis

Cell abundance and community composition were determined using microscopy [109]. Whole seawater was preserved in 2% Lugols and settled for > 24 h in an Utermöhl chamber. At least 400 cells were counted in at least five fields of view at 100×, 200×, and 400× magnification using a Leica DMIL inverted microscope.

The maximum photochemical quantum efficiency of PSII (F_v/F_m) of dark adapted cells was calculated from fluorescence induction measurements using a Satlantic FIRe as described [110–112] and blank corrected with 0.2 μm filtered seawater.

Statistical analysis

Significance between treatments within a given timepoint was determined via one-way ANOVA using the R package *stats* v.3.6.2 followed by Tukey's HSD multiple comparison test from *multcomp* v.1.4.13. When only two Fe-treatments were available for comparison a Welch two-sample t-test was used to calculate the level of significance. Community level differences in taxonomic contribution to mRNA reads were determined via PERMANOVA using the *adonis* function in the R package *vegan* v2.7. For transcript relative abundance data, normalization, differential abundance, and significance were analyzed within each taxonomic group using edgeR v.3.28.1 [113]. Significance between treatments at a given timepoint was determined using exactTest with tagwise dispersion and corrected for multiple testing using the Benjamini & Hochberg method, with a significance threshold of FDR <0.05 [114].

Data availability

All raw sequence data have been deposited in the NCBI sequence read archive under the accession no. SRP074302 (BioProject accession no. PRJNA320398) and SRP108216 (BioProject no. PRJNA388329). All data can be access through the Biological and Chemical Oceanography Data Management Office (Project number 559966, https://www.bco-dmo.org/deployment/559966).

Supplemental Information

Supplemental tables

Table S1: Dissolved macronutrient concentrations of initial upwelled water and control (Ctrl), Fe addition (+Fe), and DFB addition (+DFB) treatments at 72 and 120 h (n = 3, except for dFe concentration within the T0 saple where n = 1 and the Ctrl and +DFB treatments at 120h where n = 2).

	Silicic acid (µmol L^{-1})		Nitrate (µmol L^{-1})		Ortho-phosphate (µmol L^{-1})		Dissolved iron (nmol L^{-1})	
	Mean	St. dev	Mean	St. dev	Mean	St. dev	Mean	St. dev
T0	21.69	0.12	21.86	0.22	1.76	0.04	0.82	NA
Ctrl 72h	19.81	0.07	20.34	0.10	1.67	0.02	0.57	0.20
+Fe 72h	19.83	0.21	20.45	0.12	1.68	0.01	1.82	0.71
+DFB 72h	20.16	0.72	21.03	0.64	1.73	0.08	1.33	0.18
Ctrl 120h	14.70	2.87	15.07	2.75	1.37	0.27	0.40	0.10
+Fe 120h	16.37	1.16	15.30	1.41	1.35	0.10	1.09	0.47
+DFB 120h	15.91	0.66	17.53	0.86	1.54	0.12	1.43	0.59

Table S2: Particulate biomass concentrations of initial upwelled water and control (Ctrl), Fe addition (+Fe), and DFB addition (+DFB) treatments at 72 and 120 h (n = 3).

	TPC > 5 µm (µmol L^{-1})		TPN > 5 µm (µmol L^{-1})		bSi > 1.2 µm (µmol L^{-1})		Chl a > 5 µm (µg L^{-1})	
	Mean	St. dev	Mean	St. dev	Mean	St. dev	Mean	St. dev
T0	2.90	0.46	0.10	0.03	0.19	0.00	0.05	0.01
Ctrl 72h	6.04	2.32	0.96	0.82	0.33	0.05	0.53	0.04
+Fe 72h	6.22	1.31	1.27	0.65	0.37	0.04	0.69	0.12
+DFB 72h	4.30	1.63	0.34	0.10	0.34	0.10	0.22	0.03
Ctrl 120h	49.86	24.50	6.64	3.41	4.68	2.37	6.76	2.97
+Fe 120h	59.73	8.02	7.79	1.15	4.22	1.16	9.82	1.75
+DFB 120h	24.60	3.81	2.97	0.51	3.95	0.64	3.18	0.47

Table S3: The values of dissolved inorganic carbon, nitrate, and dissolved silicon uptake rates of initial upwelled water and control (Ctrl), Fe addition (+Fe), and DFB addition (+DFB) treatments at 72 and 120 h (n = 3). These data are presented in Fig. 1D.

	V_{DIC} (d^{-1})		V_N (d^{-1})		V_{Si} (d^{-1})	
	Mean	St. dev	Mean	St. dev	Mean	St. dev
T0	0.003	0.0006	0.06	0.02	NA	NA
Ctrl 72h	0.140	0.0700	0.54	0.25	0.79	0.01
+Fe 72h	0.210	0.0700	0.58	0.33	0.79	0.04
+DFB 72h	0.050	0.0200	0.40	0.04	0.70	0.17
Ctrl 120h	0.420	0.1100	1.32	0.03	1.30	0.37
+Fe 120h	0.510	0.0700	1.57	0.09	1.10	0.16
+DFB 120h	0.140	0.1300	0.79	0.02	1.25	0.08

Table S4: The values of the ratios of particulate biomass concentrations of initial upwelled water and control (Ctrl), Fe addition (+Fe), and DFB addition (+DFB) treatments at 72 and 120 h (n = 3). These data are presented in Fig. 1C. The mean Redfield (1963) proportions are provided in the bottom row as a reference point.

	TPC:TPN		bSi:TPC		bSi:TPN	
	Mean	St. dev	Mean	St. dev	Mean	St. dev
T0	31.48	5.49	3.35e-02	5.31e-03	2.13	0.61
Ctrl 72h	9.48	5.81	2.99e-02	1.13e-02	0.52	0.35
+Fe 72h	5.92	2.96	3.11e-02	9.01e-03	0.36	0.20
+DFB 72h	13.11	4.88	4.54e-02	2.34e-02	1.05	0.33
Ctrl 120h	7.59	0.27	4.67e-02	1.07e-03	0.71	0.01
+Fe 120h	7.68	0.12	3.49e-02	4.79e-03	0.54	0.07
+DFB 120h	8.31	0.51	8.02e-02	2.97e-03	1.33	0.03
Redfield	6.63	NA	1.51e-01	NA	1.10	NA

Supplemental figures

Figure S1: Macronutrients concentrations. Concentrations of nitrate (NO_3, black), phosphate (PO_4, blue), and silicic acid ($Si(OH)_4$, red) of the initial water mass (T0) and control (Ctrl), iron (+Fe) and DFB addition (+DFB) treatments at 72 and 120 h.

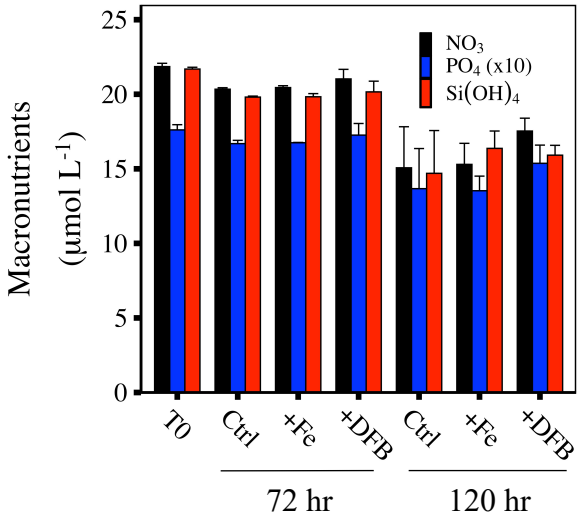

Figure S2: Percent relative abundance of diatom genera. *Chaetoceros* (black), *Pseudo-nitzschia* (gray), and *Thalassiosira* (black) percent relative abundance within diatom community in the initial water mass (T0) and control (Ctrl), iron (+Fe) and DFB addition (+DFB) treatments at 72 and 120 h based on taxonomically annotated mRNA reads.

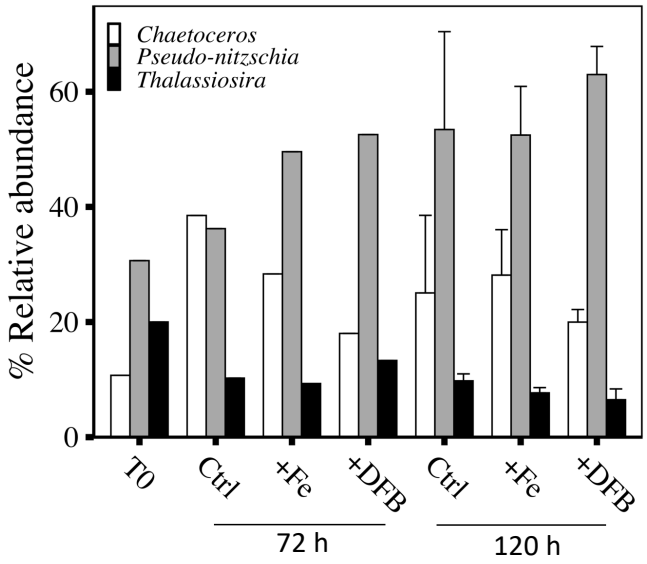

Figure S3: Molecular indicators of Fe limitation in the dominant diatom genera. Transcript abundance for iron starvation induced Protein 3 (ISIP3) in (A) *Thalassiosira* and (B) *Chaetoceros*. (C) For *Pseudo-nitzschia*, the iron limitation index (*Pseudo-nitzschia* ILI) was calculated (see Methods) with positive values >0.5 indicative of iron stress and negative values <-0.5 indicative of Fe replete growth (both thresholds indicated by the dashed lines). Statistical test results and significance are shown in Table S2.

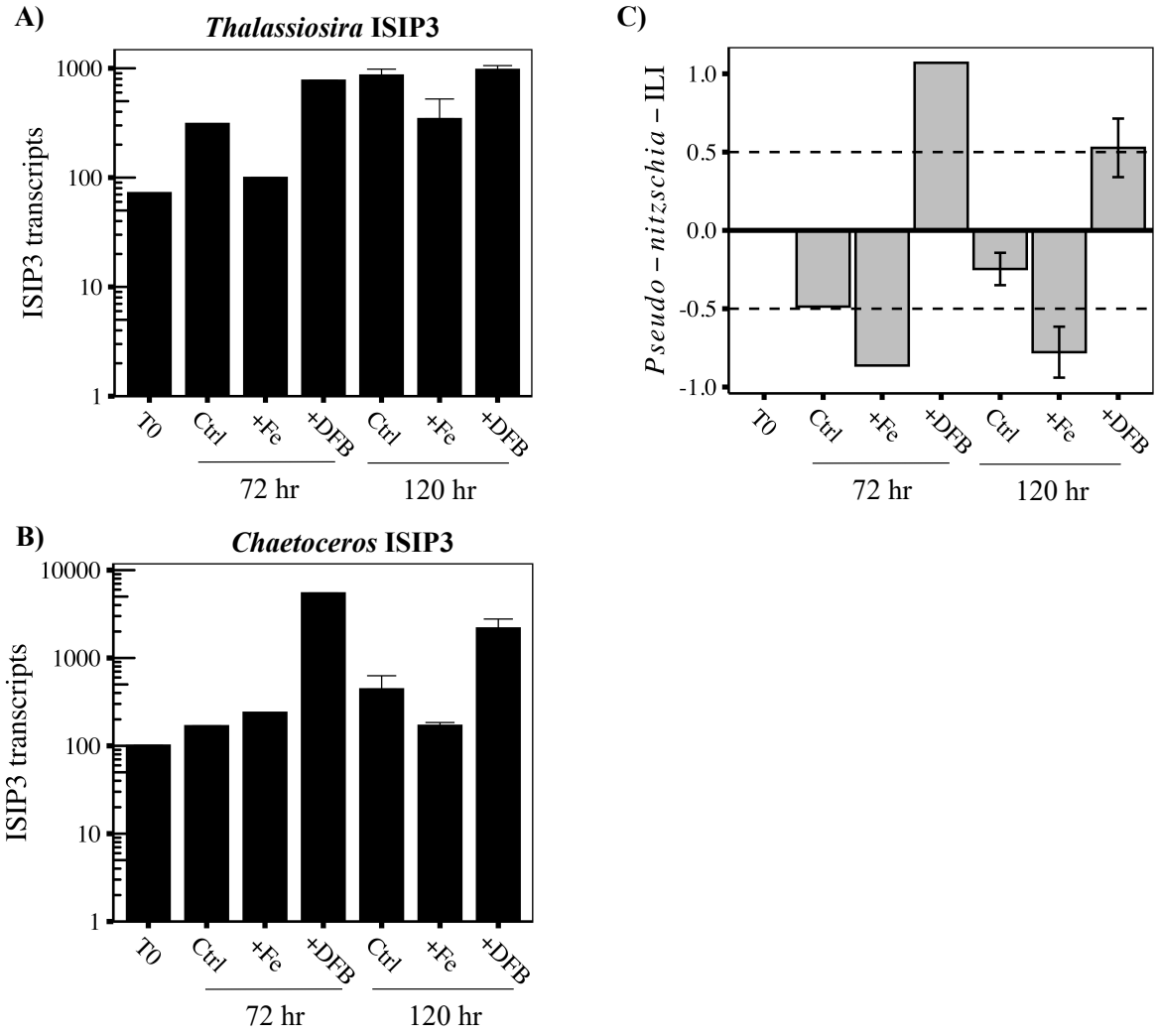

Figure S4: Silicon transporter phylogenetic tree. Phylogenetic reference tree containing 451 SIT amino acid sequences based on the reference alignment provided by Durkin et al. [52] and calculated using RAxML. Triangular nodes collapse closely related sequences together with the magnitude of the triangle proportional to the number of sequences present in the node. The tree is rooted with a clade containing SIT sequences encoded only by non-diatom organisms and labeled as "outgroup". Bootstrap values >50 are shown (100 replicates).

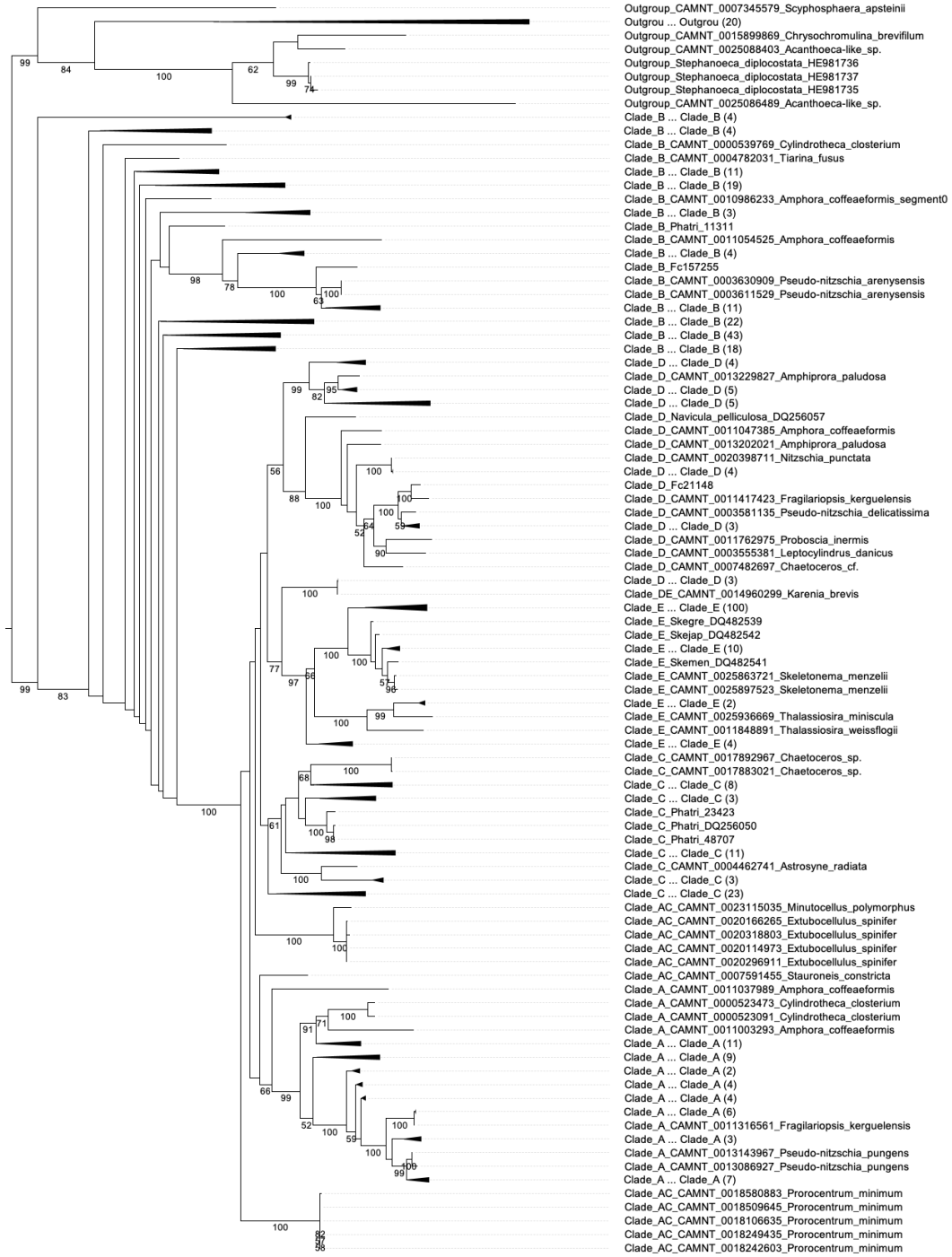

Figure S5: Confocal and 3D reconstruction images of diatom cells stained with PDMPO. PDMPO (ex 405/em 450-550 nm) is displayed in blue (panels A, D, and G), chlorophyll autofluorescence (ex 559 nm/ em 617-718 nm) is displayed in red/orange (panels B, E, and H), and a 3D reconstruction. The three diatom genera imaged are (A, B, C) a centric *Coscinodiscus*-like cell, (D, E, F), a short chain of *Chaetoceros* cells, and (G, H, I) a short chain of the ~90 µm *Pseudo-nitzschia* cells.

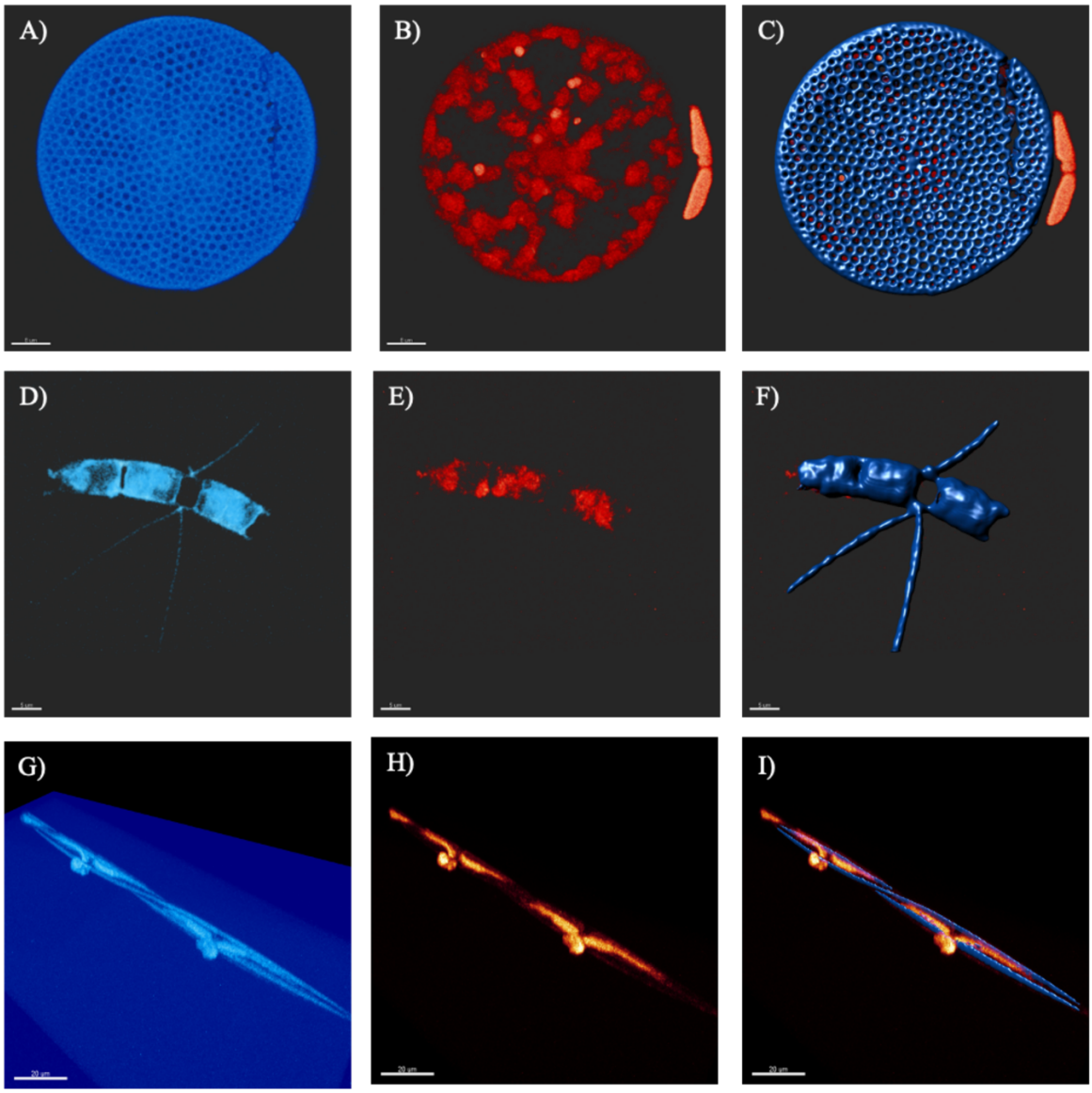

Figure S6: Morphological characteristics of diatom cells from incubations. Box and whiskerplots of (A) length normalized width measurements in *Pseudo-nitzschia* (45 and 90 µm size classes), (B) surface area to volume ratio (SA:V) for *Thalassiosira*, *Chaetoceros*, and *Pseudo-nitzschia* (45 and 90 µm size class) within the control (Ctrl; dark grey), +Fe (light grey), and +DFB (white) treatments at 72 h, (C) bSi production (pmol Si cell^{-1} d^{-1}, and (D) degree of silicification (fmol Si µm^{-2}). The center line represents the median and the boxes display the upper and lower quartiles with whiskers extending 1.5 times the interquartile range. Open diamonds represent the mean. Black dots denote data from individual cells. Samples with <5 cells were excluded and are denoted "nd". Significance was determined within each taxonomic group for A) and B) and between taxonomic groups for C) and D) by Welch two-sample t-test when comparing between two samples or one-way ANOVA and Tukey's HSD post hoc test when comparing among three samples. Lowercase letters delineate the statistically significant different groups ($p < 0.05$). The vertical axes are plotted at a logarithmic (log_{10}) scale. Statistical test results and significance are shown in Table S5.

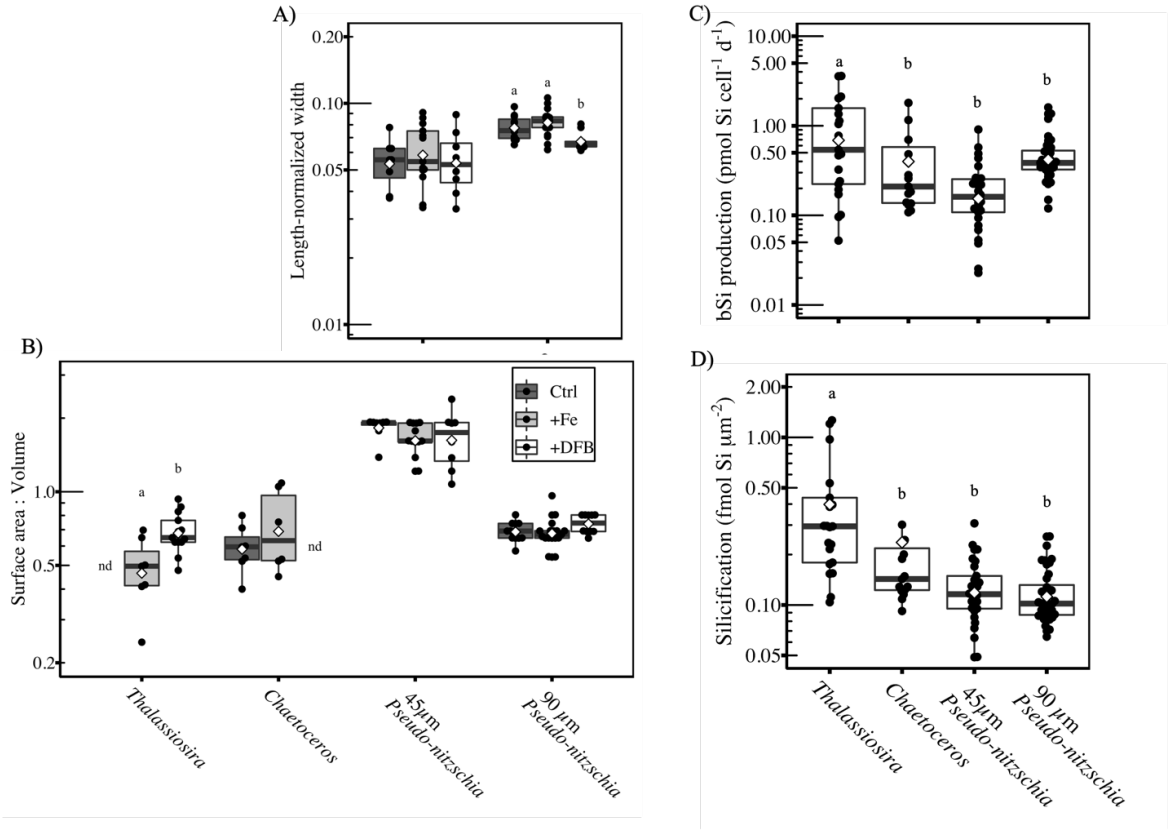

Chapter 2: Interactions between diatom nitrogen and silicon limitation investigated using metatranscriptomic analysis

Abstract:

Diatoms serve as the major link between the marine carbon (C) and silicon (Si) biogeochemical cycles through their contributions to primary productivity and their requirement for Si for cell wall formation. Although several culture-based studies have investigated the molecular response of diatoms to Si and nitrogen (N) starvation and replenishment, diatom silicon metabolism has been understudied in natural populations. In this study, we conducted a series of deck-board Si-amendment incubations using surface water collected in the California Upwelling Zone near Monterey Bay. Steep gradients in macronutrients in the surface ocean and substantial macronutrient utilization led to distinct communities that were macronutrient replete, as well as experiencing N-limitation, or N and Si co-limitation. Biogeochemical measurements of Si uptake were coupled with metatranscriptomic analysis of communities incubated with and without added dissolved Si to explore the underlying molecular response of diatom communities to different nutrient statuses. Metatranscriptomic analysis revealed that N-limited communities exhibited dynamic shifts in N and C transcriptional patterns, but despite a reduction in silica production rates from 1.21 to 0.03 d^{-1}, only modest additional changes in transcript abundance occurred with N and Si co-limitation. While well characterized Si-metabolism associated genes appeared to be poor molecular markers of the added effects of Si stress, several uncharacterized Si-responsive genes were revealed to be potential indicators of kinetic Si-limitation. Transcriptomic data implied that additional Si-limitation within N and Si co-limited samples reduced the degree of N-limitation and the associated physiological impact.

Introduction:

Diatoms serve as a critical link between ocean silicon (Si), nitrogen (N), and carbon (C) biogeochemical cycles, through an obligate Si requirement for frustule formation. Despite accounting for ~30% of marine primary production, diatom growth and productivity are limited in much of the surface ocean by depletion of nitrate (NO_3^-) as well as silicic acid ($Si(OH)_4$) [115, 116]. Here we investigate the physiological and ecological impact of, and interplay between, nitrogen and silicon limitation in a diatom bloom near Monterey Bay, CA, U.S.A. using a combination of metatransriptomic analyses and biogeochemical stock and rate measurements.

In productive coastal upwelling regimes, wind-driven upwelling events bring deep water rich in macronutrients to the surface, fueling >30 % of annual productivity [117]. In the coastal upwelling zone near Monterey Bay strong late spring and summer upwelling can bring water to the surface with $Si(OH)_4$ and NO_3^- concentrations in excess of 25 μM in a 1.2:1 ratio [118]. Diatoms can rapidly respond to the influx of nutrients and utilize $Si(OH)_4$ and NO_3^- in a 1:1 ratio [119], implying that a diatom-dominated community in Monterey Bay could account for nearly all new production within the system. Based on the mean supply and utilization ratios, even a diatom-dominated community would typically deplete NO_3^- only slightly before $Si(OH)_4$ with the possibility that both nutrients would reach low levels imposing N and Si co-limitation of diatoms. However, variation from the mean nutrient upwelling ratio, amount of regenerated nitrogen in the system [118], or community nutrient consumption ratio could each be factors relative nutrient depletion rates that drive the phytoplankton community into a specific limitation regime.

The different forms of nutrient limitation (N, Si, N & Si) can each drive a diatom community into diminished division rates and cell-cycle arrest, but they have dramatically

different impacts on cell physiology and bloom fate. Si- and N- starvation both arrest the cell-cycle, but with different physiological impact [35, 95, 120]. Nitrogen is essential to many intracellular biomolecules, including proteins, RNA, and DNA. When deprived of N, diatom cultures exhibit diminished protein concentrations and an extended lag phase upon N replenishment [120, 121]. In contrast, diatom biogenic silica is required almost exclusively for expanding the siliceous cell wall, or frustule, during cell growth and division, allowing Si starved cultures to rapidly recovering and return to optimal growth rates upon Si replenishment [120]. The relative isolation of N and Si metabolisms creates situations where NO_3^- and $Si(OH)_4$ simultaneously limit different aspects of cell growth in low-nutrient scenarios. The manner in which natural diatom communities respond to individual and coexisting N- and Si-limitations may have ecological implications on how rapidly nutrient limited communities can respond when resupplied with episodic pulses of nutrients.

Culture studies have also shown that both N- and Si-starvation can each trigger differential expression of ~40% of the diatom genome [122, 123]. For N-limitation the response includes a general down regulation of C- metabolism and a characteristic shift in the expression of N-assimilation genes, with some expressed higher and others lower under N-limitation, to allow diatoms to adjust their N metabolism to changing N availability [95, 123]. Cross-comparisons between different Si-starvation experiments have not identified consistent systemic changes in transcript expression for either photosynthesis or nitrate assimilation pathways [35], other than a notable shift in the expression of genes in the urea cycle, proposed to alter the production of polyamine peptides needed for protein-facilitated silica deposition [50].

Unlike N assimilation, the metabolic pathway of diatom silicon metabolism has not yet been fully defined, complicating efforts to develop molecular markers of silica production or Si-limitation. This has led to a reliance on the well-characterized and highly conserved multi-gene family of silicon transport proteins (*SITs)* as proxies when uptake rates are not available [124]. At the $Si(OH)_4$ concentrations typical of the Monterey Bay and greater California Current Upwelling regime (<30 μmol L^{-1} [69, 70]) active uptake of $Si(OH)_4$ is performed through *SITs*. Diatoms have also previously been shown to increase transcription of clades A and E SIT genes after Si starvation and SIT protein expression during periods of elevated biogenic silica (bSi) production [22, 73], making SITs potentially diagnostic of Si limitation in the natural communities.

The expression of genes associated with silica deposition offer a second strategy for understanding Si metabolism in field populations. Several diatom-specific proteins involved in silica biomineralization have been characterized in transcriptomic and proteomic laboratory studies [36, 67, 68, 125, 126], but most are poorly conserved with limited utility for evaluating Si limitation in diverse field communities. The sole exception to this is the silica deposition vesicle protein Silicanin-1, *Sin-1,* making it a potential molecular marker of bSi production or Si-limitation. Several proteins involved in facilitating precipitation of Si, such as silaffins, cingulins, and silicanin proteins, have been identified in *Thalassiosira pseudonana* based primarily on amino acid composition [36, 68], which may serve as useful criteria for identifying orthologous Si-related proteins in field communities. Additionally, diatom culture-based studies of the transcriptomic response to Si starvation have highlighted several, mostly uncharacterized, Si-limitation and Si production associated genes which could include a core set of conserved genes indicative of Si metabolsim [35].

With the growing abundance of marine nucleic acid sequencing data through large collaborative projects such as EXPORTS [1], BIOS-SCOPE, BioGEOTRACES [2], Global Ocean Sampling [3], Tara Oceans [4], and Bio-GO-SHIP [5], which all share an interest in moving toward linking cellular metabolism with ocean processes, there is a need to develop and test relationships between molecular markers and related biogeochemical stocks and rates. By relating metatranscriptomic patterns to biogeochemical stock and rate measurements during a diatom bloom in Monterey Bay, CA we evaluate the ecological relevance of diatom transcriptomic fingerprints of nitrogen and silicon limitations based on those previously characterized in laboratory studies, while also exploring potentially undiscovered Si related genes.

Results:

Table 1: Particulate biomass and macronutrient concentrations of initial water at sampling sites.

Station	Particulate biomass		Dissolved macronutrients		
	bSi (µmol L^{-1})	Chl a (µg L^{-1})	$[Si(OH)_4]$ (µmol L^{-1})	[N+N] (µmol L^{-1})	Incubation length (hours)
S2	5.28	8.74	9.98	8.79	24
S4	6.69	10.87	1.60	0.23	12
S11	5.56	11.83	2.85	0.59	36

This study was part of the "DYE labeling of diatom silica" (DYEatom) cruise (PS1312; 27 June–05 July 2013) that set out to examine the response of diatom communities to a spectrum of $Si(OH)_4$ concentrations within the California Current Upwelling Zone (CUZ) as previously described [127]. Upwelling favorable conditions near Monterey Bay over the 10 days prior to the start of the cruise, 10-21 June, coincided with decreased SST [127]. Satellite imagery depicted elevated (>5 µg L^{-1}) chlorophyll *a* (Chl *a*) concentration within and northwest of Monterey Bay throughout the duration of the study (Fig. 1). In situ sampling at the three sampling sites corroborated satellite data with Chl *a* concentrations

ranging between 8.74-11.84 µg L^{-1} (Table 1). Ambient bSi concentrations, between 5.3 - 6.7 µmol L^{-1}, indicated substantial diatom biomass within the phytoplankton community (Table 1). Initial macronutrient concentrations varied between the three stations, with the highest concentrations of NO_3^- + NO_2, hereafter denoted NO_3^-, 8.79 µmol L^{-1}, and $Si(OH)_4$, 9.98 µmol L^{-1}, at S2. In contrast, initial NO_3^- concentrations at both S4 and S11 were sub-micromolar at 0.23 and 0.60 µmol L^{-1}, respectively, while $Si(OH)_4$ concentrations were higher at 1.60 and 2.85 µmol L^{-1} at S4 and S11, respectively. The excess $Si(OH)_4$ relative to NO_3^- present at S2, ~1.14:1, is typical of the Monterey Bay regime, which upwells excess $Si(OH)_4$ relative to NO_3^- at a ratio of 1.2:1 to the surface, but the far higher ratios of $Si(OH)_4$: NO_3^- present at S4 (6.83) and S11 (4.81) may be linked to nitrate depletion prior to station occupation.

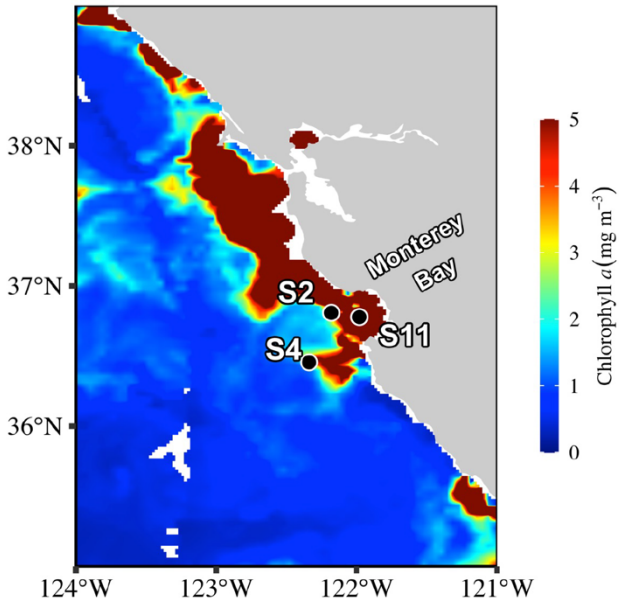

Figure 2-1: Sampling site locations overlayed on the surface chlorophyll *a* concentration from level-2 MODIS 8-day average from 2013, June 29 (https://giovanni.gsfc.nasa.gov/giovanni/).

Community Si uptake and Si stress

To investigate the impact of low Si and/or N on diatom physiology, bottle incubations were set up at each station with unamended controls (Ctrl) and 18 µmol L^{-1} Si-amended (+Si)

samples, with the latter meant to provide the diatom assemblage with enough silicic acid to operate at maximum Si uptake rates (V_{max}) for the duration of the incubations. Over the initial 12 h the specific rate of silicic acid uptake (V_b) in Ctrl treatments at S2 and S11 were similar, 0.62 - 0.66 d^{-1}, and corresponded to a doubling of initial bSi concentration in ~1.1 days. In contrast, V_b in the Ctrl treatment at S4 was ~40% lower at 0.35 d^{-1} (Fig 2A). Additional V_b measurements at 24 h within S2 Ctrl, S2 +Si, and S4 +Si treatment, which all contained initial high $Si(OH)_4$ concentrations (> 5 µmol L^{-1}), revealed nearly identical Si uptake rates to the respective 12 h measurements indicating no diurnal pattern of Si uptake (Table S1).

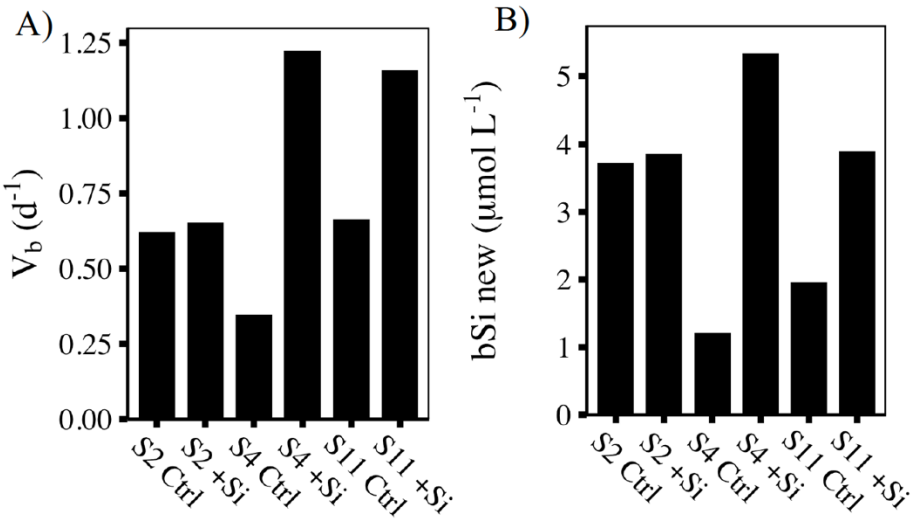

Figure 2-2: Measures of biomass specific Si uptake (d^{-1}) and new bSi produced (µmol L^{-1}) over the first 12 h of the control (Ctrl) and Si amended (+Si) incubations.

Measures of kinetic limitation of Si uptake indicated severe Si-limitation in Ctrl treatments by the termination of incubations at S4 and S11. Kinetic limitation of Si uptake was used as a measure of Si stress (V_{ctrl} /V_{max}). Si stress values >0.7 indicate no kinetic Si limitation with cells operating at > 70% of V_{max} [128, 129], 0.69-0.3 indicates moderate Si stress (i.e. uptake near $K_s = 0.5V_{max}$), and a value ≤ 0.3 indicating severe Si stress. The latter case would likely limit cell division given that diatoms can only thin frustules by 3-4 fold to

maintain doubling time despite uptake limitation [130]. At S2, the Si stress ratio measured ~1 at 24 h, indicating the Ctrl assemblage was Si replete (Table S2). In contrast, the Ctrl treatment at S4 exhibited a Si stress value of 0.28 at the time of sample harvest (12 h), which intensified further to 0.17 over the proceeding 12-24 h (Table S2). The initial Si stress of the S11 Ctrl treatment was initially minimal, 0.80, when measured at 4 h but progressed to moderately Si stressed, 0.47, over the 4-12 h interval (Table S3). Although no Si uptake rates were continued through the endpoint of the parallel RNA incubation for S11 samples, 36 h, a Michaelis-Menten based model, utilizing the initial biogeochemical measurements and kinetic values (see Methods), predicted low final V_b, 0.02, and Si stress, 0.03, values for the Ctrl treatment (Table S3).

Characterization of macronutrient depletion

Over the 12-36 h duration of the incubations, phytoplankton macronutrient utilization pushed samples from S4 and S11 deeper into NO_3^- depletion. Given that dissolved Si and N are utilized by diatoms at 1.1:1 ratio, respectively [119], the 1.2 and 5.3 μmol L^{-1} of new bSi produced in S4 Ctrl and +Si treatments, respectively, would have created a substantial debit against the initial 0.23 μmol L^{-1} of NO_3^- (Fig. 2b) even without considering uptake of N by taxa other than diatoms. Although a Si uptake may have been partially supported by regenerated sources of N, N-depletion likely resulted in a characteristic severe reduction in cell associated nitrogen content [131]. Similarly, in S11 Ctrl and +Si treatments, after 12 hr the 2.0 and 3.9 μmol L^{-1} of new bSi produced, respectively, would have created an associated N demand of 1.8 and 2.5 μmol L. Considering the initial NO_3^- concentration at S11 of only 0.59 μmol L^{-1} both treatments were likely deplete of NO_3^- by the termination of the incubation at 36 h. In contrast at S2 the 3.79 ± 0.07 μmol L^{-1} new bSi produced would have

only drawn down the initial $Si(OH)_4$ and NO_3^- to 6.19 and 5.3 μmol L^{-1}, which is not considered rate limiting (Fig. 2b [41]). Within the Ctrl treatments of S4 and S11 the >70% reduction of Si uptake relative to the +Si treatments may have affected diatom division rates reducing N demand and N limitation.

The divergent nutrient status of the stations and treatments allowed for the categorization of the transcriptomic samples based on likely physiological impact. S2 Ctrl and +Si treatments were classified as replete based on the lack of Si stress and the presence of ample NO_3^-; S4 and S11 Ctrl treatments were classified as co-limited based on negligible NO_3^- concentration and severe Si stress; and S4 and S11 +Si treatments were classified as solely N-limited similarly as Si stress was alleviated (Fig. S1). To assess the transcriptomic response to N-limitation, the abundance of transcripts within the N-limited samples was compared to replete samples. Lacking samples that exclusively experienced Si-limitation, the additional impact of Si-limitation was obtained through the comparison of co-limited samples to the N-limited treatments. The Si-limitation comparison negates the shared response to N-limitation and highlights the additional change in transcript expression that drove the observed increase in Si uptake in the S4 and S11 +Si treatments relative to the respective Ctrl treatments, as well as any additional transcriptomic impact triggered by the interplay between Si and N limitations.

Community composition

Estimates of the initial community composition, based on 18s rRNA amplicon sequencing, revealed similar diatom-dominated phytoplankton communities across all three stations. Diatoms made up 74-91% of the initial phytoplankton community with >90% of diatom associated rRNA reads belonging to the genus *Pseudo-nitzschia* as previously

reported [127, 132]. The relative proportions of taxonomically annotated mRNA reads from the incubation end-points, which represent the transcriptionally active members of the community, differed from the 18s rRNA data. Dinoflagellates and other non-diatom eukaryotes accounted for 21-56% of annotated mRNA reads, despite minor representation in 18s rRNA amplicon. *Pseudo-nitzschia* transcripts still made up the majority, 52-87%, of diatom annotated mRNA reads, but notably less than the proportion of rRNA amplicon reads. While the diatom genera *Leptocylindrus* and *Thalassiosira* each accounted for as much as 15% and 8% of diatom annotated mRNA reads, respectively, in some samples, the overall abundance of mRNA reads annotated to these diatoms in the metatranscriptome was an order of magnitude less than that of *Pseudo-nitzschia* (Table S3). As such the following sections focus on the transcriptomic response within the diatom genus *Pseudo-nitzschia* while leveraging data from other diatoms, when present, to elucidate shared or divergent responses.

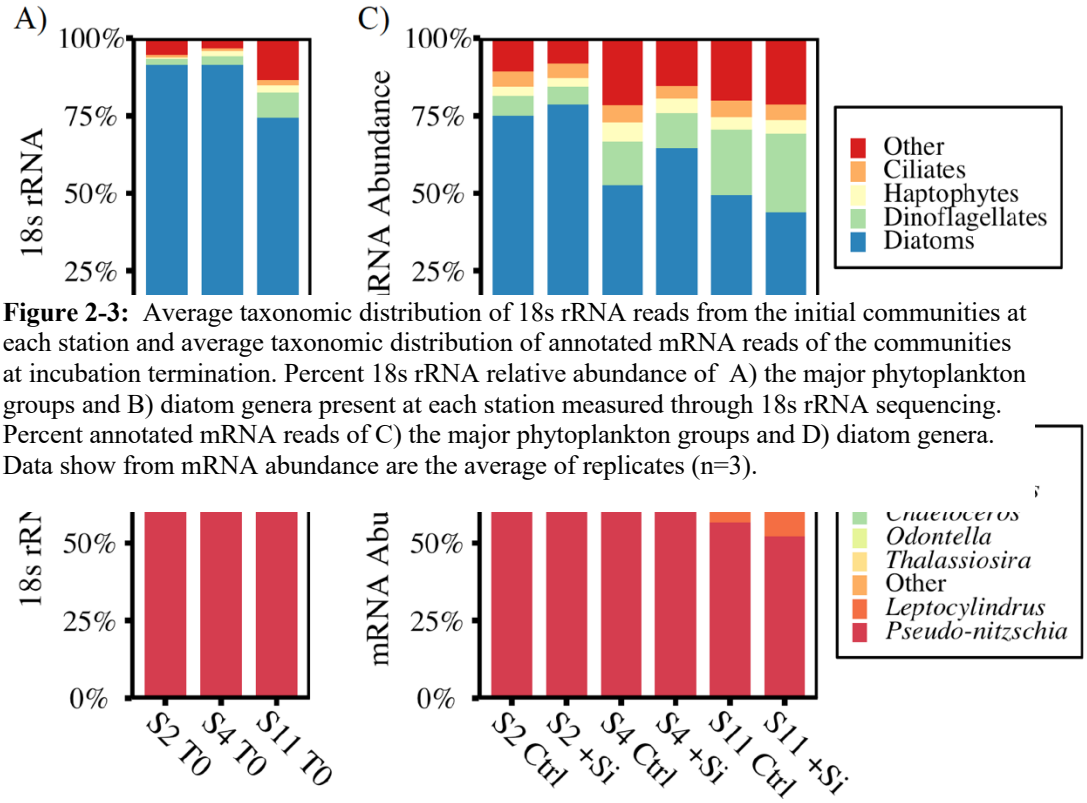

Figure 2-3: Average taxonomic distribution of 18s rRNA reads from the initial communities at each station and average taxonomic distribution of annotated mRNA reads of the communities at incubation termination. Percent 18s rRNA relative abundance of A) the major phytoplankton groups and B) diatom genera present at each station measured through 18s rRNA sequencing. Percent annotated mRNA reads of C) the major phytoplankton groups and D) diatom genera. Data show from mRNA abundance are the average of replicates (n=3).

Effect of macronutrient limitation on transcript abundance

Principle component analysis (PCA) of the transcriptomic profiles from incubation samples, using the 2500 most variable annotated genes, showed substantial separation based on macronutrient status rather than by location or treatment. PC1 accounted for 74% of the variance between samples and primarily separated the N-replete samples at S2 (Ctrl, +Si) from the N-deplete samples (+Si) and the N & Si co-limited samples (Ctrl) from S4 and S11 (Fig. 4). Furthermore, based on the loading of the core biogeochemical supplemental variables, PC1 described the absence of NO_3^- and presence of Chl *a*, informed by the high cosine square values that represented the importance of the PC to a given observation. PC2 only represented 8% of variance between samples and appeared to separate samples by geographic location rather than grouping by degree of Si stress Si-limited and Si-replete samples separation between Ctrl and +Si treatments within Si-limited stations for the S4 and S11 sites. Along PC2, $Si(OH)_4$ concentration loaded opposite of Si stress and bSi concentration with the former having a cosine squared value approximately double that of the latter two. The substantial separation between N-deplete samples relative to the N-replete sample paired with the small degree of separation between +Si and Ctrl samples provides evidence that the addition of Si stress in N & Si co-limited samples had a relatively small effect after accounting for the response to N-limitation.

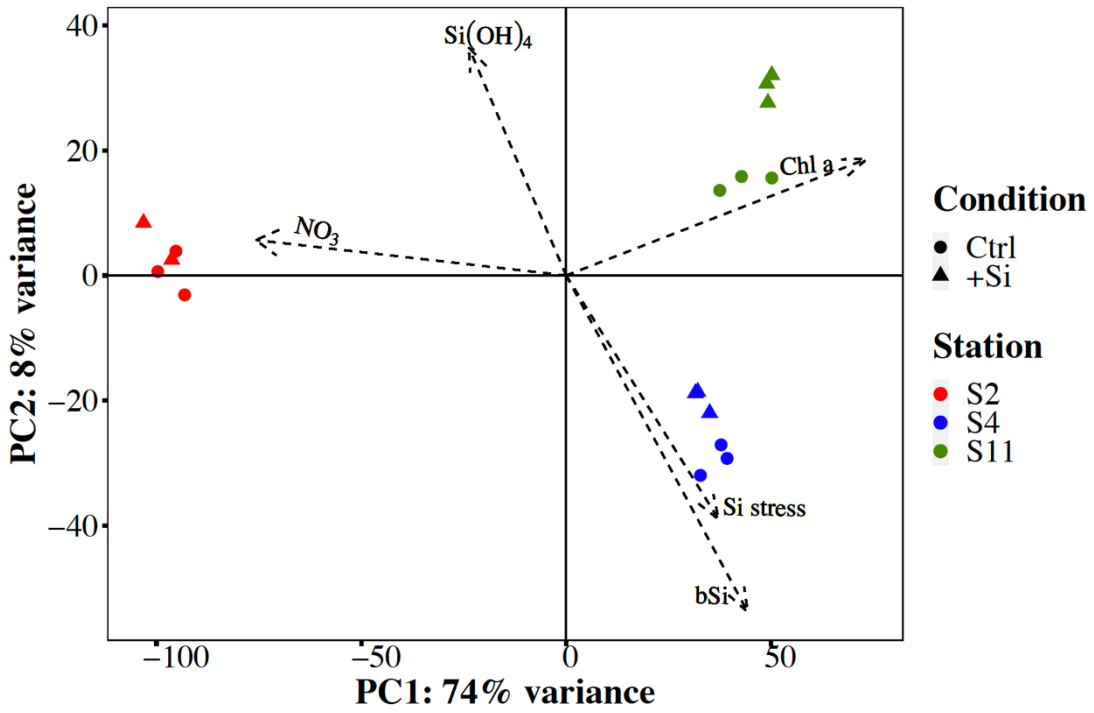

Figure 2-4: Principle component analysis biplot of gene transcript abundance (loading of principle components) and the relationship with treatment (shape), sampling site (color), and supplemental environmental variables.

Carbon assimilation transcript abundance

Depletion of NO_3^- alone triggered a dramatic shift in transcript abundance of carbon assimilation genes. Of the 44 carbon assimilation-related genes surveyed in this study, 33 were detected and differentially abundant within *Pseudo-nitzschia* (Fig. 5B). Transcripts corresponding to genes related to the light harvesting complex (LHC), photosynthetic electron transport (pet), photosystem I (psa), photosystem II (psb), glycolysis and other carbon metabolism processes were >2-fold less abundant in the N-limited samples Fig S5A, Table S4). Ribulose-5-phosphate epimerase (RPE) was the only surveyed carbon metabolism related gene that was >2-fold more abundant under N-limitation in *Pseudo-nitzschia* as well as another diatom genera, both *Leptocylindrus* and *Fragilariopsis*, possibly serving a conserved function of shuttling C into the pentose phosphate pathway.

The additional changes in the abundance of carbon assimilation transcripts when Si-limitation co-occurred with N-limitation underlie the reduced bSi production rate, but they also reflect the synergistic or antagonistic interactions between N- and Si- limitations as the transcriptomic response to Si-limitation (here after described as additional Si-limitation) was obtained by comparing the co-limited samples to the N-limited samples. Samples with additional Si-limitation exhibited an increase in the abundance of transcripts corresponding to respective C-assimilation genes that were reduced under N-limitation alone and decrease in the abundance of transcripts corresponding to C-assimilation genes that were more abundant under N-limitation. In particular, transcripts coding for genes involved in the pentose phosphate pathway (PGK and PRK), glycolysis (TPI), citric acid cycle (PEPC), and photosystem II (psb27, psb28, psbO, psbU) were >2-fold more abundant in co-limited samples compared to samples that experienced N limitation alone (Fig. 5A).

Effect of macronutrient limitation on nitrogen-related transcript abundance

Macronutrient limitation had a distinct impact on diatom N assimilation and transcription of related genes. Within a gene set of 24 highly nitrogen responsive N-assimilation genes [95], the differential abundance of 20 transcripts in N-deplete S4 and S11 Ctrl samples, relative to the replete S2 Ctrl and +Si samples, closely matched the severe responses to N-limitation described in the literature [95] lending support to the classification of S4 and S11 samples as N-limited. For example, transcripts corresponding to the genes ferredoxin-dependent nitrite reductase (nirA), glutamine synthetase II (GSII), argininosucinate synthase (ASuS), glutamate synthase (GOGAT-fd), N-acetyl-gamma-glutamyl-phosphate reductase (AGPR), and ornithine carbamoyl transferase (OTC) were all

>2-fold less abundant in N-limited samples within *Pseudo-nitzschia* as well as at least one of the next three most abundant diatom genera (Fig 5B, Table S4).

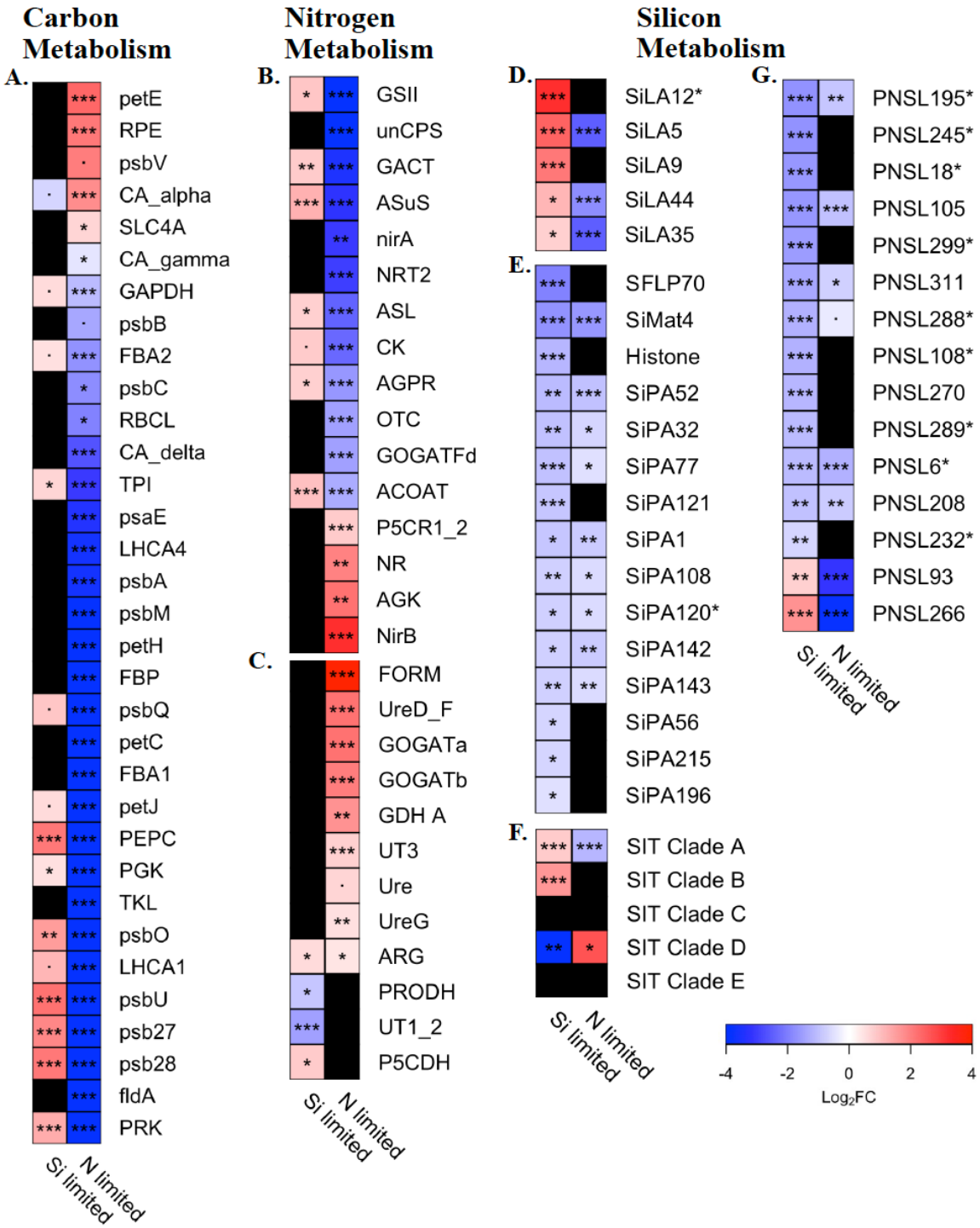

Figure 2-5: Differential abundance of transcripts corresponding to A) key carbon assimilation genes, B) nitrogen depletion induced genes, C) nitrogen depletion repressed genes, D) silicon limitation associated (SiLA) genes, E) silicon production associated (SiPA) genes, F) silicon transport genes , and G) putative *Pseudo-nitzschia* silaffin like (PNSL) genes in the diatom *Pseudo-nitzschia* under nitrogen limitation relative to controls and under nitrogen and silicon co-limitation relative to nitrogen-limited. Heatmap of transcript abundance (log_2 fold-change) in nitrogen limited samples relative to replete (right) and co-limited samples relative to nitrogen limited (left). The latter comparison reveals the added effect of Si limitation above and beyond the response to N limitation. Black boxes indicate genes that were not differentially abundant in either treatment. Asterisks denotes false discovery rate (FDR); · $p < 0.1$, * $p < 0.05$, ** $p < 0.01$, *** $p < 0.001$. Abbreviations are as follows A) Phosphoribulokinase (PRK), Flavodoxin (fldA), photosystem II 13kDa protein (psb28), photosystem II protein (psb27), photosystem II PsbU protein (psbU), light-harvesting complex I chlorophyll a/b binding protein 1 (LHCA1), photosystem II oxygen-evolving enhancer protein 1 (psbO), Transketolase (TKL), Phosphoglycerate kinase (PGK), Phosphoenolpyruvate carboxylase (PEPC), cytochrome c6 (petJ), FBA class 1 (Fructose-1, 6-bisphosphate aldolase) (FBA1), photosystem II oxygen-evolving enhancer protein 3 (psbQ), photosystem II oxygen-evolving enhancer protein 3 (psbQ), Fructose bisphosphatase (FBP), ferredoxin--NADP+ reductase [EC:1.18.1.2] (petH), photosystem II PsbM protein (psbM), photosystem II P680 reaction center D1 protein [EC:1.10.3.9] (psbA), light-harvesting complex I chlorophyll a/b binding protein 4 (LHCA4), photosystem I subunit IV (psaE), Triose phosphate isomerase (TPI), CA_delta (CA_delta), RBC large (RBCL), photosystem II CP43 chlorophyll apoprotein (psbC), FBA class 2 (Fructose-1, 6-bisphosphate aldolase) (FBA2), photosystem II CP47 chlorophyll apoprotein (psbB), Glyceraldehyde-3-phosphate dehydrogenase (GAPDH), CA_gamma (CA_gamma), SLC4A (DIC uptake) (SLC4A), CA_alpha (CA_alpha), photosystem II cytochrome c550 (psbV), Ribulose-5-P (Ru-5-P) epimerase (RPE), plastocyanin (petE) B) Formamidase (FORM), Ornithine cyclodeaminase (OCD3), Urea active transporter, mitochondrial (UT3), proline dehydrogenase (PRODH), Urease (Ure), Glutamine dehydrogenase (NADP+), mitochondria (GDH A), Urea transporter, extracellular (UT1_2), arginase (ARG), 1-pyrroline-5-carboxylate dehydrogenase (P5CDH), UreaseG (UreG), UreaseD_F (UreD_F), Cyanate lyase (CL), Glutamate synthetase (NADH), mitochondria (GOGATb), Glutamate synthetase (NADH), mitochondria (GOGATb); C) ornithine carbamoyl transferase, mitochondrial (OTC), Nitrite transport, chloroplast (NAR1), Argininosuccinate synthase (ASuS), N-acetyl-gamma-glutamyl-phosphate reductase (AGPR), glutamate kinase/glutamate-5-semialdehyde dehydrogenase (P5CS), Glutamine synthetase, chloroplast (GSII), Carbamoyl phosphate synthase (ammonia) (pgCPS), Carbamoyl phosphate synthase (ammonia) (unCPS), pyrroline-5-carboxylate reductase (P5CR1_2), argininosuccinate lyase (ASL), Glutamate synthase (ferredoxin), chloroplast (GOGATFd), Nitrate transporter (NRT2), Nitrate reductase (NADH) (NR), Nitrate reductase (NADH) (NR), Carbamate kinase (CK), Glutamine synthetase, mitochondria (GSIII), acetylornithine transaminase (ACOAT), acetylglutamate kinase (AGK), Ferredoxin-Nitrite Reductase (nirA), glutamate N-acetyltransferase (GACT), Nitrite reductase (NADPH), chloroplast (NirB), ornithine aminotransferase (OAT); and D) Si matrix protein 4 (SiMat4). Asterisks at the end of abbreviations in panels D-G signify that the gene is diatom specific.

Transcripts for a small subset of N-responsive genes, pyrroline-5-carboxylate reductase (P5CR1,2), nitrate reductase (NR), ferredoxin-independent nitrite reductase (nirB), acetylglutamate kinase (AGK), were more abundant in N-limited samples in contrast to the respective literature described responses [95]. One of these, P5CR1,2 was also elevated across *Fragilariopsis* and *Thalassiosira* and nirB transcript abundance was elevated in *Thalassiosira* as well, indicating that the transcript abundance of these two genes may have

been systematic and not an aberration (Fig S2B, Table S4). In contrast, the increased abundance of transcripts coding for NR under N-limitation in *Pseudo-nitzschia* was a genus specific response as *Leptocylindrus* and *Fragilariopsis* exhibited abundance patterns of these gene that contradicted that of *Pseudo-nitzschia* (Fig. 5C, Table S4).

In samples experiencing N and Si co-limitation the presence of Si-limitation did not trigger an additional widespread change in the transcript abundance of N assimilation genes beyond what was observed with N-limitation alone. While transcripts for 10 N-assimilation genes were differentially abundant in samples with additional Si-limitation, only the urea cycle genes proline dehydrogenase (PRODH), arginase (ARG), urea transporters 1 and 2 UT1_2, and 1-pyrroline-5-carboxylate dehydrogenase (P5CDH) were clearly driven by the added Si-limitation, potentially related to the importance of polyamine synthesis in bSi production (Fig. 5C [50]). Similar to the trend in the transcript abundance of several C-assimilation genes in samples with additional Si-limitation, the transcripts corresponding to six N-assimilation genes, glutamine synthetase (GSII), glutamate N-acetyltransferase (GACT), Argininosuccinate synthase (ASuS), argininosuccinate lyase (ASL), N-acetyl-gamma-glutamyl-phosphate reductase (AGPR), and acetylornithine transaminase (ACOAT), were more abundant in samples with additional Si-limitation while less abundant in samples only experiencing N-limitation. This pair of responses is potentially indicative of a potential easing of N-limitation by the reduced N-demand or its redirection to support Si metabolism when bSi production and growth were limited by low $Si(OH)_4$ concentration.

Effect of macronutrient limitation on silicification related transcript abundance

Fifteen silaffin like genes (PNSLs) detected within *Pseudo-nitzschia* displayed a >2-fold decrease in transcript abundance under Si and N co-limitation, compared to N-limitation

alone. While none of the 15 Si responsive PNSLs contained previously characterized functional domains, 9 were diatom specific, having homologs detected only in diatom gene databases. In particular, transcripts coding for six PSNL genes, including PNSL289 and PNSL232, were less abundant in samples with additional Si-limitation while the same genes exhibiting no discernable response to N-limitation, implying a specificity to Si availability alone, and making good potential markers of *Pseudo-nitzschia* bSi production.

Within this study a subset of genes that had previously been deemed Si-limitation associated (SiLA) and Si production associated (SiPA) through culture studies [35, 122, 133], exhibited differences in transcript abundance in response to N-limitation that were amplified by additional Si-limitation. Despite the combined 279 putative SiLA and SiPA genes queried and 157 detected, only 20 displayed significant differential abundance in co-limited samples beyond that observed under N limitation and consistent with respective literature described patterns (Fig. 5D, 5E, Table S4). Three times more SiLA and SiPA genes, 60, were differentially abundant in N-limited samples compared to the possibly due to feedbacks between slower growth under N-limitation and a reduction in the rate of frustule formation (Fig 5D, 5E, Table S4 [131]). Within the small subset of 20 SiPA and SiLA genes with transcripts differentially abundant in samples with additional Si-limitation, 75% exhibited differential abundance patterns within N-limited samples that were comparable to that of Si & N co-limited samples, making it unclear if transcript abundance correlated with changes bSi production or with a generalized macronutrient stress response. Only 4 Si related genes exhibited >2-fold changes in transcript abundance exclusively with changes in bSi production; two Si-limitation associated genes—both without homology to previously

characterized genes—and 2 bSi production associated genes—a histone gene and a silaffin-like-protein (SFLP70) (Fig. 5E [68]).

Of the previously characterized Si metabolism genes only SIT transcripts were differentially abundant in samples with additional Si-limitation (Fig. 5F, Table S4). SIT clades A and D were both differentially abundant in samples with additional Si-limitation, with the former being more abundant and the latter being less abundant relative to the N-limited samples (Fig. 5F). However, in both cases the magnitude of differential abundance was matched with an opposing direction change in abundance in the N-limited sample relative to the replete. Together the Si-limitation and N-limitation responses offset and led to no change in abundance of clade A or clade D SIT transcripts under co-limitation (Fig. 5F). In contrast the abundance of transcripts corresponding to the clade B SIT gene were >2-fold elevated under Si-limitation alone (Fig. 5F).

Discussion:

Persistence and variable physiological status of Monterey Bay diatom bloom and incubations

Satellite imagery and biogeochemical stock measurements revealed a persistent phytoplankton bloom in and near Monterey Bay during the study period dominated by the bloom forming diatom *Pseudo-nitzschia* at all three study sites. Blooms of *Pseudo-nitzschia* are not uncommon in the region as Monterey Bay is considered a "hot spot" for this toxigenic diatom [134, 135], with a persistent toxigenic bloom present during the three years proceeding this study [136].

Despite comparable concentrations of Chl *a* and bSi biomass at all three sampling sites, the final samples exhibited dissolved macronutrient concentrations and Si-stress values

characteristic of different bloom/physiological states ranging from replete, N-deplete, and varied levels of N- deplete with additional Si-limitation. By the termination of the incubations, the extended period of growth with <1μM NO_3^- present and diminished specific Si uptake rates indicated N-limitation as well as low-Si induced growth limitation in the S4 and S11 Ctrl and samples, while the respective +Si samples appeared to only be N-limited. In contrast, the specific Si uptake rates and NO_3^- concentrations in the S2 Ctrl and +Si samples would not be considered growth or rate limiting [41].

Community transcriptomic fingerprinting clearly identified nitrogen limitation

PCA of transcriptomic profiles provided evidence that N-limitation altered the abundance of a far greater number of transcripts than did additional Si-limitation. Transcriptomic profiles exhibited a large degree of separation along PC1 (Fig. 4) that explained over three quarters the variance and correlated with NO_3^- concentration. Additionally, far more transcripts for *Pseudo-nitzschia* genes were differentially abundant in response to N-limitation compared to additional Si-limitation (Fig S1). This is somewhat surprising considering genome wide studies of diatom Si- and N- limitations have shown differential expression of a similar proportion, ~40 %, of genes [122, 123]. The main difference between those studies and that reported here is that our assessment of the effect of Si-limitation only evaluated responses above and beyond those already imposed by co-occurring N-limitation. It is likely that a proportion of the diatom transcriptomic response to severe N- and Si-limitations are shared as a general macronutrient stress response minimizing any additive transcriptomic response when N- and Si- limitation co-occur. However, in three similar transcriptomic studies of the response of *Thalassiosira pseudonana* to Si-starvation and replenishment, only 1/3 of the differentially expressed genes exhibited a conserved

transcriptomic response between studies [35, 122, 133], which would imply a less tightly orchestrated transcriptomic response to $Si(OH)_4$ availability. Furthermore, as Si-starvation induces cell cycle arrest, comparing between replete and Si-starved cultures may identify a broader suite of genes involved in cell division and control of cell-cycle progression rather than primarily involved in the biomineralization of Si. Data from previous culture based transcriptomic studies of Si-starvation may not be representative of the less extreme degrees of Si stress found during this study and more common in a dynamic coastal ecosystem.

The *Pseudo-nitzschia* dominated community studied here exhibited a dramatic shift in C- and N- assimilation transcript abundance that closely corresponded with previous *Phaeodactylum tricornutum* culture experiments [95]. The less abundant diatom genera provided additional support that diatom N-limitation is resolvable within a dynamic field community. Similarly, the conserved reduction in transcripts for most C-assimilation processes in our field study supports previous culture based findings that multiple diatom genera generally down regulate carbon metabolism related genes when N-limited [123]. While the divergent evolutionary history of diatoms has led to genus-specific nutrient acquisition strategies and to varied ability to cope with low nutrients [34, 43, 53, 96, 137], the apparent shared diatom response to N-limitation may enable the discernment of the varied degrees of resilience to low nitrogen and thus the niche roles of different diatom species within a community.

The transcriptomic changes that were driven by N-limitation were likely indicative of larger physiological and biogeochemical shifts. As nitrogen is required to produce important biomolecules (e.g DNA, RNA, proteins), N-limitation and the associated reduction in key C- and N- related transcript abundance likely led to diminished diatom C- and N-assimilation

typical of N-depleted diatom assemblages [131]. The N- limitation response is also indictive of an associated shift in the stoichiometric ratios of both particulate and dissolved organic matter (POM, DOM respectively) with both becoming heavily enriched in carbon relative to nitrogen [28, 138]. N-limited samples even exhibited reduced abundance of bSi production associated transcripts, possibly indicating an impact on diatom Si affinity or bSi production.

Synergistic and antagonistic interactions between N and Si stress under co-limitation

In co-limited samples, low $Si(OH)_4$ availability dramatically reduced bSi production rates to a degree consistent with growth limitation [20, 139]. Low ambient $Si(OH)_4$ concentration causes diatom cells to reduce frustule Si content and eventually will arrest the progression of the cell-cycle if insufficient Si is available to complete a new siliceous frustule, as interrupting the DNA synthesis and cell division processes can cause damage and cell death [16, 140]. The reduced bSi production and cell division rates, driven by Si-limitation, likely triggered a decrease in the manufacture of bSi- production and growth-associated biomolecules in co-limited communities relative to N-limited communities, and further diminished N-demand. The lower N-demand associated with the additional Si-limitation manifested in the transcriptomic data as a partial offsetting of the N-limitation driven changes in C- and N- metabolism and Si- limitation associated transcripts abundance. While the community transcriptomic response to Si-limitation in the field would undoubtedly have differed if underlying N-limitation was not present, our findings complement previous culture studies that showed Si-starvation did not trigger a systematic change in transcript expression for genes involved in photosynthesis (Fig. 5A [35]). The exception to this pattern was the modulation of the abundance of transcripts corresponding to four urea cycle genes when additional Si-limitation was present, potentially related to the production of polyamines

which aide in bSi oligomerization. In contrast to the impact of Si-limitation on transcript abundance of C- and N- assimilation related genes, additional Si-limitation primarily intensified changes the N-limitation driven changes in the abundance of transcripts for Si production associated and *Pseudo-nitzschia* silaffin like genes. The pair of synergistic and antagonistic responses is potentially indicative of a potential easing of N-limitation by the reduced N-demand or it's redirection to support Si metabolism when bSi production was limited.

Based on the reduced bSi production rate and associated reduction in N-demand, our data suggest that additional Si-limitation prevented phytoplankton communities from further intensifying the co-occurring N-limitation, as would be expected with diatoms typically utilizing $Si(OH)_4$:NO_3^- in a 1.1:1 ratio under replete conditions [119]. The additional Si-limitation appeared to insulate *Pseudo-nitzschia* from further impact of N-limitation on C-assimilation, rather than acting additively and intensifying the stress response. As Si-starved diatoms have the capacity to rapidly recover upon Si-replenishment [120], exclusive or co-occurring Si-limitation may serve an ecologically important role of limiting the severity of diatom NO_3^- limitation and the heavy associated impact on physiology. Such a mechanism would help leave diatoms better poised to recover upon resupply of macronutrients.

Well characterized Si-limitation genes are poor transcriptomic makers

Well characterized Si related proteins appear to be poor transcriptomic markers of Si production and stress, despite the documented role of *SITs, Sin1,* and silaffin-like proteins in Si metabolism. While transcripts corresponding to tp-silaffin, cingulin, Sin1, tpSAP2, and tpSAP3 genes were detected in the metatranscriptome assembly, SITs were the only previously characterized Si metabolism gene differentially abundant in samples experiencing

Si-limitation within this study. The Si-limitation driven increased abundance of clade A and B SITs matched the respective literature described Si-limitation responses [22]. However, the abundance of SIT clades A and D were also driven by NO_3^- concentration in this as well as previously [52], and transcripts for all clades of SIT genes have been shown to increase in abundance in response to Fe limitation even without a concomitant change in Si uptake or silicification. The responsiveness of SIT gene transcription to changing nutrients other than $Si(OH)_4$ makes them a poor transcriptomic marker for Si uptake or production. With the disconnect between SIT transcript and protein abundance [73], it is possible that SIT protein abundance may still serve as a reliable proxy for Si status in field populations.

Potential transcriptomic markers of Si-limitation among Si responsive genes

The rapid increase in available reference genomes and transcriptomes has enabled the extensive mapping of putative marine microbial metabolic pathways [102, 141–143]. However, changing nutrient concentrations can have a complex and cascading impact on genome-wide transcription and physiology [95]. As such interpretation of community transcriptional studies is still dependent on, and in some cases lacking, a strong foundation of how transcript abundance should be *expected* to change within a group of organisms under individual and combined changes in environmental conditions (e.g. macronutrients, vitamins, trace metals, temperature, diurnal rhythm, light availability, DOM, etc). The use of an individual genes as molecular markers can be a powerful tool for broadening the understanding of ecosystems such as with *nifH* and nitrogen fixation [144].

While the use of individual diatom genes as transcriptional markers, such as nitrate or ammonium transporters for nitrogen limitation and silicon transporters for silicon limitation, has been adopted [124, 132], in some cases the utility is often less certain. Nitrate,

ammonium, and silicon transporters have all undergone gene duplication and evolution within diatom genomes with different clades of each transporter and individual genes within a clade exhibiting divergent responses to related nutrient deprivation [52, 58, 95, 145]. Furthermore, in some cases the expression of genes, that are indeed strong transcriptomic markers of a process, can be altered by confounding factors ; such is the case with diatom iron-starvation-induced-protein 2A and ferritin which are both indicators of iron limitation but are strongly modulated by changes in N availability as well [43, 123]. With the increasing availability of culture based genome wide expression profile data under numerous conditions[35, 44, 95, 146–149], moving toward using larger gene sets may be a more robust and reliable method to infer metabolic and biogeochemical processes despite initially requiring a broader understanding cellular physiology.

The substantially higher Si uptake rate in the solely N-limited samples relative to the samples with N and Si co-limitation correlated with changes in transcript abundance in a subset of genes previously deemed Si-limitation and Si-production associated in *Thalassiosira pseudonana*. The disparate evolutionary history and morphology of *Pseudo-nitzschia* and *Thalassiosira pseudonana* provide complementary evidence of conserved Si responsive transcript pattern. An additional suite PNSL genes identified through an *in-silico* search for Si biomineralization genes appear to be strong candidates for involvement in Si metabolism and potential molecular markers for the bSi production.

Conclusions:

Through temporal and spatial sampling and manipulative incubation experiments of a natural diatom bloom, this study investigated the diatom response to N-limitation and co-occurring N- and Si- limitation. In addition to validating the field-based application of

transcript-based markers of N-limitation, we found that N and Si co-limited *Pseudo-nitzschia* exhibited minimal additional transcriptomic response compared to the N-limited populations and compared to purely Si-starved diatoms in cultures. This implies that the bulk of the transcriptional response to N or Si limitation is shared across these two stressors. By comparing Si and N co-limited cells to purely N-limited cells we were able to detect the synergistic and antagonistic interactions between the two stressors. Based on the diatom transcriptomic response to Si-limitation within N-limited samples, the additional Si-limitation may have slowed the onset or lessened the degree of N-limitation and associated physiological impact. SIT transcript abundance appeared to be an unreliable marker of Si-limitation. Through leveraging previous published culture-based data and an *in-silico* screen, groups of diatom-conserved and *Pseudo-nitzschia*-specific Si-responsive genes were validated as putative markers of Si production and limitation.

Methods:

Environmental sample collection and experimental design

Incubation samples were collected during the "Dye labeling of diatoms" (DYEatom) cruise between 27 June and 05 July 2013 on board the R/V Point Sur (PS1312; 27 June 2013 to 5 July 2013; Chief Scientist: J. W. Krause) off the California coast near Monterey Bay. Stations reflecting a progression of bloom states were initially identified using satellite derived ocean color and sea surface temperature (SST; MODIS Level-2 products, NASA), high frequency radar arrays ([150]; Central and Northern California Ocean Observing System, www.cencoos. org), and the vessel's underway data acquisition system. Additional subsampling of shipboard underway seawater provided a qualitative assessment of diatom abundance to further define the type and stage of phytoplankton bloom. Stations were

sampled just after local sunrise. Water was collected using a CTD rosette containing twelve 10L Niskin bottles, Sea-Bird Electronics conductivity-temperature-depth sensor, Chelsea fluorometer, and photosynthetically active radiation (PAR) sensor from Bio-Spherical Instruments. Incident irradiance (I_0) was measured just below the surface to determine depths at which the PAR was 55%, 22%, 7%, and 1% I_0, corresponding to the neutral density-screening used to incubate samples in deck-board surface water-cooled incubators.

Phytoplankton community response to Si enhancement was investigated through a series of deckboard incubation experiments and a combination of biogeochemical measurements and metatranscriptome sequencing. Incubations consisted of an unamended control (Ctrl) and an 18.0 µmol L^{-1} $Si(OH)_4$ amendment (+Si). To initiate Si enhancement incubations water from 55% I_0 was used to fill triplicate 1.2 L acid-cleaned polycarbonate bottles to serve as Ctrl or amended with $Si(OH)_4$. Bottles were subsequently incubated deckboard at 55% I_0 for 12 h (S2), 24 h (S4), or 36 h (S11), dependent on personnel availability, before sacrificial sampling.

Silica production rate measurements

Community bSi production rates were measured using the radiotracer ^{32}Si. At the start of each incubation experiment a 250 mL polycarbonate bottle was filled to the top with 304 mL of seawater, amended with 262.8 Bq of high-specific activity ^{32}Si (>40 kBq µg Si^{-1}), and incubated in a 55% I_0 neutral density-screened surface-water-cooled deckboard incubator for 4, 12, and/or 24 h. At the termination of the incubation radiotracer samples were filtered onto 25 mm, 1.2 µm pore size polycarbonate filters and processed for ^{32}Si activity using a low-level beta counter [129]. Gross Si production rates (ρ in µmol Si L^{-1} d^{-1}) were normalized to bulk bSi concentrations (µmol Si L^{-1}) to obtain specific rates (V_b, d^{-1}). Two

methods were used to assess the degree that the ambient $Si(OH)_4$ concentration limited bSi production, both of which used the same ^{32}Si activity addition, incubation conditions, and processing as described above. The first method used eight seawater samples collected from 55% I_0 which were manipulated to make an eight-point concentration gradient between +0 through +18µmol L^{-1} $Si(OH)_4$ with the radiotracer ^{32}Si added to determine the concentration dependence of specific Si uptake rates more fully. The uptake of $Si(OH)_4$ has been shown to conform to a rectangular hyperbola described by the Michaelis-Menten equation:

$$V_{amb}\ or\ V_0 = V_{max} \times [Si(OH)_4]_{amb} \times (K_s + [Si(OH)_4]_{amb})^{-1} \quad (1)$$

Where V_{max} is the maximum specific uptake rate ($\rho \times bSi^{-1}$) and K_s is the half saturation constant where $V_b = 0.5 \times V_{max}$. Data were fit to a non-linear curve using the self-starting Michaelis-Menten function (SSmicmen) from the R *stats* package v.3.6.2. The second method used bSi production rates measured at ambient $Si(OH)_4$ concentration and +18.0 µmol L^{-1} $Si(OH)_4$ to presumably saturate Si uptake and approximate V_{max} (Eq. 1) [118]. Kinetic Si-limitation, or Si-stress, was defined as the ratio of Si production at ambient $Si(OH)_4$ concentration to +18µmol L^{-1} $Si(OH)_4$ (V_{amb}:V_{enh}) [151].

$$Si\ stress\ = V_{amb} / V_{max} \quad (2)$$

Based on the analytical error of the measurement, Si stress values >0.92 were considered within detection error and are not resolvable.

For sampling site S11 where the end point of the kinetic incubation differed from that of the incubation used for RNA extraction and sequencing, the initial kinetic variables (e.g. bSi, $Si(OH)_4$, V_{max}, V_b, and K_s) were used to estimate the final specific uptake rate and Si-stress. Eq. 1 was converted into Eqs. 3-5 to determine the bSi concentration (bSi_n) at the end

of a given time-step (t_n, iteration number n). The bSi_n and $Si(OH)_4$ concentration after t_n ($[Si(OH)_4]_n$) were then used to calculate the specific uptake rate at the end of the time-step and iteratively repeat until to extend the 4 h rate through 36 h (Eqs. 6-7).

$$V_0 = ln\left((bSi_n + bSi_0) \times (bSi_0)^{-1}\right) \times {t_n}^{-1} \quad (3)$$

$$bSi_n = bSi_0 \times e^{t_n \times V_b} \quad (4)$$

$$[Si(OH)_4]_n = [Si(OH)_4]_n - (bSi_n - bSi_0) \quad (5)$$

$$V_n = V_{max} \times [Si(OH)_4]_n \times (K_s + [Si(OH)_4]_n)^{-1} \quad (6)$$

$$V_n = ln\left((bSi_{n+1} + bSi_n) \times (bSi_n)^{-1}\right) \times {t_{n+1}}^{-1} \quad (7)$$

This simplified calculation assumes no dissolution of bSi over the duration of the incubation and that the community *Ks* did not change.

Dissolved and Particulate Analyses

Seawater samples for dissolved nutrient analyses (N, P, Si) were syringe filtered through 0.6 µm polycarbonate filters in plastic scintillation vials and immediately frozen at -20 °C. NO_2^- + NO_3^-, and PO_4^{-3} were quantified onshore at University of California, Santa Barbara Marine Science Institute using a Lachat Instruments QuikChem 8500 Series 2 [85], while dSi was quantified using a manual colorimetric method. For biogenic silica (bSi) samples, 600 mL of seawater was vacuum filtered through a 0.6 µm polycarbonate membranes and stored at -20°C, until shipboard 0.2 N NaOH digestion in Teflon tubes [152]. bSi digests were quantified alongside dissolved silicon (dSi), using the ammonium molybdate colorimetric assay [153].

To obtain chlorophyll measurements, seawater was vacuum filtered through a Millipore HAWP 0.45-µm pore-size cellulose filter, which was subsequently stored at -

20˚C. Chlorophyll *a* was extracted with 90% acetone at -20˚C for 24 h using the acidification method and measured with the Turner Designs 10-AU fluorometer [85, 154].

18s rRNA extraction, sequencing

The details of the RNA extraction and 18s sequencing of the ambient water samples were published previously, but briefly described here. Immediately prior to to RNA was extraction with TRIzol reagent (Life Technologies), each sample filter was "spiked" with one billion copies of each of two commercially available RNA standards (ArrayControl Spot and Spike standards #1 and #8, Thermo Fisher Scientific). Complementary DNA (cDNA) for each sample was prepared with 50 ng total RNA using the SuperScript III first strand synthesis system with random hexamers (Life Technologies) and amplified using an AccuPrime PCR system kit (Life Technologies). The products (2 µl sample, 5 µl no-template control) were gel purified on a 1% agarose gel with subsequent Ampure XP bead (Beckman Coulter) and resuspended in Qiagen elution buffer. The purified cDNA samples were quantified using the PicoGreen Quant-IT assay (Life Technologies). Equal masses (45 ng) of 18S amplicons were pooled for 454 pyrosequencing with TAReuk454FWD1 (5′-CCAGCASCYGCGGTAATTCC-3′) and TAReukREV3 (5′-ACTTTCGTTCTTGATYRA-3′) primers which target a 500 bp region of the v4 region37.

18s rRNA library quality control, emulsion PCR, enrichment and 454 sequencing was done according to the manufacturer's protocol (Roche Diagnostics) with the additional modifications: the KAPA Biosystems library quantification kit for qPCR was used to estimate the number of molecules needed for emPCR, automation (BioMek FX) was used to "break" the emulsions after emPCR and butanol was used for ease of handling during the breaking process. Bead enrichment was automated with a Robotic Enrichment Module

(Roche Diagnostics). 18s rRNA 454 reads were demultiplexed using the Roche/454 Sfffile utility and converted to FASTA format using sff2fastq, followed by primer removal, quality control, trimming and dereplication. Chimeric sequences were removed using USEARCH38 [155], reads were trimmed to a quality score of 10 over a 2-base window, operational taxonomic units were clustered using SWARM39 and classified using FASTA36 from the FASTA package. Taxonomic annotations were assigned using GLSEARCH36 [156] with a modified PR2 database with updates from Tara Oceans W2 [157].

mRNA preparation, sequencing, and bioinformatic workflow

Seawater samples were vacuum filtered onto triplicate 47 mm diameter, 1.2 μm pore size polycarbonate membranes, flash frozen, and stored at -80 C until sample extraction. Total RNA was extracted from filters using a Trizol-RNeasy method with an additional bead beating step. In brief, filters containing previously filtered cells were placed into a tubes of RNase/DNase free 100um zirconia/silica beads with 1mL of Trizol reagent. Each tube was vortexed for 2mins, incubated at room temperature for 5mins, and vortexed for an additional 2mins before following standard Trizol RNA extraction protocol. The upper aqueous phase was transferred to a clean 1.5mL tube with an equal volume of 70% alcohol, mixed, and to QIAgen RNAeasy column. The standard RNeasy protocol was followed with the addition of the optional on-column DNase treatment.

RNA was quantitated using The Qubit® RNA HS Assay, and RNA integrity was determined using the Agilent Bioanalyzer RNA 6000 Pico kit eukaryotic assay. 500 ng of total RNA was used for library prep with Illumina TruSeq RNA Library Prep kit v2 with mRNA selected using Oligo-dT bead capture polyA tails. Library quality was assessed on an Agilent Bioanalyzer and quantified via Qubit before being pooled in equal quantities. The

pooled libraries were sequenced at UC-Davis Genome Center on HiSeq 4000 in lanes of paired-end-150bp flow cell.

Primer and adapter sequences were removed from raw sequencing reads with trimmomatic v0.38 [98]. Paired-end reads were merged with interleave-reads.py from the khmer package v2.1.2 before removal of rRNA reads with sortmeRNA v2.0 utilizing the built in SILVA 16s, 18s, 23s, and 28s databases [158]. Remaining reads were separated (using the deinterleave_fastq.sh https://gist.github.com/nathanhaigh/3521724) and assembled into contiguous sequences (contigs) with megahit v1.1.3 using 'meta-large' setting [159]. Open reading frames (ORFs) were predicted from assembled contigs using FragGeneScan v1.31 [160], and orfs shorter than 150 bp were removed. Reads counts for remaining orfs were estimated using salmon v0.6.0 `quant` quasi-mapping with seqBias and gcBias features.

Orfs were annotated based on best homology (lowest *E*-value) using BLASTP v.2.5.0+ with an *E*-value threshold of $<10^{-3}$. Taxonomic and functional annotations were assigned using the MarineRefII (roseobase.org/data), a custom databased maintained by the Moran Lab at the University of Georgia that includes the sequences from PhyloDB v.1.076—24,509,327 peptides from 19,962 viral, 230 archaeal, 4,910 bacterial and 894 eukaryotic taxa, including peptides from KEGG, GenBank, JGI, ENSEMBL, CAMERA and various other repositories, as well as from the 410 taxa of the Marine Microbial Eukaryotic Transcriptome Sequencing Project (MMETSP)—as well as the associated KEGG functional and NCBI taxonomic annotations through a related SQL database. NCBI taxonomic annotations were further curated [45]; (https://github.com/marchettilab/metatranscriptomicsPipeline) to ensure the use of

consistent taxonomic ranks. KEGG Ortholog (KO) classifications of diatom urea transporters, nitrite reductase, ammonium transporters were manually verified against known gene phylogenies and edited accordingly [95].

Silaffin like genes were identified in *Pseudo-nitzschia multiseries* (CLN-47 v1) genome, as described previously [68], using an initial signal peptide screen of translated nucleotide sequences and subsequence sliding window search for amino acid (AA) sequences containing a 100-2000 long segment with ≥10% lysine and ≥18% serine residues. Full length *P. multiseries* putative silaffin amino acid sequences were subsequently screened for the presence of KXXK motif, with X representing a S or G residue and RXL protease cleavage motif, with X representing a Q, E, R, or K residue. Additional functional annotation was performed using BLASTP with the NCBI nr database (E-value $<10^{-10}$) and KEGG GhostKOALA (score <40). To identify the distribution of these genes in diatoms and other microalgae, BLASTP searchers were performed against a database containing the 67 translated transcriptomes from the MMETSP [102]. After decontamination based on MMETSP databast BLASTP query [161], *P. multiseries* genes with no significant hits (E-value $<10^{-10}$) to non-diatom genes were considered "diatom-specific". This process identified 326 potential *Pseudo-nitzschia* silaffin like (PNSL) genes which were used with BLASTP+ v2.5.0 (E-value $<10^{-5}$) to identify homologous sequences within the metatranscriptome assembly.

Si limitation and production associated, SiLA and SiPA respectively, genes were classified from previously published *Thalassiosira pseudonana* culture experiment data which include two whole transcriptome datasets of recovery from Si-starvation and two whole transcriptome datasets of the introduction of Si-starvation [35, 122, 133]. SiPA genes

were identified based on a >1.75-fold increase in gene expression >4 h post Si replenishment compared to Si-starved samples in both datasets without a similar response to Si starvation. Similarly, SiLA genes were identified based on a >1.75-fold increase in gene expression >4 h post removal of Si from culture medium in both datasets without a similar response to Si replenishment. The response time of >4 h was chosen to filter out genes which only responded during the initial change in $Si(OH)_4$ concentration and to ensure that the change in expression was persistent as the biogeochemical history of a field-site is often unknown prior to sampling.

For genes of interest that did not have an associated KO number, (e.g. silicon transporters (SITs), iron starvation induced proteins, *Pseudo-nitzschia granii* ferritin, silicanin-1 (Sin1), and putative Si Production and Limitation associate genes) manual annotation was performed as previously described [35, 36, 52] using BLASTP+ v2.5.0 best hit with e-value cutoff of 10^{-5}. Putative SIT sequences were further classified to clade designations, using a maximum-likelihood tree constructed from a reference alignment (Durkin et al. 2016) with RAxML version 8.2.12 – PROTGAMMAWAGF substitution model and 100 bootstrap replicates [103]. A HMM profile was constructed from the reference alignment (using hmmbuild 3.2.1) and used with hmmalign to align amino acid sequences corresponding to SIT orfs. Alignment and tree files were packaged using taxtastic v.0.8.3, and SIT orfs were placed on the reference tree using pplacer v.1.1.alpha19 with posterior probability calculated [97]. The most closely related reference sequence was assigned to each SIT orf using guppy v.1.1.alpha19 [97].

Prior to differential expression analysis, raw counts were aggregated within diatom genera by KO number. For genes lacking a KO number, e.g. *SITs*, ISIPs, Sin-1, etc.,

aggregation was done based on gene assignment through KEGG annotation or BLASTX query of supplemental databases. Prior to differential expression analysis, raw counts were aggregated within diatom genera by KO number. For genes lacking a KO number, e.g. SITs, ISIPs, Sin-1, etc., aggregation was done based on gene assignment through KEGG annotation or BLASTX query of supplemental databases. Genus-specific aggregation of functionally annotated reads reduces redundancy and allows the use of tools originally designed for single organism RNAseq analysis (e.g. DESeq2, edgeR). This is necessary for microbial community transcriptomic analysis due to methodological and computational difficulties in resolving species-level, differential transcript expression [34, 45, 104–108]. However, this approach does not resolve species-level contig expression, nor does it *a priori* resolve clade-specific expression patterns for genes that belong to multigene families. In the case of SITs, individual clades were identified through phylogenetic analysis as previously done (Durkin et al. 2012, 2016), and manually annotated to allow interrogation of SIT transcripts at the clade level. Additionally, annotations for urea transporters 1 and 2 were grouped together because of there close phylogenic relationship and shared expression pattern in response to nitrogen supply [95]. A similar approach for other multigene families, such as the ammonium transporters (AMTs) and nitrate transporters (NRT2s) was not used because 1) there are no studies reporting a clade-specific response to Fe limitation and 2) expression of these genes in response to nitrogen supply does not appear to be clade-specific (Smith et al. 2019), thus interrogating clade-level expression patterns of these genes in our metatranscriptomes would be unlikely to yield interpretable results.

Statistical analysis

For metatranscriptome data, normalization, differential abundance, and significance were analyzed within each taxonomic group using edgeR v.3.32.1 [113]. Significance between samples was determined using exactTest with tagwise dispersion and corrected for multiple testing using the Benjamini & Hochberg method, with a significance threshold of FDR <0.05 [114]. Significant differential abundance of genes related to carbon, nitrogen, and silicon metabolism was visualized through heatmaps with an additional expression threshold of ±1.75 fold-change for putative silicon related genes and PNSL genes.

Principle component analysis was performed using the log-transformed normalized counts for the 2500 most variable genes and supplemental environmental data. PCA biplots were created with ggplot2 v.3.3.5 and factoextra v.1.0.7.

Data deposition

All cruise related data can be accessed through the Biological and Chemical Oceanography Data Management Office project number 550825 (https:// www.bco-dmo.org/project/550825). All raw sequence data have been deposited in the NCBI sequence read archive. 18s sequencing data can be accessed under BioProject accession no. PRJNA528986 (BioSample accession nos SAMN11263616– SAMN11263639) and metatranscriptome data can be accessed under BioProject accession no. PRJNA790068 (BioSample accession nos SAMN11263616– SAMN11263639SAMN24193217-SAMN24193233).

Supplemental materials

Supplemental figures

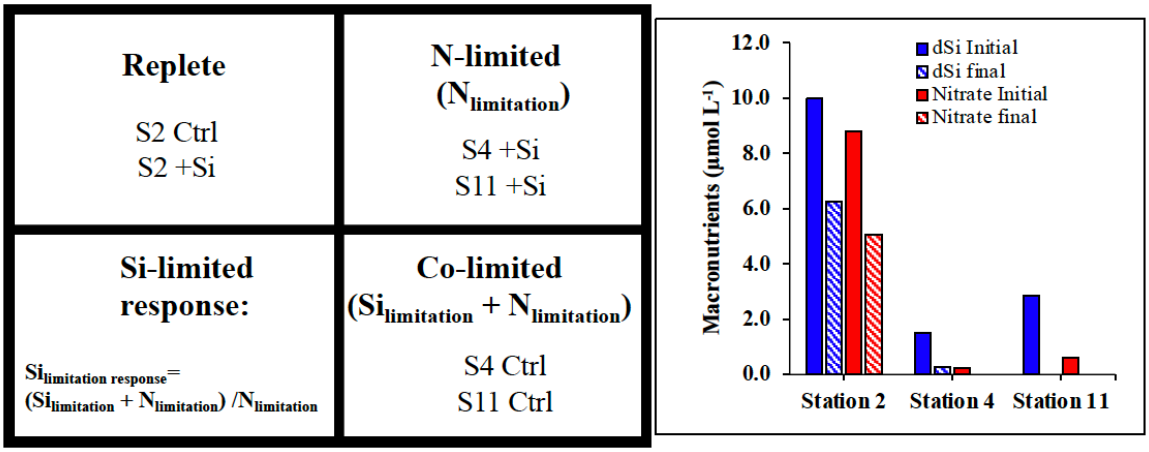

Figure S1: Diagram of macronutrient status of the Ctrl and Si amended (+Si) samples from S2, S4, and S11 paired with initial and final dissolved silicon (dSi) and nitrate concentrations.

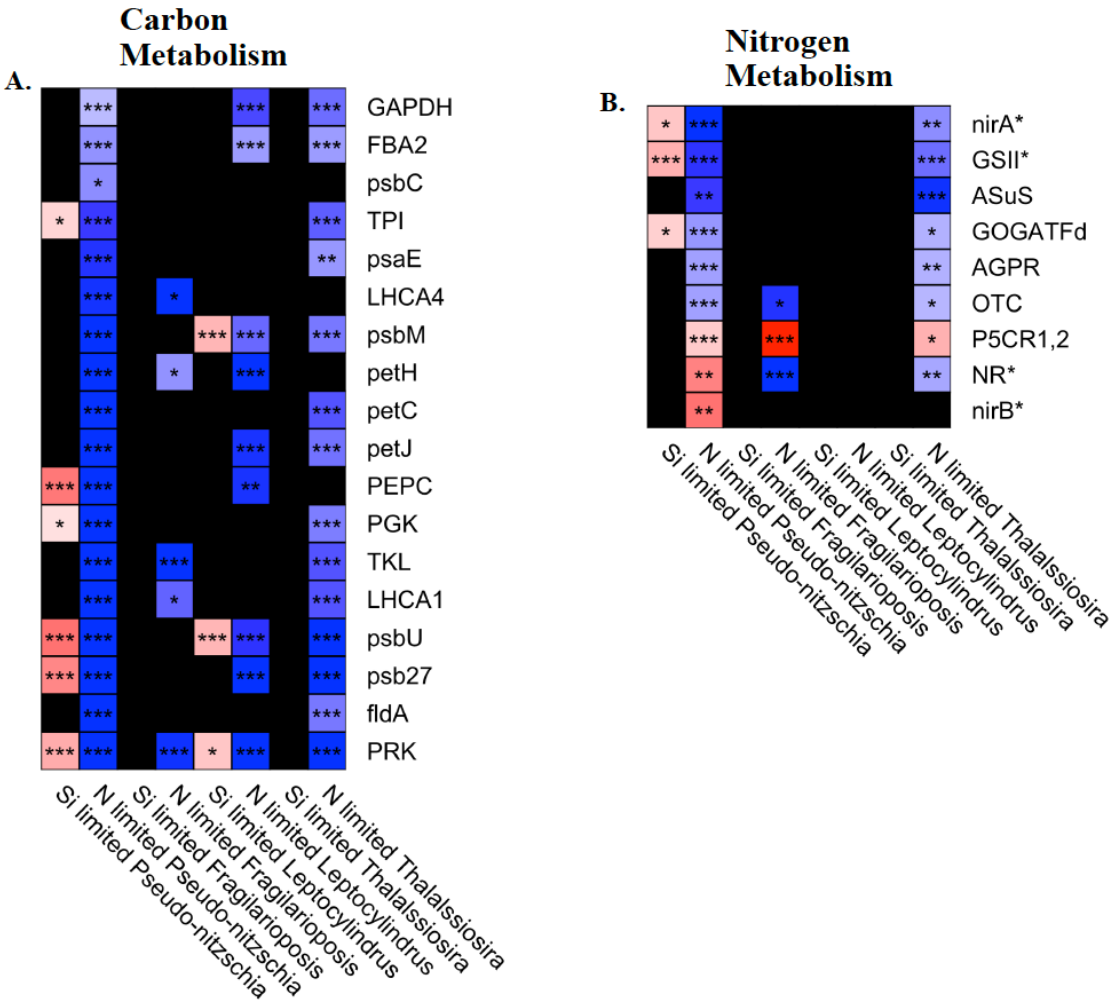

Figure S2: Additional heatmaps of (A) carbon and (B) nitrogen assimilation gene transcript abundance for the diatom genera *Pseudo-nitzschia, Fragilariopsis, Leptocylindrus,* and *Thalassiosira*

Chapter 3: Diatom molecular strategies for acclimating to diminishing light intensity in a dynamic coastal regime

Abstract:

As obligate phototrophs living in the sunlit region of the ocean, phytoplankton must have cellular mechanisms to maintain growth and productivity in response to variable light availability. An actively mixing water column can transport cells from the well-lit upper euphotic zone to much dimmer waters of the lower euphotic zone on timescales of hours, while stratification can restrict cells to a single light regime for several days. As incident irradiance diminishes with depth, so do the light-dependent processes of carbon and nitrogen assimilation. For diatoms, light-limitation can also lead to reduced silica production, which is dependent on respiration of organic carbon compounds primarily obtained through photosynthesis. We employed the ROMS model-based Coastal Upwelling Transport Index, in conjunction with biogeochemical tracers, to characterize the probable degree of mixing at four stations in the California Current Upwelling System to examine the impact of the vertical light gradient on diatom silicon, nitrogen and carbon metabolism. The extent to which diatoms reduced silica production rates and adjusted to low light conditions was investigated using a combination of silica production rate measurements and metatranscriptomic analysis. While all diatom communities exhibited reduced biomass-specific silica production under low-light, there was poor correlation between changes in rates and silicon transporter transcript abundance. Biogeochemical markers of light limitation, such as decreased ratio of chlorophyll a to particulate organic carbon, correlated with reduced transcript abundance of genes related to photosystem II as well as nitrate transport and reduction. In stratified conditions, diatom communities at the base of the

euphotic zone exhibited widespread reduction of transcripts for genes related to light harvesting, photosystem II, photosynthetic electron transport, oxidative phosphorylation, and nitrogen assimilation. However, in less stratified water columns diatom communities exhibited minimal changes in transcript abundance and were likely better poised to deal with rapid changes in light availability.

Introduction:

In eastern boundary currents such as the California Current System, strong upwelling events transport cold macronutrient-rich water to the surface and drive >30 % of annual productivity [117]. When such upwelling events are accompanied with shoaling of the mixed layer (ML) and a proceeding period of relaxation, high phytoplankton productivity can result in high phytoplankton biomass within the surface ocean [162]. Diatoms in particular are well-equipped to respond to the injection of high concentrations of nitrate and silicic acid and initially dominate upwelling-driven phytoplankton blooms [33, 163].

Within a deep ML, strong wind-driven mixing can induce physiological stress by lowering the average light intensity experienced by cells or by creating rapid shifts in light intensity over hours to days as cells are mixed vertically [164]. When substantial stratification and shoaling of the ML occurs, a steep gradient in potential density across the pynocline can serve as a strong barrier to vertical exchange. Such a barrier can separate phytoplankton communities within an actively mixed well-lit surface layer from communities in the poorly-lit lower level of the euphotic zone (EZ) below the ML [165, 166]. Mixing within a shallow ML limits turbidity-based shading and can retain phytoplankton cells at a potentially photodamaging high average light intensity [167]. However, periods of relaxation of winds can contribute to diminished mixing [168, 169] and, similar to the effect of

stratification, disconnect phytoplankton communities at the base of the ML from those at the surface, leaving each at different layers of the EZ and subject to a continuum of quantity and quality of light.

Phytoplankton communities adjust to diurnal changes in light availability through a highly orchestrated regulation of cellular processes [75, 170]. This includes carbon fixation and nitrogen assimilation which, along with cell division, often reach peak rates during the light phase of the diurnal cycle [171, 172]. During periods of saturating light, the light-dependent reactions of photosynthesis produce a surplus of energy, reductant, and carbon compounds that fuel carbon metabolism through the night. Nitrogen assimilation is similarly dependent on reductive capacity from photosynthesis to fuel inorganic nitrate and nitrite reduction and incorporation into organic matter. Light limitation can lead to decreased phytoplankton carbon fixation and lower cell division rates, as well as diminished macronutrient utilization [173–176]. Extended periods of such light limitation can lead phytoplankton cells to become chlorotic with low organic carbon and nitrogen content [37]. In contrast, the production of biogenic silica (bSi) by diatoms is driven by energy produced through respiration, and is not known to be directly dependent on photosynthesis [130, 177]. After as few as 8 h in constant darkness, the diatom cell cycle arrests and bSi production pauses [20, 178] and ceases after 24 h [179]. However, some diatom cells will continue to divide and silicify in the dark if fed certain simple carbon substrates [177, 180].

To maximize light harvesting capacity during periods of low light availability, phytoplankton employ a combination of two strategies: 1) increase the number of photosystem II (PSII) reaction centers and 2) increase the absorptive cross section of PSII by increasing the abundance of light harvesting complexes [181, 182]. However, both strategies

have associated risks as the former strategy has a comparatively higher resource cost and the latter strategy can lead to greater susceptibility to photodamage if cells are suddenly exposed to higher light intensities [182]. In the dynamic California Upwelling Zone (CUZ) where phytoplankton communities encounter shifts from a stratified light environment to rapid mixing within or below the ML, the manner in which diatom cells react to changing light may provide insight into the ability of diatoms to outcompete other taxa after strong upwelling events.

Here, we use physical and chemical measurements to define the structure of the water column, and measures of biomass-specific silica production rates to identify changes in diatom physiology at the base of the EZ. We employed metatranscriptomic analyses to assess depth resolved changes in diatom community carbon, nitrogen, and silicon metabolisms. Specifically, changes in the transcript abundance of light harvesting complex (LHC) and PSII genes were assessed and related to the transcript abundance of macronutrient uptake and reduction genes to evaluate whether diatom communities at the base of the EZ optimize transcriptomic processes to lower available light or remain poised to take advantage of higher light if mixed to the surface.

Results

Physical, chemical, and biological characteristics of the water columns

To investigate the degree that diatom communities altered transcriptomic processes in response to light, seawater was collected in the CUZ during the "*M*olecular *U*nderpinnings of *Si*licification in the *C*alifornia *C*urrent" (MUSiCC) cruise between Oregon and Point Conception (19 April – 2 May 2015; Fig. 1) as previously described [183]. At four stations, S8, S9, S11, and S14, samples were collected at 5 discrete depths within the EZ

corresponding to 55, 36, 14, 5, and 1% of incident irradiance (I_o). The Coastal Upwelling Transport Index (CUTI), a coarse estimate of the vertical transport of water within 1° latitude bins, provided an indication of the physical conditions at each station prior to sample collection [184] with values above 0.5 m^2 s^{-1} delineating upwelling favorable conditions. At all 4 stations, the CUTI exceeded 0.5 m^2 s^{-1} for at least 2 consecutive days prior to sampling

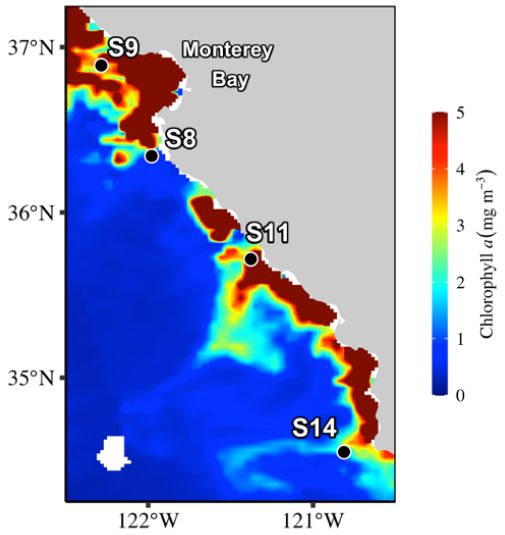

Figure 3-1: Map of coastal California showing sampling sites overlayed on the surface chlorophyll a concentration from level-2 MODIS 8-day average from 15th April- 1st May 2015 (https://giovanni.gsfc.nasa.gov/giovanni/).

(Fig. 2). At S8, S9, and S11, CUTI values exceeded 1.0 m^2 s^{-1} on the day of sampling, and for 2, 3, and 4 days prior, respectively (Fig. 2A-C). In contrast, at S14, CUTI values were >1.0 m^2 s^{-1} six days prior to sampling, but decreased to <0.5 m^2 s^{-1} two days prior to, and on the day of sampling, indicative of a period of relaxation (Fig. 2D). Collectively the CUTI values provide a spectrum of potential vertical mixing regimes present at the stations, with upwelling favorable conditions being absent from S14, intermediate in duration at S8 and S9, and of a longer duration at S11.

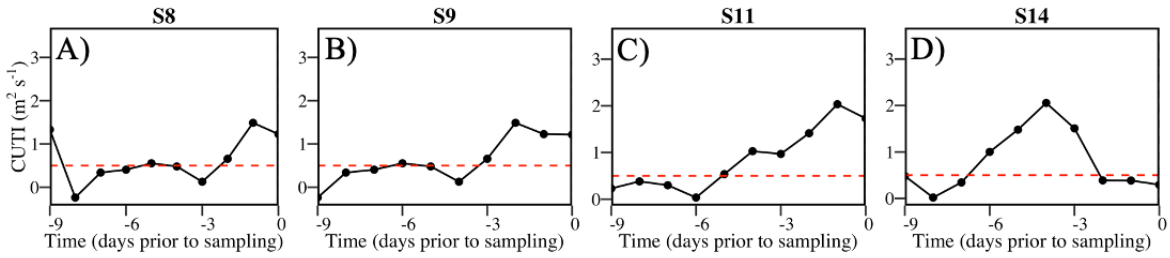

Figure 3-2: The 1˚ latitudinal bins of Coastal Upwelling Transport Index (CUTI) values of the vertical transport of water per meter of coastline ($m^3\ s^{-1}\ m^{-1}$) for the sampling date and 9 days prior at A) S8, B) S9 , C) S11 , and D) S14 . The dashed red line (0.5 $m^3\ s^{-1}\ m^{-1}$) is the threshold value used to delineate upwelling favorable conditions.

At all four stations, the potential density (σ_θ) increased with depth through the EZ rather than remaining near constant as might be expected in a well-mixed water column (Fig. 3A). However, the magnitude of $\Delta\sigma_\theta$ (difference in σ_θ at a particular depth compared to the 0-1m surface bin) and the ML depth (MLD; evaluated by $\Delta\sigma_\theta \geq 0.125$ kg m^{-3}) relative to the EZ depth provide context about the proclivity of the water at the base of the EZ to mix with the surface (Fig. 3B). Based on this MLD thresholding approach, the EZ (11.5 m at S8, 19 ± 1 m at S9 and S11, and 36 m at S14) extended below the MLD at all stations except S11 (Fig. 3B). Furthermore, the magnitude of $\Delta\sigma_\theta$ at the 1% I_o depths sorted the stations in the same manner as the CUTI values with the smallest $\Delta\sigma_\theta$ and lowest stability at S11 (0.088 kg m^{-3}), and progressively higher values at S8 (0.137 kg m^{-3}), S9 (0.184 kg m^{-3}), and S14 (0.265 kg m^{-3}; Fig. 3B).

Increased macronutrient concentrations at the lower depths of S8, S9, and S14 were consistent with incomplete mixing throughout the EZ (Fig. 4A, B, D). At S8 and S9 the concentrations of NO_3^-, 8.8-10 µmol L^{-1}, and $Si(OH)_4$, 4.7-7.5 µmol L^{-1}, remained nearly

constant in the upper EZ (55-14% I_o), indicative of well-mixed water parcels (Fig. 4A-B). At

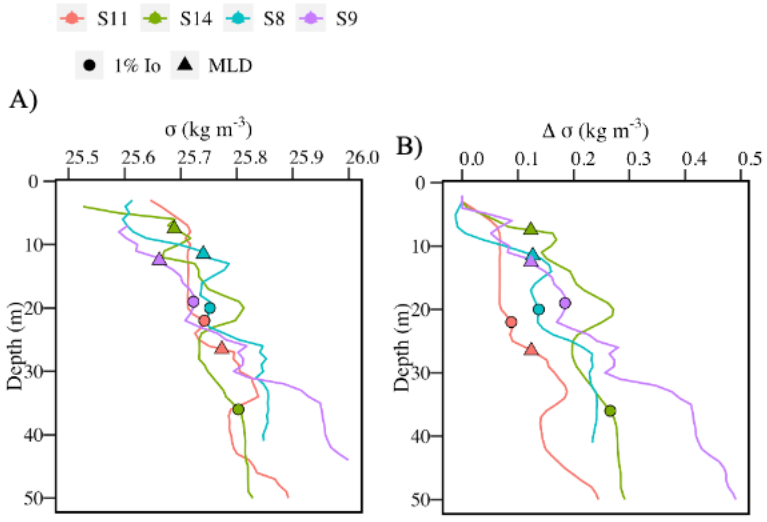

Figure 3-3: Depth profiles of A) density (kg m^{-3}) and B) change in density (Δdensity, kg m^{-3}); at S8 (turquoise), S9 (purple), S11 (salmon), and S14 (green). The filled circles mark the 1% I_o at each station, and the filled triangles mark the mixed layer depth at each station.

those same stations the base of the EZ (5-1% I_o) appeared to cross into the nutricline as NO_3^- and $Si(OH)_4$ concentrations inflected upward to 15.4 ± 0.2 µmol L^{-1} and 14.3 ± 1.1 µmol L^{-1}, respectively, in the higher σ_θ waters (Fig. 4A-B). Similar to S8 and S9, at S14 the surface concentrations of NO_3^-, 15.4 ± 0.4 µmol L^{-1}, and $Si(OH)_4$, 14.5 ± 0.5 µmol L^{-1}, each increased 2.5 and 3.5 µmol L^{-1}, respectively at the lower depths of the EZ (Fig. 4D). The same was not true at S11 where the NO_3^-, 14.5 ± 0.2 µmol L^{-1}, and $Si(OH)_4$, 14.7 ± 1.1 µmol L^{-1}, concentrations remained near constant through the EZ further supporting an actively mixed EZ at this station.

Stations S8, S9, and S11 were characterized by high phytoplankton biomass (Fig. 4E-G). At each of these stations, the upper part of the EZ (55-14% I_o) contained high bSi (3.3-6.3 µmol bSi L^{-1}) and Chl *a* (6.6-12.3 µg L^{-1}) concentrations (Fig. 4E-G). At S8 and S9 the concentrations decreased by 38-55% (bSi) and 47-56% (Chl *a*) at the base of the EZ, but both biomass indicators were nearly uniform with depth at S11 (Fig. 4E-G). Despite these

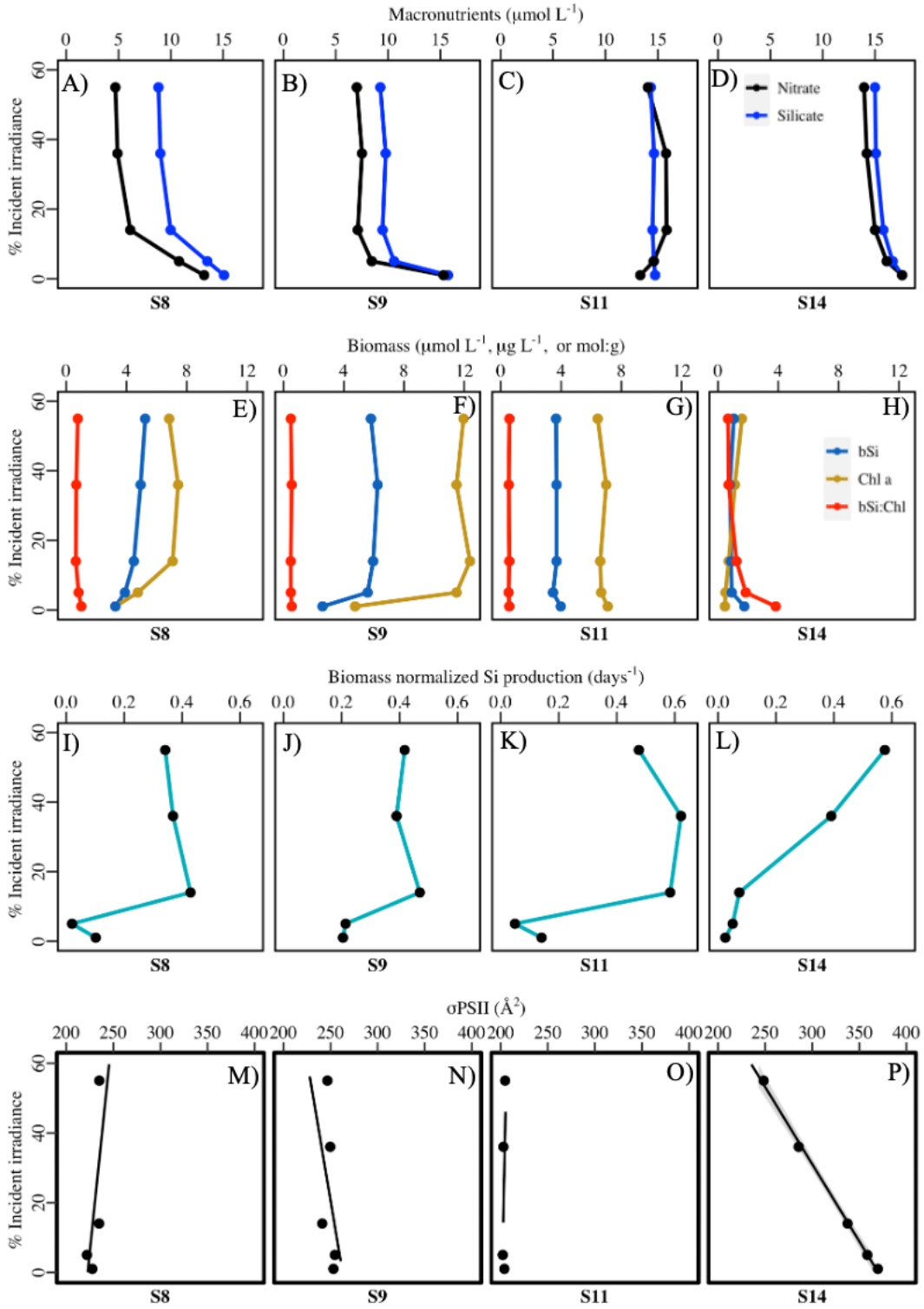

Figure 3-4: Dissolved and particulate characteristics of seawater through the euphotic zone at the four sampling stations. A-D) the concentration of the dissolved macronutrients silicic acid (µmol L^{-1}; blue) and nitrate (µmol L^{-1}; black); E-H) biogenic silica, (bSi; µmol L^{-1}; blue) and chlorophyll a (Chl a; µg L^{-1}; goldenrod), and the ratio of bSi: Chl a (µL:µg; red); I-L) biomass-specific bSi production rate (d^{-1}); and M-P) and the functional absorption cross-section of PSII (σ_{PSII}).

differences among S8, S9 and S11, bSi:Chl *a* , 0.61 ± 0.15 mol g^{-1}, did not vary greatly throughout the EZ (Fig. 4E-G). At S14, surface concentrations of bSi, 1.0 µmol L^{-1}, and Chl *a,* 1.6 µg L^{-1}, were lower than the other stations, but while Chl *a* decreased by 71% to 0.46 µg L^{-1} at the 1% I_o depth, bSi increased by 67% to 1.7 µmol L^{-1} (Fig. 4H). This resulted in elevated bSi:Chl *a*, 3.8 mol g^{-1}, at the base of the EZ (Fig. 4H). Interestingly, Chl *a*:particulate organic carbon (POC) ratios, which often increase or decrease during photoacclimation to low and high light, respectively [185, 186], did not significantly differ between the surface (0.24-0.29 g mol^{-1}) and base of the EZ (0.2-0.31 g mol^{-1}) at S8 or S11 (Table 1). However, Chl *a*:POC was 50% lower at the 1% I_o depth (0.05-0.15 g mol^{-1}) compared to the surface (0.12-0.30 g mol^{-1}) at S9 and S14 (Table 1).

Table 1: Sampling depth (m), percent incident irradiance (I_o), particulate biomass measurements, and particulate biomass ratios of the seawater at the discrete sampling depths at the surface and base of the euphotic zone at each of the four sampling stations. Particulate measurements included chlorophyll a (Chl a) and particulate organic carbon (POC), the latter of which was primarily not measured at intermediate depths within the euphotic zone. The POC samples were run in triplicate or duplicate, except at the 55% I_o of S14 where n=1.

Station	Sampling depth (m)	I_o	Chl a (µg L^{-1})	POC mean (µmol L^{-1})	POC s.d. (µmol L^{-1})	Chl a: POC mean (g:mol)	Chl a: POC stdev (g:mol)
S8	1.2	55	6.83	29.39	7.89	0.24	0.063
S8	19.6	1	3.27	16.99	3.53	0.2	0.037
S9	2.3	55	11.94	39.77	2.27	0.3	0.017
S9	18.1	1	4.75	31.99	2.27	0.15	0.01
S11	1.9	55	6.43	22.83	4.37	0.29	0.059
S11	21.1	1	7.09	23.31	3.82	0.31	0.049
S14	5.4	55	1.58	13.64	n=1	0.12	n=1
S14	15.3	14	0.7	11.42	0.72	0.06	0.004
S14	35.5	1	0.46	9.68	3.04	0.05	0.016

At all stations, the surface waters contained a high proportion of taxonomically annotated diatoms mRNA reads (52-80%, Fig. 5). These proportions were consistent throughout the EZ at S8, S9, and S11. At S14 the proportion of diatom annotated mRNA reads dropped to 26-31% at the base of the EZ, despite increased bSi concentration and bSi:Chl *a* at this depth, possibly indicative of detrital bSi or community quiescence [33]. The

taxonomic breakdown of the diatom-annotated reads were dominated by three common bloom-forming diatom genera, *Thalassiosira* (8-40%), *Chaetoceros* (1-33%), and *Pseudo-nitzschia* (15-74%), which collectively accounted for 59-84% of diatom mRNA reads within all samples (Fig. 5E-H). While the distribution of mRNA reads among these three genera was comparable between S8, S11, and S14, S9 was dominated by a single genus, *Pseudo-nitzschia*, which made up 69-74% of diatom reads throughout the EZ (Fig. 5G).

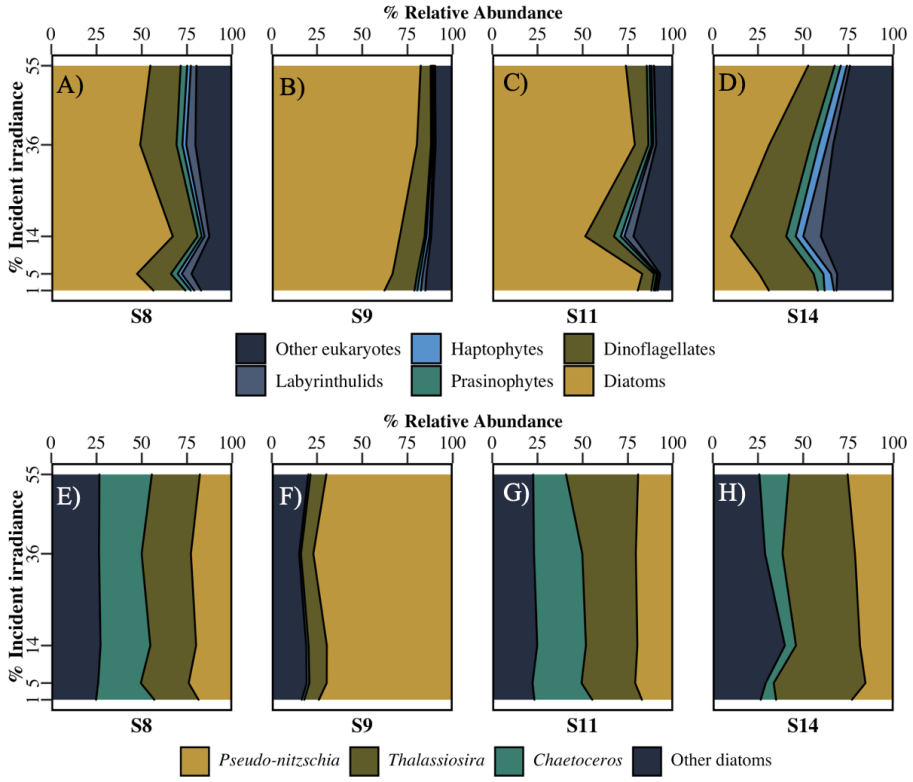

Figure 3-5: Percent relative abundance of annotated mRNA reads A-D) the major phytoplankton groups and E-F) diatom genera present through the euphotic zone at each station. Data shown from mRNA abundance are the average of replicates (n=2 or 3).

Physiological characteristics of the phytoplankton communities

Biogeochemical and biophysical measurements indicated healthy surface phytoplankton communities at all stations. The photosynthetic efficiency, F_v/F_m, was high, 0.51-0.61, throughout the EZ at each station, indicating that the phytoplankton communities were healthy and not experiencing either high-light driven oxidative stress [187] at the

surface or low light stress at depth (Table S1). At each station throughout the EZ, the concentrations of NO_3^- and $Si(OH)_4$ were above levels (>5 µmol L^{-1}) that would be considered kinetically rate limiting within the CUZ [41]. Ambient biomass-specific bSi production rates (V_b) were high, 0.34-0.62 d^{-1}, in the upper part of the EZ (55-36% I_o) and were equivalent to a bSi doubling time of 1.1-2.0 d (Fig. 4I-L). The ratio of V_b and enhanced (+18 µmol L^{-1} dSi; V_{enh}) biomass-specific bSi production measurements at S9 and S14 confirmed that the surface samples did not exhibit signs of kinetic Si-limitation (V_b:V_{enh} > 0.7; Table S1; [151]). V_{enh} was not measured at S8 or S11, but surface $Si(OH)_4$ concentrations at these stations were similar to those at S9 and S14. Despite the presence of ample nutrients, V_b decreased by 48-92% from the upper part of the EZ to the lower part (5-1% I_o; 0.03-0.21 d^{-1}; Fig. 4I-L), implicating low light availability as the underlying driver of the reduced rates. Similar to the concentrations of macronutrients and biomass in the upper EZ, at S8, S9 and S11 the near constant V_b through the changing I_o in the upper EZ was indicative of a well-mixed upper EZ with little effect of I_o phytoplankton physiological. The substantially lower V_b values at the 5 and 1% I_o depth are consistent with elevated $\Delta\sigma_\theta$ at S8, S9, and S11, but corresponded to the elevated macronutrients and lower biomass concentrations at the base of the EZ at only S8 and S9. Additionally, at S14 where $\Delta\sigma_\theta$ at 1% I_o was largest, V_b decreased through all depths rather than just the latter two, indicative of a lack of communication between all sampling depths within the upper EZ. S14 was also the only station where the functional absorption cross section of PSII ($\sigma_{PSII,}$ Fig. 4M-P, Table S1) increased with depth and was significantly correlated (linear model; p = 00018, R^2 = 0.92) to the percent I_o through the EZ (Fig. 4P).

Low light associated changes in transcript abundance

The diatom communities within the four stations employed community-specific modulation of KEGG annotated transcripts coding for the PSII complex and LHC proteins at the base of the EZ relative to the surface. In the well-mixed EZ of S11, diatom transcript abundance of contigs coding for PSII complex genes, including psbU, psbM, psb27, psbQ, psbP, psbO, were more abundant at the base of the EZ compared to the surface (Fig. 6A-B, 8A), and less abundant at the base of the EZ at S9 and S14 (Fig. 6C-D, 8A). At S8 the transcript abundance of diatom contigs coding for LHC genes were predominantly higher at the base of the EZ relative to the surface, but at S14 the opposite was true with LHC transcripts less abundant at the base of the EZ relative to the surface (Fig. 6B,D). At S9 and S11 there was no change in LHC contig transcript abundance through the EZ (Fig. 6C,D).

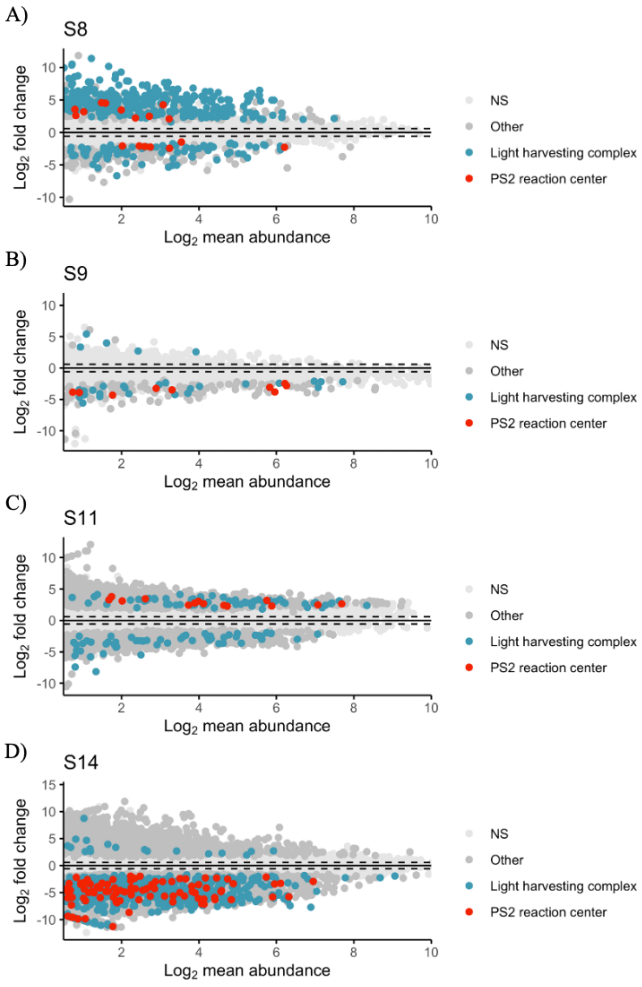

Figure 3-6: Differential abundance (log_2 fold-change) of diatom contigs between samples from 1% I_o (or 5% in the case of S14) and 55% I_o across stations as a function of mean contig abundance. In A-D) the light grey symbols are contigs that are not significantly differentially abundant between depths (NS) and the remaining colors denote genes encoding light harvesting complex proteins (blue), photosystem II reaction center proteins (red), and proteins involved in other cellular processes (dark grey) at stations B) S8, C) S9, D) S11, and E) S14.

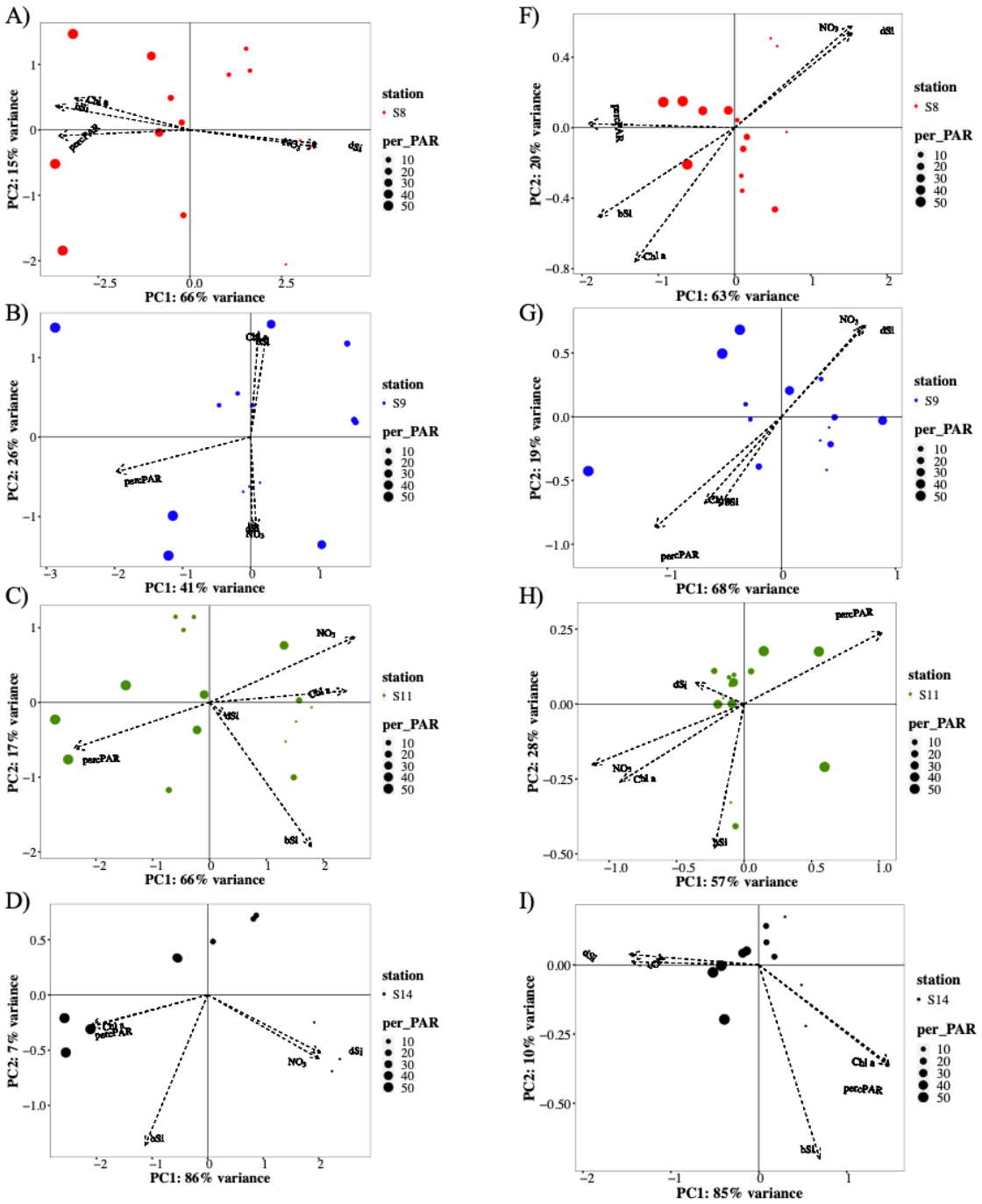

Figure 3-7: Principle component analysis biplot of light harvesting complex gene (A-D) and photosystem II gene (E-I) transcript abundances (loading of principle components) and the relationship with percent of incident irradiance at sampling depth (per_PAR; size of point), and other environmental variables.

Principal component analysis (PCA) of the aggregated normalized transcript abundance of PSII and LHC genes was used to assess where diatom communities progressively modulated transcript abundance of these genes as light diminished. Changes in

PSII gene transcripts throughout the EZ at S8 and S14 explained 63% and 86%, respectively, of the variation along PC1, which was highly correlated with I_o through the EZ at both stations (Fig. 7F,I). Similarly, PCA of the aggregated normalized transcript abundance of LHC genes separated S8 and S14 according to depth along PC1 (7A,D). Within each PCA of LHC transcripts at S8 and S14, PC1 was also highly correlated with changes in I_o and accounted for 66% and 86% of variation in LHC transcript, indicating a strong light-associated response of LHC transcript abundance at S8 and S14 (Fig. 7A,D). No clear separation along an I_o spectrum was evident at S9 and S11 from PCA of LHC or PSII transcript abundance data, indicating that light was not driving the global transcriptomic changes through all depths at these stations. However, PC1 and PC2 may poorly capture the changes in transcript abundance, and associated environmental variables, between any two discreet depths within a station, such as 55% and 1% I_o as they highlight the variation among all depths.

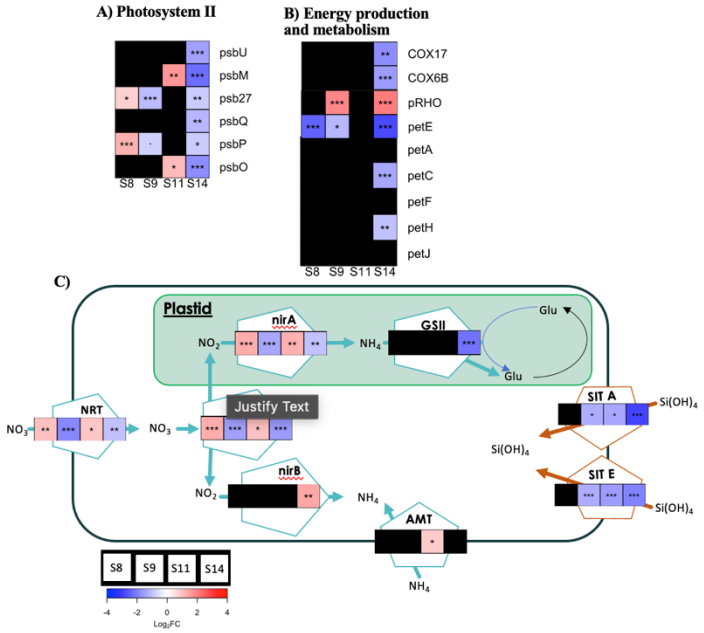

Figure 3-8: The heatmap of differential abundance (log_2 fold-change) of diatom genes (rows) at the four stations (columns) for aggregated mRNA reads for KEGG annotated diatom genes between samples from 1% I_o (or 5% in the case of S14) and 55% I_o across stations. Data from within station comparisons are

Figure 3-8 continued: displayed from left to right as follows S8, S9, S11, and then S14. Black boxes indicate genes that were not differentially abundant in either treatment. Asterisks denotes false discovery rate (FDR); · $p < 0.1$, * $p < 0.05$, ** $p < 0.01$, *** $p < 0.001$ with $p < 0.05$ used as the significance threshold. Gene abbreviations are as follows: A) photosystem II genes: photosystem II M protein (*psbM*), photosystem II oxygen-evolving enhancer protein 1 (*psbO*), photosystem II oxygen-evolving enhancer protein 2 (*psbP*), photosystem II oxygen-evolving enhancer protein 3 (*psbQ*), photosystem II protein U (*psbU*), photosystem II protein 27 (psb27); B) cytochrome oxidase 17 (COX17), cytochrome oxidase 6B (*COX6B*), proteorhodopsin (*pRHO*), plastocyanin (*petE*), apocytochrome f (*petA*), cytochrome b6-f (*petC*), ferredoxin (petF), ferredoxin--NADP+ reductase (*petH*), cytochrome c6 (*petJ*); C) ammonium transporter (*AMT*), nitrogen transporters (*NRT*), ferredoxin-dependent nitrite reductase (*nirA*), NADH-nitrite reductase (*nirB*), nitrate reductase (*NR*), glutamine synthetase II (*GSII*), clade A silicon transporter (SIT A), and clade E silicon transporter (*SIT E*).

Diatom communities at the base of the EZ exhibited progressively broader changes in the abundance of transcripts coding for energy production and metabolism as $\Delta\sigma_\theta$ increased. Transcripts for the photosynthetic electron transport chain protein plastocyanin (*petE*), an analog of cytochrome b_6f, were >2-fold less abundant at the base of the EZ at all stations except S11, which had the smallest $\Delta\sigma_\theta$ at the 1% I_o (Fig. 8B). At S9 and S14, where $\Delta\sigma_\theta$ was indicative of a more stable water column, diatom communities exhibited increased transcript abundance of genes of proteorhodopsin (*pRHO*) genes, which may help supplement energy generation at low light (Fig. 8B). Exclusively at S14, larger scale decreases in diatom transcript abundance for genes involved in carbon metabolism were evident at the base of the EZ. This included a >2-fold decrease in transcripts corresponding to proteins involved in the rate-limiting electron transfer steps of oxygenic photosynthesis, cytochrome b_6f (*petC*; [188, 189]), and oxidative phosphorylation, cytochrome c oxidase (*COX*; [190, 191]) at the base of the EZ compared to surface samples (Fig. 8B,C, E).

Lower available light also coincided with changes in transcript abundance of genes related to macronutrient utilization. Transcripts of nitrate transporters (NRT), nitrate reductase (NR), and ferredoxin- and NADH- dependent nitrite reductase (nirA, nirB) genes, were >2-fold more abundant at the base of the EZ compared to the surface at S8 and S11, but

>2-fold less abundant at S9 and S14 where $\Delta\sigma_\theta$ was larger at the base of the EZ (Fig. 8C). At S14 transcripts of nirB and glutamine synthetase (GSII) genes were >2-fold more and less abundant, respectively, at the base of the EZ relative to the surface, but these genes were not differentially abundant at other stations (Fig. 8C). Corresponding with decreased bSi-specific production rates, at S9, S11, and S14 diatom transcripts of clade A and E silicon transporters (SITs), which are specific to the pennate and Thalassiosirales diatoms lineages, respectively, were >2-fold less abundant at the base of the EZ (Fig. 8C). However, no SIT genes were differentially abundant at the base of the EZ at S8 (Fig. 8C), and clades B, C, and D, were not differentially abundant at the base of the EZ relative to the surface at any of the 4 stations sampled (Fig. 8B).

Discussion:

Spectrum of stability through the EZ present among stations

Figure 9 summarizes the physical, biophysical, and biogeochemical measurements for the four stations and reveals a spectrum of stability and water mass history within the EZ across stations. At S11 the lower $\Delta\sigma_\theta$ at 1% I_o delineated this station as the only one with a MLD below the EZ. The positive and strong upwelling favorable conditions at S11 on the day of and 4 prior days to sampling combined with the near constant macronutrient and biomass concentrations through depth were collectively indicative of a well-mixed EZ. The EZ of stations S8 and S9 appeared to be more stratified than S11 based on progressively higher $\Delta\sigma_\theta$ values at S8 and S9 and weaker and shorter duration upwelling favorable conditions compared to S11. Additionally, at S8 and S9 the nutricline depths and decreased biomass concentrations at 5% Io and below were indicative of incomplete mixing through the lower depths of the EZ. At S14 the $\Delta\sigma_\theta$ at 1% I_o was indicative of the most substantial

physical barrier to mixing of the four stations. Additionally, the CUTI values at S14 were indicative of a period of relaxation from wind driven vertical mixing on the day of and 2 days prior to sampling. Not only were the variable macronutrient and biomass concentrations through the EZ at S14 representative of a poorly mixed EZ, but the physical history based on CUTI in addition to the high macronutrient concentrations, relatively low biomass concentrations, lower proportion of diatom mRNA reads below the surface [33], and potentially detrital dominated biomass at the base of the EZ, seemed indicative of a water column at the early stages of post upwelling bloom development.

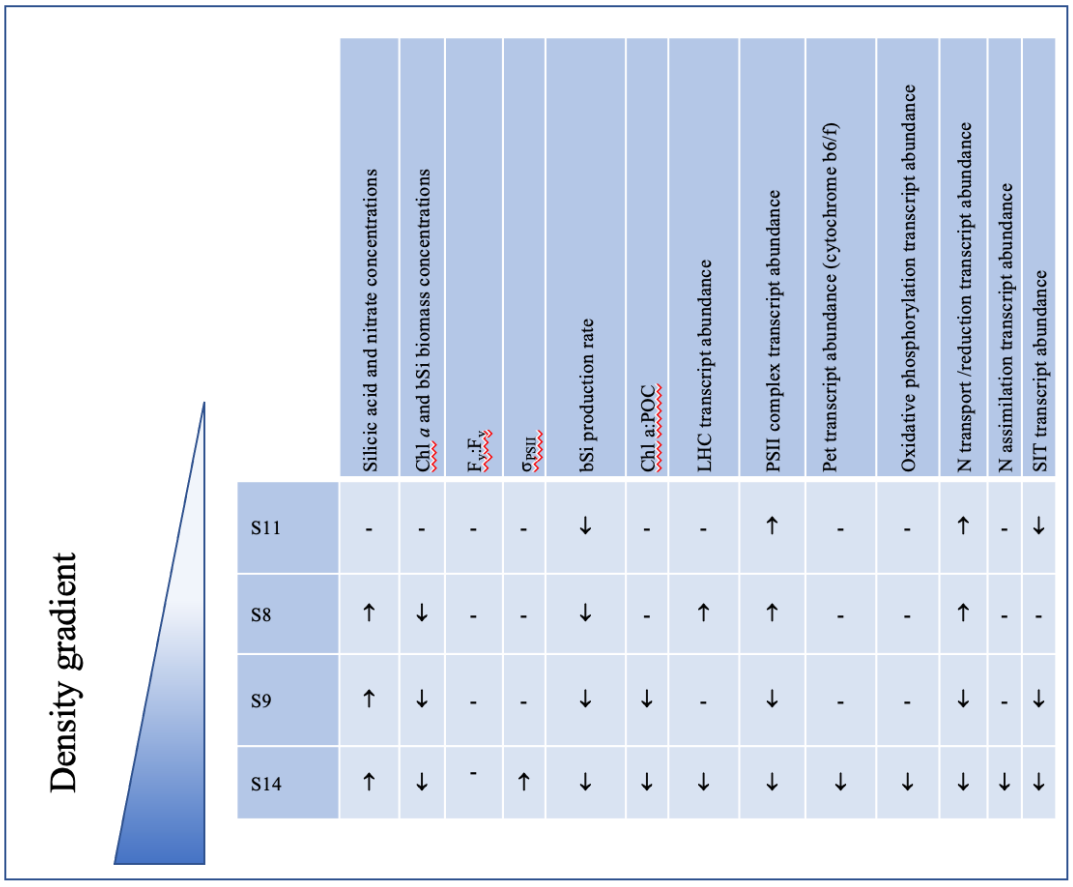

Figure 3-9: Diagram describing the relationship between change in density (Δdensity) and the biogeochemical and physiological measurements at the surface (55% I_o) and base of the EZ (5-1% I_o). Upward facing arrows represent increased values at depth relative to the surface, downward facing arrows represent decreased values at depth relative to the surface, and dashes represent no change.

Silica production rates were particularly sensitive to light limitation

The biomass-specific bSi production rates were at least 48% lower at the base of the EZ compared to the surface at all four stations, despite substantial differences among sites in transcriptomic changes, photoacclimation strategies, and physical connectivity between the surface and depth. The decrease in V_b does not come as a surprise as silicification is tightly linked to cell division [65, 192], which decreases and eventually halts under light limitation and deprivation [20, 178, 179, 193]. However, the magnitude of changes in bSi production at the base of the EZ did not correlate with any transcriptomic changes in silicon uptake or photosynthesis, highlighting the disconnect between silicon metabolism and the light dependent process of photosynthesis [65]. In particular, clade A and E SIT transcript abundances were lower at the base of the EZ relative to the surface at all stations except S8, but the reported V_b values at the base of the EZ at S8 were among the lowest measured. There is evidence that SITs are post-transcriptionally regulated [73, 194], and at least in some cases there does not appear to be a relationship between SIT transcription and bSi production in diatom communities (Maniscalco et al. 2022). There is currently a lack of mechanistic understanding of if and how silicon metabolism is controlled on the transcriptomic level in diatoms [195], as well as in other silicifying organisms, but future exploration of the genetic control of silica production may be able to elucidate a light-associated transcriptomic control of silica production.

Difficulties in interpreting and connecting biomass-specific bSi production rates to molecular measurements also exist, in part, from the interspecies variation in bSi production and the necessary biomass-normalization of gross production rates. Similar to other rate measurements, the biomass concentration used for normalization of bSi production rates may

contain varying proportions of active cells, inactive cells, and detrital matter; the latter two leading to underestimates of specific-production rates. Estimates of detrital bSi range from near zero to 80% of the total pool, underscoring the uncertainty that can be introduced, particularly in less active communities [152]. Within a community of active diatom cells, the amount of bSi per unit area of diatom frustule and the rate of new frustule production can vary as much as an order of magnitude between species [53]. Therefore, changes in diatom community composition can complicate the assessment of differences in physiology based on comparisons between bulk production rates from discrete samples. However, the diatom communities did remain stable at the genus level through depth at each station within this study, limiting the influence of interspecific diversity.

Differing shifts in allocation of transcript related to photo-acclimation

The phytoplankton communities at the base of the EZ at the two less stratified stations, S8 and S11, maintained light absorbing capability at the lower light irradiances not evident in the more stratified stations (S9 and S14). In some cases light-limited phytoplankton communities [196] and diatom cultures [185, 186] have been reported to increase σ_{PSII}, Chl *a*, and Chl *a*:POC under low light. These changes allow cells to maximize light absorption and minimize the impact of light limitation [182, 197], but changes in pigment and LHC concentrations are slow and can take days to reach a new equilibrium [185, 186]. With the comparatively lower stability of S8 and particularly S11, where the 1% I_o was within the ML, the duration of light limitation may not have been prolonged enough to induce an increase in σ_{PSII} or Chl *a*. However, the increase in diatom LHC transcript abundance at 1% I_o of S8 (Fig. 6B), the more stratified of this pair of stations, may be indicative of an increasing degree of light limitation. The higher diatom LHC transcript

abundance without an increase in σ_{PSII}, may be related to a time lag between transcription and LHC protein expression driven by post-transcriptional regulation of LHC protein expression as has been reported in phytoplankton [198].

The diatom communities at base of the EZ at S11 exhibited elevated transcript abundance of PSII reaction center genes in response to low incident irradiance (Fig. 6D), potentially as an alternative strategy of increasing energy absorbing capacity without increasing the relative area of the absorptive cross section of each PSII reaction centers [199]. An increase in PSII reaction centers while maintaining σ_{PSII} limits the drop in photosynthetic rates under potential future exposure to photoinhibiting light intensities compared to increasing σ_{PSII} [182]. The lower photoinhibition risk associated with this strategy may more adequately serve the communities at 1% I_o at S11, which is less stratified. The higher transcript abundance for PSII reaction center genes was accompanied by increased transcript abundance of inorganic nitrogen transport and nitrate reduction reflective of the link between photosynthesis and nitrate reduction [200, 201]. However, changes in transcript abundance did not extend to genes related to the assimilation of reduced nitrate or the rate limiting steps of photosynthetic or oxidative phosphorylation electron transport chains. The narrow rather than widespread set of transcriptomic changes under low light growth, is comparable to that of *Fragilariopsis kerguelensis* cultures maintained in a 24 h low-light cycle [149], and may keep diatom cells poised to readily take up and process nitrate while minimizing photodamage and limiting the need for wider metabolic restructuring upon return to higher I_o. Such a strategy may be particularly helpful for short- to medium- term light limitation in a physically dynamic regime such as the CUZ.

Shared responses to low incident irradiance

Substantial reductions in Chl *a*:POC were evident at the two more stratified stations, S9 and S14, but were unchanged at the less stratified S8 and S11 implying that stronger stratification resulted in severely light limited diatom communities at the base of the EZ. Other culture based diatom studies have shown that as little as 24 h of light deprivation can induce cell cycle arrest [202], and even regular exposure to sub-saturating light (1-3 h of 20 μmol m^{-2} s^{-1} per photoperiod) is not enough to prevent cell cycle arrest and reduction in Chl *a* content [193]. Nutrient limitation has the potential to similarly effect the Chl *a*:POC of phytoplankton communities [203, 204], but at S9 or S14 the macronutrient concentrations and F_v/F_m were not at levels indicative of macronutrient limitation. While shifts in community composition toward a more heterotrophic community could also explain part of the observed decreases in Chl *a*:POC at S14, at S9 the taxonomic fingerprint of the communities, based on mRNA reads, were comparable at 55% and 1% I_o. Unlike the short term increased Chl *a*:POC observed in phytoplankton photoacclimating to growth at lower light irradiance [185, 186], longer term (1-9 days) light deprivation of diatom and haptophyte cultures [38] and quiescent field communities [33] exhibit decreased Chl *a*:POC comparable in magnitude to the ~2-fold reduction observed at S9 and S14 within this study. Based on the physical stratification, nutrient replete characterizations, and reduced Chl *a*:POC, it seems likely that the lower depths of the EZ at S9 and S14 were severely energy limited possibly due to prolonged lack of adequate light intensity and/or duration.

The diatom communities at the base of the EZ at S9 and 14 exhibited changes in transcript abundance that were unique from the less stratified stations S8 and S11. At S9 and S14 diatom communities exhibited lower abundance of diatom transcripts of PSII complex genes, similar to the transcriptomic response of *Phaeodactylum tricornutum* to prolonged

darkness [146]. This is potentially indicative of reduced growth rate and likely related to the greater degree of light limitation present relative to the low light communities at S8 and S11. The proteins associated with PSII complexes in diatoms become inactivated when exposed to saturating light-intensities and the associated proteins are rapidly turned over [205], longer periods of light limitation would yield reduced photoinactivation and lower demand for production of new PSII proteins and related transcripts. The diatom communities at the base of the EZ at S9 and S14 also exhibited lower transcript abundance for inorganic nitrogen acquisition and reduction genes, again underscoring the link between photosynthesis and nitrogen acquisition [201].

The two more severely energy-limited communities at the base of the EZ at S9 and S14 also exhibited signs of increased rhodopsin-based phototrophy. Diatoms as well as other microbial eukaryotes possess a retinal-based proteorhodopsin gene (pRHO), homologous to bacterial green light absorbing rhodopsins [206, 207]. Prior *in silico* work investigating diatom pRHOs amino acid sequence secondary structure has deemed it highly likely that pRHO genes encode light-driven proton pumping rhodopsins which generate supplemental energy for metabolism and growth [25, 207, 208]. Culture-based diatom studies have shown that pRHO transcription is elevated under Fe- and low-light-based growth limitation [149, 207]. It seems likely that the increased diatom transcript abundance of pRHO genes at the base of the EZ of S9 and S14 may be linked to a strategy to generate supplemental light-driven energy and mitigate the severe light limitation exhibited by these communities.

The phytoplankton community at the base of the EZ at S14, the station with the greatest physical barrier to mixing between the surface and lower depths, exhibited additional physiological changes associated with extended light deprivation. At S14 the absorptive cross

section of PSII at the base of the EZ was nearly twice that of the surface suggestive of a long-term photoacclimation response [182, 209, 210]. The phytoplankton community at the base of the EZ also exhibited signs of deeper metabolic quiescence through the lower abundance of transcripts for light harvesting complex proteins, nitrogen assimilation (glutamine synthetase), and the genes corresponding to the rate limiting steps of photosynthetic and oxidative phosphorylation electron transport chains.

Implications for diatom response to variable mixing regimes

Aligning transcriptomic responses to light in discrete samples is complicated by the dynamic nature of the upper water column. In particular, within the shallow euphotic zones of this study, internal waves, which have been measured to be ~4 m in the California Upwelling system during late spring [211], can produce order-of-magnitude changes in the light intensity within the pycnocline near the base of the EZ creating large discrepancies between the light intensity measured when a community is sampled and the longer-term light history of that community. While all communities at the base of the EZ within this study exhibited decreases in biomass-specific bSi production rates and signs of light limitation, station specific responses to low light differed substantially and were likely driven by the duration and intensity of light deprivation.

Despite these complexities the patterns of biogeochemical and physiological changes from the less stratified S11 to S8, S9, and the most stratified S14 appeared to reflect different stages of progression into severe energy limitation. While the less stratified communities at the base of the EZ of S11 and S8 possessed higher abundance of transcripts of PSII genes, nitrate acquisition, and nitrate reduction and remained poised to return to the surface, communities at the base of the EZ at the more stratified stations appeared to progress into

quiescence and decrease the abundance of transcripts for those same genes. The quicker and more extensive transcriptional changes and associated metabolic plasticity, relative to other taxa, may allow diatoms to more quickly recover from both short and long term light limitation and take advantage of available resources upon return to saturating light irradiance [33, 38, 193].

Methods:

Samples were collected during the "Molecular Underpinnings of Silicification in the California Current" MUSiCC cruise onboard the R/V Oceanus (OC1504A; 19 April to 1 May 2015; Chief Scientist: Kimberlee Thamatrakoln). Nearshore stations were sampled along the coast of California from Point Reyes to Point Conception from 44°N to 34°N [183]. Stations with moderate to high biomass that also represented a gradient of macronutrient concentrations were targeted based on satellite derived ocean color and sea surface temperature(MODIS Level-2 products, NASA) and the vessel's underway data acquisition system. Subsampling of shipboard underway seawater for near-real-time microscopic and dissolved silicon analyses provided an indication of diatom abundance.

Sampling occurred just after local sunrise using a CTD rosette system equipped with twelve 10-L Niskin bottles, Sea-Bird Electronics conductivity-temperature-depth sensor, Chelsea fluorometer, and photosynthetically active radiation (PAR) sensor from Bio-Spherical Instruments. Seawater was collected at discrete depths corresponding to 55, 36, 14, 5, and 1% I_o to assess differences in phytoplankton physiology at different levels of light availability within the euphotic zone. Niskin bottles were immediately drained and pooled into acid-washed carboys, shaded, and subsampled for chlorophyll, biogenic silica, dissolved silicon, silica production, macronutrient, biophysical, and molecular (RNA) analyses. Mixed

layer depth was determined using a 0.125 kg m^{-3} threshold of change in density ($\Delta\sigma_\theta$) from the surface, 0-1m bin, value similar to previous studies within this region as well over the global ocean [127, 212, 213].

Dissolved and particulate analyses

Seawater samples for dissolved nutrient analysis ($Si(OH)_4$, NO_3+NO_2, PO_4^{-}) were syringe filtered through 0.6 µm polycarbonate filters and stored at -20°C. Samples for NO_2^{-} + NO_3^{-}, and PO_4^{-3} were processed post-cruise at the University of California Santa Barbara Analytical Lab on a Lachat flow injection system [85]. Samples for biogenic silica (bSi) measurements were collected by filtration onto 0.6 µm polycarbonate filters and stored at -20°C until analysis. The bSi samples were digested shipboard with 0.2 N NaOH in Teflon® tubes [152], and measured, alongside dSi using the ammonium molybdate colorimetric assay [153]. Seawater for chlorophyll measurements were vacuum filtered onto 5 µm pore-size HAWP membrane filters and stored at -20°C. Chlorophyll *a* was extracted with 90% acetone at -20˚C for 24 h and quantified on a Turner Designs 10-AU fluorometer using the acidification method [85, 154].

Silica production rate measurements

Community bSi production rates were measured using the radiotracer ^{32}Si to assess the degree that ambient $Si(OH)_4$ concentration may have limited the bSi production of the phytoplankton communities at each sampling depth within the euphotic zone. Incubations consisted of an unamended control (Ctrl) and an 18.0 µmol L^{-1} $Si(OH)_4$ amendment (+Si) to presumably saturate Si production [118]. Both incubations were set up in 250 mL polycarbonate bottles, filled to the top with 304 mL of water, spiked with 262.8 Bq of high-specific activity ^{32}Si (15,567 Bq μg^{-1} Si). Following radiotracer addition bottles were placed

in neutral-density screened bags within surface water-cooled deckboard incubators to simulate the light level at the depth of collection. Radiotracer samples were filtered onto 25 mm, 1.2 μm pore-size polycarbonate filters and processed for ^{32}Si activity using a low-level beta counter according to Krause et al. (2011). Gross Si production rates (ρ in μmol Si L^{-1} d^{-1}) were normalized to bulk bSi (μmol Si L^{-1}) to obtain biomass-specific rates (V_b, d^{-1}).

Coastal Upwelling Transport Index

The Coastal Upwelling Transport Index (CUTI) was used to assess the timing and strength of nearshore event-scale upwelling for the 10 days prior to sampling at a given site. Similar to the well-known Bakun index, the CUTI uses a combination of geostrophic and Ekman transport to estimate the total volume of upwelled (positive values) or downwelled (negative values) water into or out of the surface layer over a given time period—volume of vertical transport per meter of coastline per day [184]. The CUTI measurements were calculated in 1-degree longitudinal bins, along the California coastline. Positive Coastal Upwelling Transport Index values are the result of equatorward wind stress and indicate upwelling favorable winds, whereas negative values indicate downwelling favorable conditions. While any positive CUTI values are indicative of upwelling favorable conditions, a higher threshold of 0.5 m^2 day^{-1} was applied because of potential high spatial variability within the 1-degree bins and the limited geographic scale of sampling.

Biophysical measurements

The minimum, F_o, and maximum, F_m, fluorescence yield of photosystem II and the relative measure of the functional absorption cross-section of PSII (σ_{PSII}) were measured from low light adapted water samples using a custom Fluorescence Induced Relaxation (FIRe) system [110–112]. The variable fluorescence F_v was calculated as the difference

between F_m and F_o and the maximum efficiency of photosystem II (photosynthetic efficiency; F_v/F_m) was calculated as $F_v/F_m = (F_m - F_o)/F_m$. The FIRe measurements were taken from a single turnover saturating flash (20,000 µmol photons m^{-2} s^{-1}) of a 450nm LED, single turn over flash sample delay 100 µs, 50 samples, 100 µs single turn over flash (STF), 40 single Turnover Relaxation Phase (STRP), and 60 µs single turnover relation interval (STRI). Measurements were blank corrected with 0.2 µm filtered seawater.

RNA sampling extraction and sequencing

Biomass for RNA extraction was collected in triplicate from 0.4-2.4L of seawater through vacuum filtration onto 47 mm, 1.2 µm pore-size polycarbonate membrane filters. Samples were flash frozen in liquid nitrogen and stored at -80 C until sample extraction.

For total RNA extraction, filters were transferred into vials containing 1 mL of Trizol, RNase/DNase-free ,100 µm zirconia/silica beads and1-billion copies each of Array Control Spots and Spikes RNA standards 1 and 8 (Ambion) to allow for quantification of contigs in reads L^{-1}. Tubes were vortexed for 2 min, incubated at room temperature for 5 mins, and vortexed for an additional 2 mins prior to following the standard Trizol-RNeasy extraction protocol with the addition of the on-column DNase treatment. The Qubit® RNA HS Assay was used to determine RNA concentrations and Agilent Bioanalyzer RNA 6000 Pico kit eukaryotic assay was used to determine RNA integrity. Libraries were prepared with 500 ng of total RNA using TruSeq RNA Library Prep kit v2 with mRNA selected using Oligo-df bead capture polyA tails. Individual library quality was determined using an Agilent Bioanalyzer, quantified via Qubit, pooled in equimolar concentration, and quality checked again on an Agilent Bioanalyzer. The pooled libraries were sequenced at UC-Davis Genome Center on a NovaSeq S4 instrument on one lane of a paired-end-150bp flow cell.

RNA-Seq Assembly, Annotation, and Analysis

Raw sequencing reads were initially processed with fastp v.0.19.7 to remove primer and adapter sequences [214]. Trimmed paired-end (PE) reads were assembled into contiguous sequences (contigs): in brief: PE reads were merged with interleave-reads.py, rRNA reads were removed with sortmeRNA v2.0 utilizing the built in SILVA 16s, 18s, 23s, and 28s databases [158], remaining reads were separated back to paired-end reads using the deinterleave_fastq.sh (https://gist.github.com/nathanhaigh/3521724), and assembled into contigs with megahit v1.1.3 using 'meta-large' mode [159]. Predicted open reading frames (ORFs) were identified within assembled contigs using FragGeneScan v1.31 [160], and orfs shorter than 150 bp were removed. Reads counts for remaining orfs were quantified using salmon v0.6.0 `quant` quasi-mapping with seqBias and gcBias features [215].

Taxonomic and functional annotations were assigned based on lowest *E*-value ($<10^{-3}$) using BLASTP v.2.5.0+ and the MarineRefII reference database (roseobase.org/data), a custom database maintained by the Moran Lab at the University of Georgia that includes the sequences from PhyloDB v.1.076—24 ,509,327 peptides from 19,962 viral, 230 archaeal, 4,910 bacterial and 894 eukaryotic taxa, including peptides from KEGG, GenBank, JGI, ENSEMBL, CAMERA and various other repositories, as well as from the 410 taxa of the Marine Microbial Eukaryotic Transcriptome Sequencing Project. KEGG functional and NCBI taxonomic annotations were associated with orfs through related .sql tables within the MarineRefII database and NCBI taxonomic annotations were curated according to Cohen 2017; (https://github.com/marchettilab/metatranscriptomicsPipeline). Diatom genera that

accounted for <5% of total reads in the metatranscriptome were consolidated as “other diatoms”.

Genes presented in diatom photosystem II and photosynthetic electron transport chain genesets were based on KEGG pathways or modules for the diatoms *Thalassiosira pseudonana, Phaedactylum tricornutum*, and *Fragilariopsis cylindrus.* The genes encoding transcripts for without KO identifiers, such as marnavirus RDRP, silicon transporters (SITs), silicanin-1 (Sil-1), putative Pn silaffin-like genes (Maniscalco et al. in 2022), and putative Si Related Genes, were manually annotated as previously described [36, 52, 216] using BLASTP v.2.5.0+ based on best hit with e-value cutoff of $<10^{-5}$. To assign clade designations to putative SIT orfs, a maximum-likelihood tree was created from a reference alignment (Durkin et al. 2016) with RAxML version 8.2.12 – PROTGAMMAWAGF substitution model and 100 bootstrap replicates [103]. Amino acid sequences corresponding to SIT orfs were aligned (using hmmalign v3.2.1) to the reference alignment with an HMM profile constructed with hmmbuild v3.2.1. SIT orfs were placed on the reference tree with posterior probability calculated using pplacer v.1.1.alpha19 [217]. The most recent common ancestor of putative SIT orfs were assigned using guppy v.1.1.alpha19 [217].

Prior to differential expression analysis, raw counts were aggregated within diatom genera by KO number. For genes lacking a KO number, e.g. *SITs*, ISIPs, Sin-1, etc., aggregation was done based on gene assignment through KEGG annotation or BLASTX query of supplemental databases. Group (e.g. diatoms and dinoflagellates) and genus-specific aggregation of functionally annotated reads reduces redundancy and allows the use of tools originally designed for single organism RNAseq analysis (e.g. DESeq2, edgeR). This is necessary for microbial community transcriptomic analysis due to methodological and

computational difficulties in resolving species-level, differential transcript expression [34, 45, 104–108].

Statistical analysis

For metatranscriptome data, normalization, differential abundance, and significance were analyzed within each taxonomic group using edgeR v.3.32.1 [113]. Significance between samples was determined using exactTest with tagwise dispersion and corrected for multiple testing using the Benjamini & Hochberg method, with a significance threshold of FDR <0.05 [114]. Linear regressions between variables were run using the *lm* function from the stats v.3.6.2 package in R. Principle component analysis was performed using the log-transformed normalized counts for the 2500 most variable genes and supplemental environmental data. PCA biplots were created with ggplot2 v.3.3.5 and factoextra v.1.0.7.

Data deposition

All cruise related data can be accessed through the Biological and Chemical Oceanography Data Management Office project number 651685 (https:// www.bco-dmo.org/project/651685). All raw sequence data have been deposited in the NCBI sequence read archive. Metatranscriptome data can be accessed under BioProject accession no. PRJNA790632 (BioSample accession nos. SAMN24217379 – SAMN24217438).

Acknowledgements:

We acknowledge funding from the National Science Foundation (OCE-1334387 to M.A.B and OCE-1333929 to K.T). We thank the captain and crew of R/V Oceanus. Computing resources were administered by the Center for Scientific Computing (CSC) with funds from the National Science Foundation (CNS-1725797). The CSC is supported by the California NanoSystems Institute and the Materials Research Science and Engineering Center (MRSEC;

NSF DMR 1720256) at UC Santa Barbara. We would also like to thank Janice Jones, Heather McNair, and Christopher Johns for assistance during the cruise as well as Nicole Wagner and Jason Lathom for sample preparation.

Supplemental Materials:

Table S1: Mixed layer depth (MLD), percent incident irradiance (I_o), biogeochemical measurements, and photophysiological parameters of the seawater at the discrete sampling depths within the euphotic zone at each of the four sampling stations. Measurements included silicic acid ($[Si(OH)_4]$), nitrate+nitrite ([N+N]), orthophosphate($[PO_4]$), chlorophyll a (Chl a), and biogenic silica (bSi) concentrations, biomass-specific bSi production rate (V_b), Si stress ratio (V_{amb}: V_{enh}), the maximum photosynthetic efficiency of PSII (F_v:F_m), the functional absorption cross-section of PSII (σ_{PSII}), and change in seawater density from surface value ($\Delta\sigma$). The letters NM denote when no measurement was taken at site and/or depth.

Station	MLD	Sampling depth	I_o	$[Si(OH)_4]$ (µmol L^{-1})	[N+N] (µmol L^{-1})	$[PO_4]$ (µmol L^{-1})	Chl a (µg L^{-1})	bSi (µmol L^{-1})	V_b (d^{-1})	V_{amb}: V_{enh}	F_v:F_m	σ_{PSII}	$\Delta\sigma$
S8	11.5												
		1.2	55	4.7	8.81	0.65	6.83	5.24	0.34	NM	0.51	235.1	0
		3.4	36	4.9	9	0.65	7.42	4.93	0.37		NM	NM	-0.003
		6.9	14	6.12	9.97	0.74	7.06	4.49	0.43		0.51	234.9	-0.008
		13.1	5	10.78	13.48	1.01	4.75	3.89	0.02		0.54	222	0.156
		19.6	1	13.18	15.07	1.12	3.27	3.26	0.1		0.53	227.7	0.137
S9	12.5												
		2.3	55	7	9.25	0.59	11.94	5.8	0.42	1.1266	0.52	246.6	0
		4.6	36	7.5	9.77	0.63	11.48	6.25	0.39		0.52	249.6	0.049
		8.2	14	7.1	9.46	0.6	12.37	5.95	0.47		0.54	241.1	0.051
		12.2	5	8.44	10.57	0.69	11.48	5.58	0.21		0.55	254.5	0.118
		18.1	1	15.29	15.72	1.14	4.75	2.59	0.21		0.54	253	0.184
S11	26.5												
		1.9	55	14.05	14.33	0.97	6.43	3.67	0.48	NM	0.58	204.6	0
		5.2	36	15.79	14.64	1.01	6.99	3.7	0.62		0.57	202.8	0.035
		8.6	14	15.85	14.5	0.99	6.6	3.7	0.58		0.57	198.7	0.069
		13.8	5	14.61	14.63	1.05	6.66	3.46	0.05		0.57	202.1	0.068
		21.1	1	13.33	14.75	1.04	7.09	3.98	0.14		0.6	203.8	0.08
S14	7.5												
		5.4	55	13.95	14.99	1.13	1.58	1.04	0.58	1.2518	0.59	248.4	0.037
		8.6	36	14.21	15.08	1.15	1.12	0.79	0.39		0.6	285.6	0.169
		15.3	14	14.99	15.79	1.19	0.7	0.86	0.07		0.52	337.5	0.199
		23.5	5	16.12	16.69	1.27	0.49	0.91	0.05		0.59	358.5	0.218
		35.5	1	17.59	17.59	1.36	0.46	1.74	0.03		0.61	369.7	0.261

References:

1. Siegel DA, Buesseler KO, Behrenfeld MJ, Benitez-Nelson CR, Boss E, Brzezinski MA, et al. Prediction of the export and fate of global ocean net primary production: The exports science plan. *Front Mar Sci* 2016; **3**: 22.

2. Biller SJ, Berube PM, Dooley K, Williams M, Satinsky BM, Hackl T, et al. Marine microbial metagenomes sampled across space and time. *Sci Data 2018 51* 2018; **5**: 1–7.

3. Rusch DB, Halpern AL, Sutton G, Heidelberg KB, Williamson S, Yooseph S, et al. The Sorcerer II Global Ocean Sampling Expedition: Northwest Atlantic through Eastern Tropical Pacific. *PLOS Biol* 2007; **5**: e77.

4. Bork P, Bowler C, de Vargas C, Gorsky G, Karsenti E, Wincker P. Tara Oceans studies plankton at Planetary scale. *Science (80-)* 2015; **348**: 873.

5. Larkin AA, Garcia CA, Garcia N, Brock ML, Lee JA, Ustick LJ, et al. High spatial resolution global ocean metagenomes from Bio-GO-SHIP repeat hydrography transects. *Sci Data 2021 81* 2021; **8**: 1–6.

6. Tréguer PJ, Sutton JN, Brzezinski MA, Charette MA, Devries T, Dutkiewicz S, et al. Reviews and syntheses: The biogeochemical cycle of silicon in the modern ocean. *Biogeosciences* 2021; **18**: 1269–1289.

7. Hutchins DA, Bruland KW. Iron-limited diatom growth and Si:N uptake ratios in a coastal upwelling regime. *Nature* 1998; **393**: 561–564.

8. King AL, Barbeau KA. Evidence for phytoplankton iron limitation in the southern

California Current System. *Mar Ecol Prog Ser* 2007; **342**: 91–103.

9. Pichevin LE, Ganeshram RS, Geibert W, Thunell R, Hinton R. Silica burial enhanced by iron limitation in oceanic upwelling margins. *Nat Geosci* 2014; **7**: 541–546.

10. Brzezinski MA, Krause JW, Bundy RM, Barbeau KA, Franks P, Goericke R, et al. Enhanced silica ballasting from iron stress sustains carbon export in a frontal zone within the California Current. *J Geophys Res Ocean* 2015; **120**: 4654–4669.

11. Baines SB, Twining BS, Vogt S, Balch WM, Fisher NS, Nelson DM. Elemental composition of equatorial Pacific diatoms exposed to additions of silicic acid and iron. *Deep Res Part II Top Stud Oceanogr* 2011; **58**: 512–523.

12. de Baar HJW, van Heuven SMAC, Middag R. Ocean Biochemical Cycling and Trace Elements. *Encycl Earth Sci Ser* 2017; 1–21.

13. Assmy P, Smetacek V, Montresor M, Klaas C, Henjes J, Strass VH, et al. Thick-shelled, grazer-protected diatoms decouple ocean carbon and silicon cycles in the iron-limited Antarctic Circumpolar Current. *Proc Natl Acad Sci* 2013; **110**: 20633–20638.

14. Leynaert A, Bucciarelli E, Claquin P, Dugdale RC, Martin-jézéquel V, Pondaven P, et al. Effect of iron deficiency on diatom cell size and silicic acid uptake kinetics. *Limnol Oceanogr* 2004; **49**: 1134–1143.

15. Marchetti A, Harrison PJ. Coupled changes in the cell morphology and the elemental (C, N, and Si) composition of the pennate diatom *Pseudo-nitzschia* due to iron deficiency. *Limnol Oceanogr* 2007; **52**: 2270–2284.

16. McNair HM, Brzezinski MA, Krause JW. Diatom populations in an upwelling

environment decrease silica content to avoid growth limitation. *Environ Microbiol* 2018; **20**: 4184–4193.

17. Glibert PM, McCarthy JK. Uptake and assimilation of ammonium and nitrate by phytoplankton: Indices of nutritional status for natural assemblages. *J Plankton Res* 1984; **6**: 677–697.

18. Takeda S. Influence of iron availability on nutrient consumption ratio of diatoms in oceanic waters. *Nature* 1998; **393**: 774–777.

19. Timmermans KR, Van Der Wagt B, De Baar HJW. Growth rates, half-saturation constants, and silicate, nitrate, and phosphate depletion in relation to iron availability of four large, open-ocean diatoms from the Southern Ocean. *Limnol Oceanogr* 2004; **49**: 2141–2151.

20. Brzezinski MA, Olson R, Chisholm SSW. Silicon availability and cell-cycle progression in marine diatoms. *Mar Ecol Prog Ser* 1990; **67**: 83–96.

21. Hildebrand M, Volcani BE, Gassmann W, Schroeder JI. A gene family of silicon transporters. *Nat 1997 3856618* 1997; **385**: 688–689.

22. Durkin CA, Marchetti A, Bender SJ, Truong T, Morales RL, Mock T, et al. Frustule-related gene transcription and the influence of diatom community composition on silica precipitation in an iron-limited environment. *Limnol Oceanogr* 2012; **57**: 1619–1633.

23. Allen AE, LaRoche J, Maheswari U, Lommer M, Schauer N, Lopez PJ, et al. Whole-cell response of the pennate diatom *Phaeodactylum tricornutum* to iron starvation.

Proc Natl Acad Sci 2008; **105**: 10438–10443.

24. Meyerink SW, Ellwood MJ, Maher WA, Dean Price G, Strzepek RF. Effects of iron limitation on silicon uptake kinetics and elemental stoichiometry in two Southern Ocean diatoms, *Eucampia antarctica* and *Proboscia inermis*, and the temperate diatom Thalassiosira pseudonana. *Limnol Oceanogr* 2017; **62**: 2445–2462.

25. Marchetti A, Schruth DM, Durkin CA, Parker MS, Kodner RB, Berthiaume CT, et al. Comparative metatranscriptomics identifies molecular bases for the physiological responses of phytoplankton to varying iron availability. *Proc Natl Acad Sci U S A* 2012; **109**: E317–E325.

26. Boyd PW, Muggli DL, Varela DE, Goldblatt RH, Chretien R, Orians KJ, et al. In vitro iron enrichment experiments in the NE subarctic pacific. *Mar Ecol Prog Ser* 1996; **136**: 179–193.

27. Marchetti A, Sherry ND, Kiyosawa H, Tsuda A, Harrison PJ. Phytoplankton processes during a mesoscale iron enrichment in the NE subarctic Pacific: Part I-Biomass and assemblage. *Deep Res Part II Top Stud Oceanogr* 2006; **53**: 2095–2113.

28. La Roche J, Geider RJ, Graziano LM, Murray H, Lewis K. Induction of specific proteins in eukaryotic algae grown under iron-, phosphorus-, or nitrogen-deficient conditions. *J Phycol* 1993; **29**: 767–777.

29. Peers G, Price NM. Copper-containing plastocyanin used for electron transport by an oceanic diatom. *Nature* 2006; **441**: 341–344.

30. Boyd PW, Berges JA, Harrison PJ. In vitro iron enrichment experiments at iron-rich

and -poor sites in the NE subarctic pacific. *J Exp Mar Bio Ecol* 1998; **227**: 133–151.

31. Timmermans KR, Stolte W, de Baar HJW. Iron-mediated effects on nitrate reductase in marine phytoplankton. *Mar Biol* 1994; **121**: 389–396.

32. Jin. X, Gruber N, Dune JP, Sarmiento JL, Armstrong RA. Diagnosing the contributions of phytoplankton functional groups to the production and export of particulate organic carbon, $CaCO_3$, and opal from global nutrient and alkalinity distributions. *Global Biogeochem Cycles* 2006; **20**: 1–17.

33. Lampe RH, Cohen NR, Ellis KA, Bruland KW, Maldonado MT, Peterson TD, et al. Divergent gene expression among phytoplankton taxa in response to upwelling. *Environ Microbiol* 2018; **20**: 3069–3082.

34. Lampe RH, Mann EL, Cohen NR, Till CP, Thamatrakoln K, Brzezinski MA, et al. Different iron storage strategies among bloom-forming diatoms. *Proc Natl Acad Sci* 2018; **115**: E12275–E12284.

35. Brembu T, Chauton MS, Winge P, Bones AM, Vadstein O. Dynamic responses to silicon in Thalasiossira pseudonana - Identification, characterisation and classification of signature genes and their corresponding protein motifs. *Sci Rep* 2017; **7**: 4865.

36. Kotzsch A, Gröger P, Pawolski D, Bomans PHH, Sommerdijk NAJM, Schlierf M, et al. Silicanin-1 is a conserved diatom membrane protein involved in silica biomineralization. *BMC Biol* 2017; **15**: 9–11.

37. Fawcett SE, Ward BB. Phytoplankton succession and nitrogen utilization during the development of an upwelling bloom. *Mar Ecol Prog Ser* 2011; **428**: 13–31.

38. Lampe RH, Hernandez G, Lin YY, Marchetti A. Representative Diatom and Coccolithophore Species Exhibit Divergent Responses throughout Simulated Upwelling Cycles. *mSystems* 2021; **6**.

39. Bruland KW, Rue EL, Smith GJ. Iron and macronutrients in California coastal upwelling regimes: Implications for diatom blooms. *Limnol Oceanogr* 2001; **46**: 1661–1674.

40. Redfield AC, Ketchum BH, Richards FA. The influence of organisms on the composition of sea-water. *sea ideas Obs Prog study seas* 1963.

41. White KK, Dugdale RC. Silicate and nitrate uptake in the Monterey Bay upwelling system. *Cont Shelf Res* 1997; **17**: 455–472.

42. Chappell PD, Whitney LP, Wallace JR, Darer AI, Jean-Charles S, Jenkins BD. Genetic indicators of iron limitation in wild populations of *Thalassiosira oceanica* from the northeast Pacific Ocean. *ISME J* 2015; **9**: 592–602.

43. Marchetti A, Moreno CM, Cohen NR, Oleinikov I, deLong K, Twining BS, et al. Development of a molecular-based index for assessing iron status in bloom-forming pennate diatoms. *J Phycol* 2017; **53**: 820–832.

44. Thamatrakoln K, Korenovska O, Niheu AK, Bidle KD. Whole-genome expression analysis reveals a role for death-related genes in stress acclimation of the diatom *Thalassiosira pseudonana*. *Environ Microbiol* 2012; **14**: 67–81.

45. Cohen NR, Ellis KA, Lampe RH, McNair HM, Twining BS, Maldonado MT, et al. Diatom Transcriptional and Physiological Responses to Changes in Iron

Bioavailability across Ocean Provinces. *Front Mar Sci* 2017; **4**: 1–20.

46. La Roche J, Boyd PW, McKay RML, Geider RJ. Flavodoxin as an in situ marker for iron stress in phytoplankton. *Nature* 1996; **382**: 802–805.

47. Hervás M, Navarro JAJ a, Diaz A, Bottin HH, De la Rosa MA, Díaz A, et al. Laser-flash kinetic analysis of the fast electron transfer from plastocyanin and cytochrome c6 to photosystem I. Experimental evidence on the evolution of the reaction mechanism. *Biochemistry* 1995; **34**: 11321–11326.

48. Franck VM, Bruland KW, Hutchins DA, Brzezinski MA. Iron and zinc effects on silicic acid and nitrate uptake kinetics in three high-nutrient, low-chlorophyll (HNLC) regions. *Mar Ecol Prog Ser* 2003; **252**: 15–33.

49. Brown KL, Twing KI, Robertson DL. Unraveling the regulation of nitrogen assimilation in the marine diatom *Thalassiosira pseudonana* (bacillariophyceae): Diurnal variations in transcript levels for five genes involved in nitrogen assimilation. *J Phycol* 2009; **45**: 413–426.

50. Allen AE, Dupont CL, Oborník M, Horák A, Nunes-Nesi A, McCrow JP, et al. Evolution and metabolic significance of the urea cycle in photosynthetic diatoms. *Nature* 2011; **473**: 203–207.

51. Görlich S, Pawolski D, Zlotnikov I, Kröger N. Control of biosilica morphology and mechanical performance by the conserved diatom gene Silicanin-1. *Commun Biol* 2019; **2**.

52. Durkin CA, Koester JA, Bender SJ, Armbrust VE. The evolution of silicon

transporters in diatoms. *J Phycol* 2016; **52**: 716–731.

53. McNair HM, Brzezinski MA, Till CP, Krause JW. Taxon-specific contributions to silica production in natural diatom assemblages. *Limnol Oceanogr* 2018; **63**: 1056–1075.

54. King AL, Barbeau KA. Dissolved iron and macronutrient distributions in the southern California Current System. *J Geophys Res Ocean* 2011; **116**: 1–18.

55. Hoffmann LJ, Peeken I, Lochte K. Effects of iron on the elemental stoichiometry during EIFEX and in the diatoms *Fragilariopsis kerguelensis* and *Chaetoceros dichaeta*. *Biogeosciences* 2007; **4**: 569–579.

56. Matsumoto K, Sarmiento JL, Brzezinski MA. Silicic acid leakage from the Southern Ocean: A possible explanation for glacial atmospheric pCO2. *Global Biogeochem Cycles* 2002; **16**.

57. Geider RJ, Greene RM, Kolber ZS, MacIntyre HL, Falkowski PG. Fluorescence assessment of the maximum quantum efficiency of photosynthesis in the western North Atlantic. *Deep Res Part I* 1993; **40**: 1205–1224.

58. Durkin CA, Bender SJ, Chan KYK, Gaessner K, Grünbaum D, Armbrust VE. Silicic acid supplied to coastal diatom communities influences cellular silicification and the potential export of carbon. *Limnol Oceanogr* 2013; **58**: 1707–1726.

59. Kudo I, Miyamoto M, Noiri Y, Maita Y. Combined effects of temperature and iron on the growth and physiology of the marine diatom *Phaeodactylum tricornutum* (Bacillariophyceae). *J Phycol* 2000; **36**: 1096–1102.

60. Eldridge ML, Trick CG, Alm MB, DiTullio GR, Rue EL, Bruland KW, et al. Phytoplankton community response to a manipulation of bioavailable iron in HNLC waters of the subtropical Pacific Ocean. *Aquat Microb Ecol* 2004; **35**: 79–91.

61. Sunda WG, Huntsman SA. Iron uptake and growth limitation in oceanic and coastal phytoplankton. *Mar Chem* 1995; **50**: 189–206.

62. Morel FMM, Rueter JG, Price NM. Iron nutrition of phytoplankton and its possible importance in the ecology of ocean regions with high nutrient and low biomass. *Oceanography* 1991; **4**: 56–61.

63. Coale TH, Moosburner M, Horák A, Oborník M, Barbeau KA, Allen AE. Reduction-dependent siderophore assimilation in a model pennate diatom. *Proc Natl Acad Sci U S A* 2019; **116**: 23609–23617.

64. De La Rocha CL, Hutchins DA, Brzezinski MA, Zhang Y. Effects of iron and zinc deficiency on elemental composition and silica production by diatoms. *Mar Ecol Prog Ser* 2000; **195**: 71–79.

65. Claquin P, Martin-Jézéquel V, Kromkamp JC, Veldhuis MJW, Kraay GW. Uncoupling of silicon compared with carbon and nitrogen metabolisms and the role of the cell cycle in continuous cultures of *Thalassiosira pseudonana* (Bacillariophyceae) under light, nitrogen, and phosphorus control. *J Phycol* 2002; **38**: 922–930.

66. Wang WX, Dei RCH. Biological uptake and assimilation of iron by marine plankton: influences of macronutrients. *Mar Chem* 2001; **74**: 213–226.

67. Kröger N, Deutzmann R, Sumper M. Polycationic peptides from diatom biosilica that

direct silica nanosphere formation. *Science (80-)* 1999; **286**: 1129–1132.

68. Scheffel A, Poulsen N, Shian S, Kröger N. Nanopatterned protein microrings from a diatom that direct silica morphogenesis. *Proc Natl Acad Sci* 2011; **108**: 3175–3180.

69. Knight MJ, Senior L, Nancolas B, Ratcliffe S, Curnow P. Direct evidence of the molecular basis for biological silicon transport. *Nat Commun* 2016; **7**: 1–11.

70. Shrestha RP, Hildebrand M. Evidence for a regulatory role of diatom silicon transporters in cellular silicon responses. *Eukaryot Cell* 2015; **14**: 29.

71. Thamatrakoln K, Hildebrand M. Silicon uptake in diatoms revisited: A model for saturable and nonsaturable uptake kinetics and the role of silicon transporters. *Plant Physiol* 2008; **146**: 1397–1407.

72. Conway HL, Harrison PJ. Marine diatoms grown in chemostats under silicate or ammonium limitation. IV. Transient response of *Chaetoceros debilis*, *Skeletonema costatum*, and *Thalassiosira gravida* to a single addition of the limiting nutrient. *Mar Biol* 1977; **43**: 33–43.

73. Thamatrakoln K, Hildebrand M. Analysis of *Thalassiosira pseudonana* silicon transporters indicates distinct regulatory levels and transport activity through the cell cycle. *Eukaryot Cell* 2007; **6**: 271–279.

74. Sapriel G, Quinet M, Heijde M, Jourdren L, Tanty V, Luo G, et al. Genome-wide transcriptome analyses of silicon metabolism in *Phaeodactylum tricornutum* reveal the multilevel regulation of silicic acid transporters. *PLoS One* 2009; **4**.

75. Ashworth J, Coesel SN, Lee A, Armbrust VE, Orellana M V., Baliga NS. Genome-

wide diel growth state transitions in the diatom *Thalassiosira pseudonana*. *Proc Natl Acad Sci U S A* 2013; **110**: 7518–7523.

76. Chauton MS, Winge P, Brembu T, Vadstein O, Bones AM. Gene regulation of carbon fixation, storage, and utilization in the diatom *Phaeodactylum tricornutum* acclimated to light/dark cycles. *Plant Physiol* 2013; **161**: 1034–1048.

77. Chisholm SW, Costello JC. Influence of environmental factors and population composition on the timing of cell division in Thalassiosira fluviatilis (Bacillariophyceae) grown on light/dark cycles. *J Phycol* . 1980. , **16**: 375–383

78. Smith SR, Glé C, Abbriano RM, Traller JC, Davis AK, Trentacoste E, et al. Transcript level coordination of carbon pathways during silicon starvation-induced lipid accumulation in the diatom *Thalassiosira pseudonana*. *New Phytol* 2016; **210**: 890–904.

79. Vaulot D, Olson RJ, Chisholm SW. Light and dark control of the cell cycle in two marine phytoplankton species. *Exp Cell Res* 1986; **167**: 38–52.

80. Marchetti A, Parker MS, Moccia LP, Lin EO, Arrieta AL, Ribalet FF, et al. Ferritin is used for iron storage in bloom-forming marine pennate diatoms. *Nature* 2009; **457**: 467–470.

81. Goldman JAL, Schatz MJ, Berthiaume CT, Coesel SN, Orellana M V., Armbrust VE. Fe limitation decreases transcriptional regulation over the diel cycle in the model diatom Thalassiosira pseudonana. *PLoS One* 2019; **14**: 1–25.

82. Assmy P, Smetacek V, Montresor M, Klaas C, Henjes J, Strass VH, et al. Thick-

shelled, grazer-protected diatoms decouple ocean carbon and silicon cycles in the iron-limited Antarctic Circumpolar Current. *Proc Natl Acad Sci U S A* 2013; **110**: 20633–20638.

83. Kranzler CF, Brzezinski MA, Cohen NR, Lampe RH, Maniscalco M, Till CP, et al. Impaired viral infection and reduced mortality of diatoms in iron-limited oceanic regions. *Nat Geosci* 2021; **14**: 231–237.

84. Hutchins DA, Franck VM, Brzezinski MA, Bruland KW. Inducing phytoplankton iron limitation in iron-replete coastal waters with a strong chelating ligand. *Limnol Oceanogr* 1999; **44**: 1009–1018.

85. Parsons TR, Maita Y, Lalli CM. A manual of chemical and biological methods for seawater analysis. 1984. Pergamon Press.

86. Krause JW, Nelson DM, Lomas MW. Biogeochemical responses to late-winter storms in the Sargasso Sea, II: Increased rates of biogenic silica production and export. *Deep Res Part I Oceanogr Res Pap* 2009; **56**: 861–874.

87. Biller D V., Coale TH, Till RC, Smith GJ, Bruland KW. Coastal iron and nitrate distributions during the spring and summer upwelling season in the central California Current upwelling regime. *Cont Shelf Res* 2013; **66**: 58–72.

88. Parker CE, Brown MT, Bruland KW. Scandium in the open ocean: A comparison with other group 3 trivalent metals. *Geophys Res Lett* 2016; **43**: 2758–2764.

89. Biller D V., Bruland KW. Sources and distributions of Mn, Fe, Co, Ni, Cu, Zn, and Cd relative to macronutrients along the central California coast during the spring and

summer upwelling season. *Mar Chem* 2013; **155**: 50–70.

90. Dugdale RC, Wilkerson FP. The use of 15N to measure nitrogen uptake in eutrophic oceans; experimental considerations,. *Limnol Oceanogr* 1986; **31**: 673–689.

91. Bronk DA, Gilbert PM, Ward BB. Nitrogen Uptake, Dissolved Organic Nitrogen Release, and New Production. *Science (80-)* 1994; **265**: 1843–1846.

92. McNair HM, Brzezinski MA, Krause JW. Quantifying diatom silicification with the fluorescent dye, PDMPO. *Limnol Oceanogr Methods* 2015; **13**: 587–599.

93. Robertson G, Schein J, Chiu R, Corbett R, Field M, Jackman SD, et al. De novo assembly and analysis of RNA-seq data. *Nat Methods* 2010; **7**: 909–912.

94. Kanehisa M, Furumichi M, Tanabe M, Sato Y, Morishima K. KEGG: new perspectives on genomes, pathways, diseases and drugs. *Nucleic Acids Res* 2017; **45**: D353--D361.

95. Smith SR, Dupont CL, McCarthy JK, Broddrick JT, Oborník M, Horák A, et al. Evolution and regulation of nitrogen flux through compartmentalized metabolic networks in a marine diatom. *Nat Commun* 2019; **10**: 4552.

96. Morrissey J, Sutak R, Paz-Yepes J, Tanaka A, Moustafa A, Veluchamy A, et al. A novel protein, ubiquitous in marine phytoplankton, concentrates iron at the cell surface and facilitates uptake. *Curr Biol* 2015; **25**: 364–371.

97. Matsen FA, Kodner RB, Armbrust VE. pplacer: linear time maximum-likelihood and Bayesian phylogenetic placement of sequences onto a fixed reference tree. *BMC Bioinformatics* 2010; **11**: 538.

98. Bolger AM, Lohse M, Usadel B. Trimmomatic: A flexible trimmer for Illumina sequence data. *Bioinformatics* 2014; **30**: 2114–2120.

99. Birol I, Jackman SD, Nielsen CB, Qian JQ, Varhol R, Stazyk G, et al. De novo transcriptome assembly with ABySS. *Bioinformatics* 2009; **25**: 2872–2877.

100. Gremme G, Steinbiss S, Kurtz S. Genome tools: A comprehensive software library for efficient processing of structured genome annotations. *IEEE/ACM Trans Comput Biol Bioinforma* 2013; **10**: 645–656.

101. Patro R, Duggal G, Love MI, Irizarry RA, Kingsford C. Salmon provides fast and bias-aware quantification of transcript expression. *Nat Methods* 2017; **14**: 417–419.

102. Keeling PJ, Burki F, Wilcox HM, Allam B, Allen EE, Amaral-Zettler LA, et al. The Marine Microbial Eukaryote Transcriptome Sequencing Project (MMETSP): Illuminating the Functional Diversity of Eukaryotic Life in the Oceans through Transcriptome Sequencing. *PLoS Biol* 2014; **12**.

103. Stamatakis A. RAxML version 8: A tool for phylogenetic analysis and post-analysis of large phylogenies. *Bioinformatics* 2014; **30**: 1312–1313.

104. Cohen NR, McIlvin MR, Moran DM, Held NA, Saunders JK, Hawco NJ, et al. Dinoflagellates alter their carbon and nutrient metabolic strategies across environmental gradients in the central Pacific Ocean. *Nat Microbiol* 2021; **6**: 173–186.

105. Alexander H, Rouco M, Haley ST, Wilson ST, Karl DM, Dyhrman ST. Functional group-specific traits drive phytoplankton dynamics in the oligotrophic ocean. *Proc Natl Acad Sci U S A* 2015; **112**: E5972–E5979.

106. Hu SK, Liu Z, Alexander H, Campbell V, Connell PE, Dyhrman ST, et al. Shifting metabolic priorities among key protistan taxa within and below the euphotic zone. *Environ Microbiol* 2018; **20**: 2865–2879.

107. Toseland A, Moxon S, Mock T, Moulton V. Metatranscriptomes from diverse microbial communities: Assessment of data reduction techniques for rigorous annotation. *BMC Genomics* 2014; **15**: 1–7.

108. Kopf A, Kostadinov I, Wichels A, Quast C, Glöckner FO. Metatranscriptome of marine bacterioplankton during winter time in the North Sea assessed by total RNA sequencing. *Mar Genomics* 2015; **19**: 45–46.

109. Utermöhl H. Methods of collecting plankton for various purposes are discussed. *SIL Commun 1953-1996* 1958; **9**: 1–38.

110. Falkowski PG, Kiefer DA. Chlorophyll-A fluorescence in phytoplankton - relationship to photosynthesis and biomass. *J Plankton Res* 1985; **7**: 715–731.

111. Kolber ZS, Prasil O, Falkowski PG. Measurements of variable chlorophyll fluorescence using fast repetition rate techniques: defining methodology and experimental protocols. *Biochim Biophys ACTA-BIOENERGETICS* 1998; **1367**: 88–106.

112. Gorbunov MY, Falkowski PG. Fluorescence induction and relaxation (FIRe) technique and instrumentation for monitoring photosynthetic processes and primary production in aquatic ecosystems. *Photosynth Fundam Asp to Glob Perspect 13th Int Congr Photosynth* 2004; 1029–1031.

113. Robinson MD, McCarthy DJ, Smyth GK. edgeR: a Bioconductor package for differential expression analysis of digital gene expression data. *Bioinformatics* 2010; **26**: 139–40.

114. Benjamini Y, Hochberg Y. Controlling the false discovery rate: a practical and powerful approach to multiple testing. *Journal of the Royal Statistical Society. Series B (Methodological)* . 1995.

115. Tréguer PJ, Sutton JN, Brzezinski MA, Charette MA, Devries T, Dutkiewicz S, et al. Reviews and syntheses: The biogeochemical cycle of silicon in the modern ocean. *Biogeosciences* 2021; **18**: 1269–1289.

116. Moore JK, Doney SC, Kleypas JA, Glover DM, Fung IY. An intermediate complexity marine ecosystem model for the global domain. *Deep Res Part II Top Stud Oceanogr* 2001; **49**: 403–462.

117. Krause JW, Brzezinski MA, Siegel DA, Thunell RC. Biogenic silica standing stock and export in the Santa Barbara Channel ecosystem. *J Geophys Res Ocean* 2013; **118**: 736–749.

118. Brzezinski MA, Phillips DR, Chavez FP, Friederich GE, Dugdale RC. Silica production in the Monterey, California, upwelling system. *Limnol Oceanogr* 1997; **42**: 1694–1705.

119. Brzezinski MA. The Si:C:N ratio of marine diatoms: interspecific variability and the effect of some environmental variables. *J Phycol* 1985; **21**: 347–357.

120. De La Rocha CL, Passow U. Recovery of Thalassiosira weissflogii from nitrogen and

silicon starvation. *Limnol Oceanogr* 2004; **49**: 245–255.

121. Hockin NL, Mock T, Mulholland F, Kopriva S, Malin G. The response of diatom central carbon metabolism to nitrogen starvation is different from that of green algae and higher plants. *Plant Physiol* 2012; **158**: 299–312.

122. Smith SR, Glé C, Abbriano RM, Traller JC, Davis A, Trentacoste E, et al. Transcript level coordination of carbon pathways during silicon starvation-induced lipid accumulation in the diatom T halassiosira pseudonana. *New Phytol* 2016; **210**: 890–904.

123. Bender SJ, Durkin CA, Berthiaume CT, Morales RL, Armbrust VE. Transcriptional responses of three model diatoms to nitrate limitation of growth. *Front Mar Sci* 2014; **1**: 1–15.

124. Zielinski BL, Allen AE, Carpenter EJ, Coles VJ, Crump BC, Doherty M, et al. Patterns of transcript abundance of eukaryotic biogeochemically-relevant genes in the Amazon river plume. *PLoS One* 2016; **11**: 1–20.

125. Wenzl S, Hett R, Richthammer P, Sumper M. Silacidins: Highly acidic phosphopeptides from diatom shells assist in silica precipitation in vitro. *Angew Chemie - Int Ed* 2008; **47**: 1729–1732.

126. Tesson B, Lerch SJL, Hildebrand M. Characterization of a new protein family associated with the silica deposition vesicle membrane enables genetic manipulation of diatom silica. *Sci Rep* 2017; **7**: 1–13.

127. Krause JW, Brzezinski MA, Largier JL, McNair HM, Maniscalco M, Bidle KD, et al.

The interaction of physical and biological factors drives phytoplankton spatial distribution in the northern California Current. *Limnol Oceanogr* 2020; **65**: 1974–1989.

128. Nelson D, Brzezinski MA. Kinetics of silicic acid uptake by natural diatom assemblages in two Gulf Stream warm-core rings. *Mar Ecol Prog Ser* 1990; **62**: 283–292.

129. Krause JW, Brzezinski MA, Jones JL. Application of low-level beta counting of 32Si for the measurement of silica production rates in aquatic environments. *Mar Chem* 2011; **127**: 40–47.

130. Martin-Jézéquel V, Hildebrand M, Brzezinski MA. Silicon metabolism in diatoms: Implications for growth. *J Phycol* 2000; **36**: 821–840.

131. Harrison PJ, Conway H., Holmes R, Davis C. Marine diatoms grown in chemostats under silicate or ammonium linitation. III. Chaetoceros debilis, Skeletonema costatum, and Thalassiosira gravida*. *Mar Biol* 1977; **43**: 19–31.

132. Kranzler CF, Krause JW, Brzezinski MA, Edwards BR, Biggs WP, Maniscalco M, et al. Silicon limitation facilitates virus infection and mortality of marine diatoms. *Nat Microbiol* 2019; **4**: 1790–1797.

133. Shrestha RP, Tesson B, Norden-Krichmar T, Federowicz S, Hildebrand M, Allen AE. Whole transcriptome analysis of the silicon response of the diatom *Thalassiosira pseudonana*. *BMC Genomics* 2012; **13**: 1.

134. Trainer VL, Adams NG, Bill BD, Stehr CM, Wekell JC, Moeller P, et al. Domoic acid

production near California coastal upwelling zones, June 1998. *Limnol Oceanogr* 2000; **45**: 1818–1833.

135. Trainer VL, Bates SS, Lundholm N, Thessen AE, Cochlan WP, Adams NG, et al. Pseudo-nitzschia physiological ecology, phylogeny, toxicity, monitoring and impacts on ecosystem health. *Harmful Algae* 2012; **14**: 271–300.

136. McCabe RM, Hickey BM, Kudela RM, Lefebvre KA, Adams NG, Bill BD, et al. An unprecedented coastwide toxic algal bloom linked to anomalous ocean conditions. *Geophys Res Lett* 2016; **43**: 10,366-10,376.

137. Benoiston AS, Ibarbalz FM, Bittner L, Guidi L, Jahn O, Dutkiewicz S, et al. The evolution of diatoms and their biogeochemical functions. *Philos Trans R Soc B Biol Sci* 2017; **372**.

138. Wetz MS, Wheeler PA. Production and partitioning of organic matter during simulated phytoplankton blooms. *Limnol Oceanogr* 2003; **48**: 1808–1817.

139. Paasche E. Silicon and the ecology of marine plankton diatoms. I. Thalassiosira pseudonana (Cyclotella nana) grown in a chemostat with silicate as limiting nutrient. *Mar Biol* 1973; **19**: 117–126.

140. Sullivan CW, Volcani BE. Role of silicon in diatom metabolism III. The effects of silicic acid on DNA polymerase, TMP kinase and DNA synthesis in Cylindrotheca fusiformis. *Biochim Biophys Acta - Nucleic Acids Protein Synth* 1973; **308**: 212–229.

141. Armbrust VE, Berges JA, Bowler C, Green BR, Martinez D, Putnam NH, et al. The genome of the diatom *Thalassiosira Pseudonana*: Ecology, evolution, and

metabolism. *Science (80-)* 2004; **306**: 79–86.

142. Bowler C, Allen AE, Badger JH, Grimwood J, Jabbari K, Kuo A, et al. The *Phaeodactylum* genome reveals the evolutionary history of diatom genomes. *Nature* 2008; **456**: 239–244.

143. Tully BJ, Graham ED, Heidelberg JF. The reconstruction of 2,631 draft metagenome-assembled genomes from the global oceans. *Sci Data 2018 51* 2018; **5**: 1–8.

144. Zehr JP, Montoya JP, Jenkins BD, Hewson I, Mondragon E, Short CM, et al. Experiments linking nitrogenase gene expression to nitrogen fixation in the North Pacific subtropical gyre. *Limnol Oceanogr* 2007; **52**: 169–183.

145. Thamatrakoln K. Molecular insights into the function and regulation of diatom silicon transporters. 2006; 137.

146. Nymark M, Valle KC, Hancke K, Winge P, Andresen K, Johnsen G, et al. Molecular and Photosynthetic Responses to Prolonged Darkness and Subsequent Acclimation to Re-Illumination in the Diatom Phaeodactylum tricornutum. *PLoS One* 2013; **8**.

147. Brembu T, Mühlroth A, Alipanah L, Bones AM. The effects of phosphorus limitation on carbon metabolism in diatoms. *Philos Trans R Soc B Biol Sci* 2017; **372**.

148. Alipanah L, Rohloff J, Winge P, Bones AM, Brembu T. Whole-cell response to nitrogen deprivation in the diatom Phaeodactylum tricornutum. *J Exp Bot* 2015; **66**: 6281–6296.

149. Moreno CM, Gong W, Cohen NR, DeLong K, Marchetti A. Interactive effects of iron and light limitation on the molecular physiology of the Southern Ocean diatom

Fragilariopsis kerguelensis. *Limnol Oceanogr* 2020; **65**: 1511–1531.

150. Kaplan DM, Largier JL. HF radar-derived origin and destination of surface waters off Bodega Bay, California. *Deep Res Part II* 2006; **25**–**26**: 2906–2930.

151. Nelson DM, Brzezinski MA, Sigmon DE, Franck VM. A seasonal progression of Si limitation in the Pacific sector of the Southern Ocean. *Deep Res Part II Top Stud Oceanogr* 2001; **48**: 3973–3995.

152. Krause JW, Brzezinski MA, Landry MR, Baines SB, Nelson DM, Selph KE, et al. The effects of biogenic silica detritus, zooplankton grazing, and diatom size structure on silicon cycling in the euphotic zone of the eastern equatorial Pacific. *Limnol Oceanogr* 2010; **55**: 2608–2622.

153. Brzezinski MA, Nelson DM. The annual silica cycle in the Sargasso Sea near Bermuda. *Deep Res Part I* 1995; **42**: 1215–1237.

154. Strickland JDH, Parsons TR. Practical Handbook of Seawater Analyis. 1972.

155. Edgar RC, Bateman A. Search and clustering orders of magnitude faster than BLAST. *Bioinformatics* 2010; **26**: 2460–2461.

156. Pearson WR. Finding Protein and Nucleotide Similarities with FASTA. *Curr Protoc Bioinforma* 2016; **53**: 3.9.1-3.9.25.

157. De Vargas C, Audic S, Henry N, Decelle J, Mahé F, Logares R, et al. Eukaryotic plankton diversity in the sunlit ocean. *Science (80-)* 2015; **348**.

158. Kopylova E, Noé L, Touzet H. SortMeRNA: Fast and accurate filtering of ribosomal RNAs in metatranscriptomic data. *Bioinformatics* 2012; **28**: 3211–3217.

159. Li D, Liu CM, Luo R, Sadakane K, Lam TW. MEGAHIT: An ultra-fast single-node solution for large and complex metagenomics assembly via succinct de Bruijn graph. *Bioinformatics* 2015; **31**: 1674–1676.

160. Rho M, Tang H, Ye Y. FragGeneScan: Predicting genes in short and error-prone reads. *Nucleic Acids Res* 2010; **38**: 1–12.

161. Marron AO, Ratcliffe S, Wheeler GL, Goldstein RE, King N, Not F, et al. The evolution of silicon transport in eukaryotes. *Mol Biol Evol* 2016; **33**: 3226–3248.

162. Largier JLL, Lawrence CAA, Roughan M, Kaplan DMM, Dever EPP, Dorman CEE, et al. WEST: A northern California study of the role of wind-driven transport in the productivity of coastal plankton communities. *Deep Sea Res Part II Top Stud Oceanogr* 2006; **53**: 2833–2849.

163. Margalef R. Life-forms of phytoplankton as survival alternatives in an unstable environment. *Oceanol Acta* 1978; **1**: 493–509.

164. Boyd PW, Crossley AC, DiTullio GR, Griffiths FB, Hutchins DA, Queguiner B, et al. Control of phytoplankton growth by iron supply and irradiance in the subantarctic Southern Ocean: Experimental results from the SAZ Project. *J Geophys Res Ocean* 2001; **106**: 31573–31583.

165. Kudela RM, Dugdale RC. Nutrient regulation of phytoplankton productivity in Monterey Bay, California. *Deep Res Part II Top Stud Oceanogr* 2000; **47**: 1023–1053.

166. Lewis M, Cullen J, Piatt T. Relationships between vertical mixing and photoadaptation of phytoplankton: similarity criteria. *Mar Ecol Prog Ser* 1984; **15**: 141–149.

167. Mitchell BG, Brody EA, Holm-Hansen O, McClain C, Bishop J. Light limitation of phytoplankton biomass and macronutrient utilization in the Southern Ocean. *Limnol Oceanogr* 1991; **36**: 1662–1677.

168. Price JF, Weller RA, Pinkel R. Diurnal Cycling: observations and models of the upper ocean response to diurnal heating, cooling, and wind mixing. 1986.

169. Pellichero V, Boutin J, Claustre H, Merlivat L, Sallée JB, Blain S. Relaxation of Wind Stress Drives the Abrupt Onset of Biological Carbon Uptake in the Kerguelen Bloom: A Multisensor Approach. *Geophys Res Lett* 2020; **47**: e2019GL085992.

170. Muratore D, Boysen AK, Harke MJ, Becker KW, Casey JR, Coesel SN, et al. Complex marine microbial communities partition metabolism of scarce resources over the diel cycle. *Nat Ecol Evol 2022 62* 2022; **6**: 218–229.

171. Huppe HC, Turpin DH. Integration of Carbon and Nitrogen Metabolism in Plant and Algal Cells. *Annu Rev Plant Physiol Plant Mol Biol* 1994; **45**: 577–607.

172. Vergara JJ, Berges JA, Falkowski PG. Diel periodicity of nitrate reductase activity and protein levels in the marine diatom Thalassiosira weissflogii (Bacillariophyceae). *J Phycol* 1998; **34**: 952–961.

173. Karl DM. A sea of change: Biogeochemical variability in the North Pacific Subtropical Gyre. *Ecosystems* 1999; **2**: 181–214.

174. Goldman JC, McGillicuddy DJ. Effect of large marine diatoms growing at low light on episodic new production. *Limnol Oceanogr* 2003; **48**: 1176–1182.

175. Krause JW, Nelson DM, Brzezinski MA. Biogenic silica production and the diatom

contribution to primary production and nitrate uptake in the eastern equatorial Pacific Ocean. *Deep Res Part II Top Stud Oceanogr* 2011; **58**: 434–448.

176. Krause JW, Brzezinski MA, Villareal TA, Wilson C. Biogenic silica cycling during summer phytoplankton blooms in the North Pacific subtropical gyre. *Deep Res Part I Oceanogr Res Pap* 2013; **71**: 49–60.

177. Lewin JC, Hellebust JA. Heterotrophic nutrition of the marine pennate diatom Nitzschia angularis var. affinis. *Mar Biol* 1976; **36**: 313–320.

178. Vaulot D, Olson RJ, Chisholm SW. Light and dark control of the cell cycle in two marine phytoplankton species. *Exp Cell Res* 1986; **167**: 38–52.

179. Blank GS, Sullivan CW. Diatom mineralization of silicic acid. *Arch Microbiol 1979 1232* 1979; **123**: 157–164.

180. Tuchman NC, Schollett MA, Rier ST, Geddes P. Differential heterotrophic utilization of organic compounds by diatoms and bacteria under light and dark conditions. *Hydrobiologia* 2006; **561**: 167–177.

181. Falkowski PG, Owens TG, Ley AC, Mauzerall DC. Effects of Growth Irradiance Levels on the Ratio of Reaction Centers in Two Species of Marine Phytoplankton. *Plant Physiol* 1981; **68**: 969–973.

182. Behrenfeld MJ, Prasil O, Kolber ZS, Babin M, Falkowski PG. Compensatory changes in Photosystem II electron turnover rates protect photosynthesis from photoinhibition. *Photosynth Res* 1998; **58**: 259–268.

183. Closset I, McNair HM, Brzezinski MA, Krause JW, Thamatrakoln K, Jones JL.

Diatom response to alterations in upwelling and nutrient dynamics associated with climate forcing in the California Current System. *Limnol Oceanogr* 2021; **66**: 1578–1593.

184. Jacox MG, Edwards CA, Hazen EL, Bograd SJ. Coastal Upwelling Revisited: Ekman, Bakun, and Improved Upwelling Indices for the U.S. West Coast. *J Geophys Res Ocean* 2018; **123**: 7332–7350.

185. Anning T, MacIntyre HL, Pratt SM, Sammes PJ, Gibb S, Geider RJ. Photoacclimation in the marine diatom Skeletonema costatum. *Limnol Oceanogr* 2000; **45**: 1807–1817.

186. Cullen JJ, Lewis MR. The kinetics of algal photoadaptation in the context of vertical mixing. *J Plankton Res* 1988; **10**: 1039–1063.

187. Rijstenbil JW. Assessment of oxidative stress in the planktonic diatom Thalassiosira pseudonana in response to UVA and UVB radiation. *J Plankton Res* 2002; **24**: 1277–1288.

188. Avron M, Chance B. Relation of phosphorylation to electron transport in isolated chloroplasts. *Brookhaven Symp Biol* 1966; **19**: 149–160.

189. Saif Hasan S, Cramer WA. On rate limitations of electron transfer in the photosynthetic cytochrome b6f complex. *Phys Chem Chem Phys* 2012; **14**: 13853–13860.

190. Villani G, Attardi G. In vivo control of respiration by cytochrome c oxidase in wild-type and mitochondrial DNA mutation-carrying human cells. *Proc Natl Acad Sci U S A* 1997; **94**: 1166–1171.

191. Villani G, Greco M, Papa S, Attardi G. Low Reserve of Cytochrome c Oxidase Capacity in Vivo in the Respiratory Chain of a Variety of Human Cell Types. *J Biol Chem* 1998; **273**: 31829–31836.

192. Brzezinski MA. Cell-cycle effects on the kinetics of silicic acid uptake and resource competition among diatoms. *J Plankton Res* 1992; **14**: 1511–1539.

193. Walter B, Peters J, van Beusekom JEE. The effect of constant darkness and short light periods on the survival and physiological fitness of two phytoplankton species and their growth potential after re-illumination. *Aquat Ecol* 2017; **51**: 591–603.

194. Lopez PJ, Desclés J, Allen AE, Bowler C. Prospects in diatom research. *Curr Opin Biotechnol* 2005; **16**: 180–186.

195. Hildebrand M, Lerch SJL, Shrestha RP. Understanding diatom cell wall silicification-moving forward. *Front Mar Sci* 2018; **5**: 1–19.

196. Graff JR, Westberry TK, Milligan AJ, Brown MB, Dall'Olmo G, Reifel KM, et al. Photoacclimation of natural phytoplankton communities. *Mar Ecol Prog Ser* 2016; **542**: 51–62.

197. Barber J, Andersson B. Too much of a good thing: light can be bad for photosynthesis. *Trends Biochem Sci* 1992; **17**: 61–66.

198. Durnford DG, Price JA, McKim SM, Sarchfield ML. Light-harvesting complex gene expression is controlled by both transcriptional and post-transcriptional mechanisms during photoacclimation in Chlamydomonas reinhardtii. *Physiol Plant* 2003; **118**: 193–205.

199. Falkowski PG, Owens TG. Light- Shade Adaptation. *Cell* 1980; 592–595.

200. Escoubas JM, Lomas M, La Roche J, Falkowski PG. Light intensity regulation of cab gene transcription is signaled by the redox state of the plastoquinone pool. *Proc Natl Acad Sci U S A* 1995; **92**: 10237–10241.

201. Giordano M, Chen YB, Koblížek M, Falkowski PG, Koblizek M, Falkowski PG. Regulation of nitrate reductase in Chlamydomonas reinhardtii by the redox state of the plastoquinone pool. *Eur J Phycol* 2005; **40**: 345–352.

202. Huysman MJJ, Martens C, Vandepoele K, Gillard J, Rayko E, Heijde M, et al. Genome-wide analysis of the diatom cell cycle unveils a novel type of cyclins involved in environmental signaling. *Genome Biol* 2010; **11**.

203. Laws EA, Bannister TT. Nutrient- and light-limited growth of Thalassiosira fluviatilis in continuous culture, with implications for phytoplankton growth in the ocean1. *Limnol Oceanogr* 1980; **25**: 457–473.

204. Halsey KH, Jones BM. Phytoplankton Strategies for Photosynthetic Energy Allocation. *http://dx.doi.org/101146/annurev-marine-010814-015813* 2015; **7**: 265–297.

205. Li G, Woroch AD, Donaher NA, Cockshutt AM, Campbell DA. A hard day's night: Diatoms continue recycling photosystem II in the dark. *Front Mar Sci* 2016; **3**: 218.

206. Slamovits CH, Okamoto N, Burri L, James ER, Keeling PJ. A bacterial proteorhodopsin proton pump in marine eukaryotes. *Nat Commun 2011 21* 2011; **2**: 1–7.

207. Marchetti A, Catlett D, Hopkinson BM, Ellis K, Cassar N. Marine diatom proteorhodopsins and their potential role in coping with low iron availability. *ISME J* 2015; **9**: 2745–2748.

208. Kloer DP, Ruch S, Al-Babili S, Beyer P, Schulz GE. The structure of a retinal-forming carotenoid oxygenase. *Science (80-)* 2005; **308**: 267–269.

209. Kolber ZS, Zehr J, Falkowski PG. Effects of Growth Irradiance and Nitrogen Limitation on Photosynthetic Energy Conversion in Photosystem II. *Plant Physiol* 1988; **88**: 923–929.

210. Ley AC, Mauzerall DC. Absolute absorption cross-sections for Photosystem II and the minimum quantum requirement for photosynthesis in Chlorella vulgaris. *Biochim Biophys Acta - Bioenerg* 1982; **680**: 95–106.

211. Woodson CB, Barth JA, Cheriton OM, McManus MA, Ryan JP, Washburn L, et al. Observations of internal wave packets propagating along-shelf in northern Monterey Bay. *Geophys Res Lett* 2011; **38**: 1605.

212. de Boyer Montégut C, Madec G, Fischer AS, Lazar A, Iudicone D. Mixed layer depth over the global ocean: An examination of profile data and a profile-based climatology. *J Geophys Res Ocean* 2004; **109**: 1–20.

213. Kara AB, Rochford PA, Hurlburt HE. An optimal definition for ocean mixed layer depth. *J Geophys Res Ocean* 2000; **105**: 16803–16821.

214. Chen S, Zhou Y, Chen Y, Gu J. fastp: an ultra-fast all-in-one FASTQ preprocessor. *Bioinformatics* 2018; **34**: i884–i890.

215. Patro R, Duggal G, Love MI, Irizarry RA, Kingsford C. Salmon provides fast and bias-aware quantification of transcript expression. *Nat Methods* 2017; **14**: 417–419.

216. Brembu T, Chauton MS, Winge P, Bones AM, Vadstein O. Dynamic responses to silicon in Thalasiossira pseudonana - Identification, characterisation and classification of signature genes and their corresponding protein motifs. *Sci Rep* 2017; **7**: 4865.

217. Matsen FA, Kodner RB, Armbrust EV. pplacer: linear time maximum-likelihood and Bayesian phylogenetic placement of sequences onto a fixed reference tree. *BMC Bioinformatics* 2010; **11**.